Relativistic aspects of time in quantum mechanics

Kacper Dębski

Doctoral dissertation under the supervision of

prof. dr hab. Andrzej Dragan

Institute of Theoretical Physics
Faculty of Physics, University of Warsaw
Warsaw, 2024

Podziękowania

Niniejsza praca doktorska jest zwieńczeniem wieloletnich badań prowadzonych pod opieką profesora Andrzeja Dragana, któremu chciałbym złożyć serdeczne podziękowania za wszystkie lata, podczas których wspierał mój rozwój naukowy. Jego pasja, zaangażowanie oraz niezliczone godziny poświęcone na konsultacje i dyskusje sprawiły, że mogłem rozwijać swoje zainteresowania i umiejętności od pracy licencjackiej, przez magisterską, aż po ten doktorat. Dzięki jego wsparciu i inspiracji mogę dzisiaj z pewnością powiedzieć, że odnalazłem to, co naprawdę ważne, i czemu chciałbym poświęcić moje życie zawodowe.

Ponadto, chciałbym serdecznie podziękować mojej najbliższej rodzinie i przyjaciołom, którzy nieustannie wspierali mnie przez wszystkie lata mojej edukacji i badań. Szczególne podziękowania kieruję do moich rodziców, którzy od samego początku wierzyli we mnie i w sens moich działań. Ich wiara, wsparcie duchowe i materialne były dla mnie nieocenione i pozwoliły mi na realizację moich celów.

Na koniec chciałbym złożyć szczególne podziękowania mojej przyszłej żonie, Zuzannie. Dzięki jej wsparciu, wszystkie godziny spędzone na pisaniu tej pracy i żmudnych poprawkach były dla mnie czystą przyjemnością.

Abstract

This dissertation presents an in-depth study of the relativistic aspects of time in quantum mechanics, focusing on two primary themes: quantum time dilation and the concept of indefinite temporal order, including the implications of temporal Bell inequalities.

The research investigates quantum time dilation, a phenomenon where time dilation, well-known in relativity, also occurs at the quantum level. Our findings reveal that quantum time dilation is universal, similar to classical time dilation, meaning it does not depend on the specific mechanisms of the clocks used. This universality suggests that quantum time dilation is a fundamental property of quantum systems, expanding our understanding of time in the quantum realm. However, the dissertation also explores gravitational quantum time dilation and finds that it is not universal. Different clocks experience varying amounts of time dilation due to gravity, depending on their internal structures. This discovery mirrors the classical understanding of gravitational time dilation and highlights the complex interplay between quantum mechanics and gravity.

The second focus of this dissertation is the concept of indefinite temporal order. In classical physics, events occur in a definite sequence, but in the quantum world, events can exist in a superposition of different orders. This means that the sequence of events is not fixed and can be indefinite. We developed a scenario where accelerating particles interact with quantum fields to demonstrate this indefinite order. By using special relativistic time dilation, we established a protocol that shows a violation of Bell's inequalities, traditionally used to test definite temporal order. Our results indicate that events can indeed occur in an indefinite order, challenging classical perceptions of time.

Our research highlights that the assumptions necessary for proving Bell inequalities for temporal order are not always satisfied in practical scenarios. This insight led to a critical reassessment of these assumptions, revealing the complexities of disentangling the free dynamics of a system from local operations. These findings are significant for both theoretical and experimental investigations into the nature of time. To address these challenges, we propose using more general operations that include measurements with classical outcomes. This approach facilitates the direct examination of causal relationships between events without relying on specific theoretical models.

This dissertation advances our understanding of quantum time dilation and indefinite temporal order. It challenges conventional notions of time and causality, providing new perspectives on the fundamental nature of the universe. As research progresses in this field, the exploration of quantum mechanics and the nature of time promises to remain a fascinating and profound endeavor.

This doctoral thesis is based on four publications [1–4], two of which were first-authored [3, 4]. Furthermore, the writer of this thesis has contributed to several other articles that may provide context for the present considerations [5–10].

Contents

1 Introduction

> For what is time? Who can easily and briefly explain it? Who even in thought can comprehend it, even to the pronouncing of a word concerning it? But what in speaking do we refer to more familiarly and knowingly than time? And certainly we understand when we speak of it; we understand also when we hear it spoken of by another. What, then, is time? If no one ask of me, I know; if I wish to explain to him who asks, I know not.
>
> *(St. Augustine [11])*

This chapter provides a comprehensive exploration of the concept of time across different scientific fields, including its philosophical foundations and recent theories in physics. The dissertation aims to investigate various aspects of time and their implications. The research topics include the nature of time, the role of time in classical mechanics, quantum mechanics, and general relativity. Additionally, the structure of the dissertation will be presented, outlining the specific areas of study and the organization of the research.

Not only is time one of the most fundamental quantities present in science, but also it is a concept that we intuitively know from daily life. For physicists—and not only for them—it is a mysterious phenomenon somehow connected with motion and space. Since antiquity, natural philosophers have struggled to comprehend its true nature and provide a strict definition that would satisfy everyone [12].

Throughout history, various civilizations have explored the relationship between time and natural cycles. The Egyptians created calendars based on the regular flooding of the Nile River, which helped them plan their farming activities [13]. Similarly, the Mayans, known for their

advanced astronomy, built calendars that included celestial cycles and planetary movements [14]. These ancient civilizations understood time as something being linked to the natural rhythms of the world [15].

Religious traditions have also played a significant role in shaping our understanding of time [16]. Ancient and indigenous belief systems, including Hinduism, Buddhism, and certain indigenous cultures, embrace a cyclical perception of time [15]. Within these frameworks, time manifests as a recurring cycle of creation, existence, and dissolution, symbolizing the cosmic rhythm [17]. Conversely, Christianity introduced a shift from cyclical time, emphasizing a linear progression of history leading to the Second Coming of Christ and the ultimate fulfillment of God's plan [16]. This shift in Christian thought influenced Western perspectives and initiated subsequent philosophical discussions on the understanding of time [15]. One of the first scientific-like approaches to the problem of time was initiated by Ancient Greek thinkers [18]. Philosophers such as Zeno of Elea enriched the discourse on time with their paradoxes [19]. Zeno's paradoxes, including the Achilles and the Tortoise paradox and the Dichotomy paradox, presented profound challenges to our intuitive understanding of time. These paradoxes probed the concepts of motion, continuity, and the divisibility of time, stimulating contemplation on the fundamental nature of temporal existence [20].

The idea of time has been a topic of analysis for many thinkers throughout the ages. One of them was Immanuel Kant, the great eighteenth-century Prussian philosopher [21]. His works, particularly the "Critique of Pure Reason", contain some of the most intriguing arguments regarding time as a fundamental element of human experience. Contrary to empiricist philosophers like Locke, Kant argued that time is not a concept derived from experience but a form of our sensibility that we impose on our experiences [20]. His theory of temporal idealism aimed to resolve skeptical concerns about the possibility of scientific knowledge, demonstrating that the organization of experiences in time is a necessary condition for coherent thought [22].

Even in more contemporary times, philosophers continue to engage with the complexities of time. In the realm of more modern philosophy, Friedrich Nietzsche's idea, first presented in the work "The Gay Science" significantly contributed to our understanding of time [23]. Nietzsche challenged the prevailing linear perception of time and emphasized the profound significance of embracing the present moment. He criticized the excessive fixation on the past and future, positing that genuine fulfillment and meaning reside solely in the immediate experience of life. Nietzsche introduced the concept of the "eternal recurrence", proposing that time is cyclical, with all past events infinitely repeating in the future [24]. This concept urges individuals to wholeheartedly engage with each moment, recognizing its eternal repetition and extracting profound meaning from the present experience [24, 25].

Moreover, the philosophical debate on the significance of time did not end with the close

of the nineteenth century. New discoveries in quantum mechanics have shed light on existing problems that touch upon philosophical issues related to time. For example, the discovery that quantum mechanics is fundamentally an indeterministic theory has provided another opportunity to explore the old philosophical problem of free will [20]. These questions have intrigued many thinkers of the past, such as St. Augustine, St. Thomas Aquinas, Descartes, Spinoza, Leibniz, and others [26, 27] but this is not the appropriate place for such a discussion. We need to focus more on physical theories and the physical perception of time. However, the topic of determinism, particularly the possibility of verifying the indeterminism inherent in quantum mechanics, will reemerge, especially when we discuss the problem of indefinite temporal order arising from the interplay of quantum mechanics and theory of relativity (see chapter 3).

1.1 Concept of time in physics

While the philosophical discourse on time flourished in the humanities, a parallel discussion developed within the field of physics. Physics, as a scientific discipline, investigates the fundamental laws governing the physical world, and time plays a central role in this pursuit. The significance of time in physics extends beyond philosophical contemplations; it serves as a crucial dimension for describing and predicting physical phenomena.

Since the times of Newton and Leibniz, philosophers' efforts to comprehend these concepts have been seen as a conflict between the absolute concepts of space, time, and motion, and the relational approach proposed by Leibniz [20]. The revolution in physics caused by Newton seemed to solve the problem of an appropriate definition of time until the beginning of the twentieth century. Physicists forgot about the subtleties related to this topic because everything in physics seemed to work according to Newton's classical dynamics.

The classical notion of reality began to collapse when Einstein introduced his theory of relativity [28]. He defined time as what is measured by a clock, as shown in this quote: [29]:

> "[Time is] considered measurable by a clock (ideal periodic process) of negligible spatial extent. The time of an event taking place at a point is then defined as the time shown on the clock simultaneous with the event."

As such, this notion of time was closer to the opinion presented by Leibniz, not Newton. Moreover, the special and general theories of relativity show that time is just one of the four coordinates that can be transformed between different reference frames. The next great revolution in physics was caused by quantum mechanics, which changed the classical point of view. Every measurable quantity was now described by an operator acting on a Hilbert space [30]. Only the definition of time that was introduced to the quantum mechanic stays the same as in the classical Newto-

nian interpretation. Time in quantum mechanics is still only a scalar parameter that labels the evolution of the system. Attempts to construct a time operator ended in failure, expressed in Pauli's famous objection [31].

He argues that the time operator would necessarily commute with the Hamiltonian of a given system, and as such, they would share the same spectrum. The typical spectrum of the latter is discrete and bounded from below, which stays in conflict with our expectations of time as a continuous, real quantity. This simple argumentation meant that physicists got stuck with classical time in a fully quantum theory.

Dealing with these contradictions is one of the crucial aims of modern theoretical physics. Exploring phenomena lying at the boundary of the two great branches of physics: the theory of relativity and quantum mechanics, can be an impulse to develop a better theory reconciling different points of view on the nature of time. Recent publications show a new way of treating time in quantum mechanics. Based on Bridgman's conception of physics expressed in the quote [32]:

> "Einstein, in seizing on the act of the observer as the essence of the situation, is actually adopting a new point of view as to what the concepts of physics should be; namely, the operational view."

One can try to extend the operational view to quantum theory. This extension has been made, and now time can be understood through measurements of quantum systems serving as clocks [33]. For example, this perspective on quantum clocks has been studied in the context of quantum metrology [34–37].

Recently it was also shown how to construct time observables as positive-operator valued measures (POVMs) that transform covariantly with respect to the group of time translations acting on the employed clock system [38, 39]. What is even more important, such covariant time observables not only can be used for a rigorous formulation of the time-energy uncertainty relation [34–37], but also to avoid the above-mentioned Pauli's objection [40]. Also, this way of defining time in quantum mechanics plays an important role in the so-called relational quantum dynamics [41–45]. Using this kind of quantum clock has significant consequences in the context of the theory of relativity. It was shown that a quantum clock can simultaneously experience different proper times if it spread along different trajectories. However, if it is well localized in space, the rate of its ticking agree with special and general relativity, as examined in numerous studies [46–53].

Quantum treatment of clocks no longer invites us to consider them as a background to some dynamic evolution of a given system, but rather as an intrinsic part of a fully quantum setup. As such, it is only natural to exploit the quantumness of the time measurement in order to ask fundamental questions and introduce quantities that may work as a testbed for relativistic and

quantum theories. Among many other proposals, we are most interested in two of them—the phenomenon of quantum time dilation and indefinite temporal order.

The first one emerges after asking the question: What happens when a clock is in a quantum superposition of two different velocities? It was demonstrated that, in addition to the classical contributions from a mixture of two different time dilations, there is an additional effect that arises solely due to quantum coherence. This effect is known as quantum time dilation [54].

The second issue involves the possibility that the *order* of two events could be in a superposition, similar to how we could have superpositions of different positions in quantum mechanics [55–57].

We plan to work with these ideas in order to devise schemes that would test the relationship of quantum and relativistic theories, uncovering phenomena that might provide us with further insight into the interlayer between these frameworks.

Recent theoretical advancements in this field have sparked a rapidly growing interest. Researchers are exploring a variety of fascinating topics. For example, some studies have investigated whether a charged decaying particle can act as an ideal clock in the presence of a magnetic field [58], and whether it is even possible to construct an ideal clock at all [59]. Other investigations have examined whether the time dilation on Earth is strong enough to cause decoherence in micro-scale quantum systems [60]. Researchers have also studied how detectors behave when they follow a quantum superposition of different accelerated paths in Minkowski spacetime [61]. Additionally, they have focused on establishing proper relational dynamics in quantum mechanics [62] and ensuring that physical laws remain consistent across different quantum reference frames [63].

Experimental efforts have also highlighted numerous regimes where the gravitational and quantum worlds intersect. Some studies have shown that quantum interference effects allow two detectors to gain information on field correlations that would otherwise be inaccessible [64]. Other research has demonstrated how free-falling objects in a uniform gravitational field can be used to test the equivalence principle [65, 66]. Moreover, a recent paper by Sougato Bose *et al.* proposed an idea to test whether gravity is a quantum entity [67]. A similar idea was proposed by Chiara Marletto and Vlatko Vedral, who suggested an experiment to observe the quantumness of the gravitational field by examining the induced entanglement between two massive particles [68].

The author of this dissertation has also been involved in other research related to the aforementioned topics. His other work includes studies on quantum effects through the theory of Gaussian states in uniformly accelerated frames [5], which, for example, was used to demonstrate the effect of relativistic acceleration on tripartite entanglement in Gaussian states [6]. Additionally, he has studied the Casimir-Polder potential with Unruh-DeWitt detector excitations [7], as well as the Casimir effect in conformally flat spacetimes [8].

Recently, the author has also worked on the theory of hypothetical superluminal particles. This research culminated in the theory of relativity for superluminal observers in 1+3 spacetime [9], and the quantum version of the theory of tachyons [10].

While all these topics are indeed fascinating, they are not directly related to the subject of this dissertation, and thus, will not be elaborated upon further.

1.2 Structure of this work

This dissertation is structured as follows: In Chapters 2 and 3, we present the original results of this research based on four publications [1–4]. Consequently, all the plots presented in this dissertation are sourced from these references, although each plot will not be individually cited. Chapter 2 focuses on the properties of quantum time dilation, while Chapter 3 explores indefinite temporal order without gravity. At the start of each chapter, we will introduce the basic theories that underpin our work, such as the concept of quantum time dilation and indefinite temporal order. These introductions will set the stage for the key topics of this dissertation, like the universality of quantum time dilation and other related subjects. Additionally, Chapter 4 contains conclusions drawn from this dissertation. It also presents possible future research directions based on these findings.

2 Quantum time dilation

> [Time is] considered measurable by a clock (ideal periodic process) of negligible spatial extent. The time of an event taking place at a point is then defined as the time shown on the clock simultaneous with the event.
>
> *(Hermann Weyl [69])*

This chapter delves into the phenomenon of quantum time dilation, focusing on the definition put forth by Alexander Smith and Mehdi Ahmadi [70]. The impact of this concept is explored through the study of a clock interacting with an electromagnetic field. We examine the consistency of spectral measurements with theoretical predictions based on the time operator. Additionally, a quantum clock model, represented by a two-level system, is employed to investigate both kinematic and gravitational time dilation effects, demonstrating significant alignment with theoretical expectations derived from the more abstract analysis of the time operator. The chapter concludes by confirming the non-coincidental nature of the observed effects and identifying the conditions under which the universality of quantum time dilation occurs.

Contents

2.1 Useful tools

In this section, we will introduce the fundamental concepts used in this chapter. These theories and ideas serve as an introduction to the topic of further considerations that are the focus of this work.

2.1.1 Quantum time dilation - time operator approach

The superposition principle is a fundamental aspect of quantum mechanics. When combined with relativistic effects, it leads to various intriguing phenomena and theories like communications without definite causal structure [57], decoherence due to gravitational time dilation [47], gravitationally induced entanglement between particles [68], Bells's theorem for temporal order [71] or Unruh effect for detectors in superposition of accelerations [61], as we mentioned in the introduction. Consequently, a natural question arises: does quantum mechanics contribute to the observed time dilation of a clock moving in a superposition of relativistic speeds? This question has been investigated in various scenarios, such as modified twin-paradox situations with one twin in a superposition of motions [72], analogue twin-paradox scenarios in superconducting circuits [73], interferometry experiments where a clock experiences a superposition of proper

times [52, 53, 74, 75], and sequential boosts of quantum clocks emulating twin-like scenarios, leading to nonclassical effects in ion trap atomic clocks [76].

Recently, a probabilistic formulation of relativistic time dilation observed by quantum clocks has been developed [54]. It has been demonstrated that a clock moving in a localized momentum wave packet, on average, observes classical time dilation in accordance with special relativity. However, when a clock moves in a coherent superposition of two momentum wave packets, it experiences quantum corrections to the observed time dilation compared to a classical clock moving in a probabilistic mixture of the same wave packets. This quantum time dilation effect has been established within an idealized model of a clock. However, the question of whether quantum time dilation is universal, analogous to how classical time dilation affects all clocks uniformly, remains an open question, one of the main topic of this dissertation.

The original goal of this work is to demonstrate the universality of quantum time dilation and to provide conditions under which it occurs. However, before delving into the discussion of the results obtained by the author of this dissertation, it is necessary to present a precise description of the phenomenon of the quantum time dilation.

To illustrate the quantum time dilation measured by a quantum clock, we can examine a relativistic particle with an internal degree of freedom. This internal degree of freedom is described by a Hamiltonian, which captures the particle's dynamics and interactions within the framework of quantum mechanics

$$\hat{H} = \sqrt{\hat{\boldsymbol{p}}^2 c^2 + \hat{M}^2 c^4}, \tag{2.1}$$

where the momentum of the particle is represented by $\hat{\boldsymbol{p}}$, and the mass operator is defined as $\hat{M} \equiv m + \hat{H}_{\text{clock}}/c^2$. The mass operator combines the particle's rest mass m with the dynamical mass $\hat{H}_{\text{clock}}/c^2$, which arises from the energy associated with the internal degree of freedom governed by the Hamiltonian $\hat{H}_{\text{clock}}$.

The internal degree of freedom of the particle can function as a clock that measures the particle's proper time. This is achieved through a time observable $\hat{T}_{\text{clock}}$ that undergoes covariant transformations with respect to the group generated by $\hat{H}_{\text{clock}}$. The time observable $\hat{T}_{\text{clock}}$ is defined as a positive operator valued measure with effect operators $\hat{E}(t)$ satisfying the covariance condition $\hat{E}(t+t') = e^{-it'\hat{H}_{\text{clock}}}\hat{E}(t)e^{it'\hat{H}_{\text{clock}}}$ [35, 37, 40]. It is assumed that this time observable is sharp and can be associated with a self-adjoint operator $\hat{T}_{\text{clock}}$.

Let us consider the particle prepared in a superposition of momentum wave packets, which

can be expressed, up to normalization, as

$$|\psi\rangle \propto \cos\theta \left|\varphi_{\bar{\boldsymbol{p}}_1}\right\rangle + e^{i\phi}\sin\theta \left|\varphi_{\bar{\boldsymbol{p}}_2}\right\rangle, \tag{2.2}$$

where $\theta \in [0, \frac{\pi}{2})$, $\phi \in [0, \pi)$, and $\langle \boldsymbol{p}|\varphi_{\bar{\boldsymbol{p}}_i}\rangle = e^{-(\boldsymbol{p}-\bar{\boldsymbol{p}}_i)^2/2\Delta^2}/\pi^{1/4}\sqrt{\Delta}$ with Δ being the spread of the wave packet in momentum space. Consider a clock characterized by the Hilbert space $L^2(\mathbb{R})$, where the Hamiltonian is given by $\hat{H}_{\text{clock}} = c\hat{P}_{\text{clock}}$ and the covariant time observable satisfies the commutation relation $[\hat{T}_{\text{clock}}, \hat{H}_{\text{clock}}] = i\hbar$. The average time measured by the clock, denoted as $\langle \hat{T}_{\text{clock}}\rangle$, when observed by an observer relative to whom the Hamiltonian in (2.1) generates an evolution corresponding to a time t, can be shown to be equal to [54]

$$\langle \hat{T}_{\text{clock}}\rangle = \left(\gamma_C^{-1} + \gamma_Q^{-1}\right) t, \tag{2.3}$$

where to leading relativistic order

$$\gamma_C^{-1} \equiv 1 - \frac{\bar{\boldsymbol{p}}_1^2\cos^2\theta + \bar{\boldsymbol{p}}_2^2\sin^2\theta - \Delta^2/2}{2m^2c^2}, \tag{2.4}$$

is associated with the classical time dilation of a clock moving in a statistical mixture of momenta $\bar{\boldsymbol{p}}_1$ and $\bar{\boldsymbol{p}}_2$ with probabilities $\cos^2\theta$ and $\sin^2\theta$, and

$$\gamma_Q^{-1} \equiv \frac{\cos\phi\sin 2\theta\left[(\bar{\boldsymbol{p}}_2 - \bar{\boldsymbol{p}}_1)^2 - 2\left(\bar{\boldsymbol{p}}_2^2 - \bar{\boldsymbol{p}}_1^2\right)\cos 2\theta\right]}{8m^2c^2\left[\cos\phi\sin 2\theta + e^{\frac{(\bar{\boldsymbol{p}}_2-\bar{\boldsymbol{p}}_1)^2}{4\Delta^2}}\right]}, \tag{2.5}$$

quantifies the deviations from classical time dilation that arise due to the coherence between the momentum wave packets associated with the internal clock. It can be considered as a generalization of the classical time dilation formula, taking into account the potential motion of the clock in nonclassical states and accounting for non-zero γ_Q^{-1} that leads to quantum time dilation effects.

The previous discussions were centered around an ideal clock model, where the proper time of the clock was associated with an operator that was canonically conjugate to the specific clock Hamiltonian $\hat{H}_{\text{clock}}$. However, it remains uncertain whether quantum time dilation is a universal phenomenon that affects all clocks in a similar manner, as observed in classical time dilation.

2.1.2 Rindler coordinates

In the further sections of this dissertation, we will employ Rindler transformations to simulate the behavior of a clock in the presence of a gravitational field. At this point, let us recall the

basic facts about Rindler coordinates.
An accelerating frame of reference can be described using the following coordinate transformation [77]

$$ct = \chi \sinh\left(\frac{g\tau}{c}\right), \qquad z = \chi \cosh\left(\frac{g\tau}{c}\right), \tag{2.6}$$

where (ct, z) are Minkowski coordinates, τ is the Rindler time, χ is the Rindler distance, and g is a reference proper acceleration corresponding to an observer measuring proper time τ. For simplicity, we will focus on positive Rindler distances. In this case, observers with fixed Rindler coordinates χ experience constant proper acceleration c^2/χ, and their proper times can be related to the parameter g through the expression $\frac{g\chi}{c^2}\tau$. We restrict our considerations only to the region of spacetime with $z > |ct|$, i.e. to one Rindler wedge. The inverse transformation can be written as [77]

$$c\tau = \frac{c^2}{g}\operatorname{atanh}\left(\frac{ct}{z}\right), \qquad \chi = \sqrt{z^2 - c^2t^2}. \tag{2.7}$$

It is also convenient to use the so-called radar coordinates $(c\tau, \xi)$ with ξ defined by the relation $\chi = \frac{c^2}{g}e^{g\xi/c}$. These new coordinate system is especially useful to quantization procedure of the electromagnetic field as was shown in [78].

2.1.3 Post-Newtonian approximation

In the further sections of this dissertation, we will use Schwarzschild coordinates to investigate the behavior of a clock in the presence of a gravitational field. Let us now examine the so-called post-Newtonian expansion of the metric.
Let us consider the standard Schwarzschild metric in Schwarzschild coordinates, which corresponds to a set of stationary observers. The metric is given by

$$\mathrm{d}s^2 = \left(1 - \frac{2GM}{rc^2}\right)c^2\mathrm{d}t^2 - \left(1 - \frac{2GM}{rc^2}\right)^{-1}\mathrm{d}r^2 - r^2\mathrm{d}\Omega^2, \tag{2.8}$$

where $\mathrm{d}\Omega^2 = \mathrm{d}\theta^2 + \sin^2\theta\mathrm{d}\phi^2$.

To simplify the metric and make the spatial component isotropic, we can reparameterize the radial coordinate as $r(\varrho) = \varrho\left(1 + \frac{GM}{2\varrho c^2}\right)^2$. This leads to the metric

$$\mathrm{d}s^2 = \underbrace{\left(\frac{1 - \frac{GM}{2\varrho c^2}}{1 + \frac{GM}{2\varrho c^2}}\right)^2}_{g_{00}(\varrho)}c^2\mathrm{d}t^2 - \left(1 + \frac{GM}{2\varrho c^2}\right)^4\left(\mathrm{d}\varrho^2 + \varrho^2\mathrm{d}\Omega^2\right). \tag{2.9}$$

In these coordinates, the spatial part (ϱ, θ, ϕ) is proportional to the Euclidean metric.

Next, we introduce a reparameterized temporal coordinate τ_0 that corresponds to the proper time measured by a stationary ideal clock placed at ϱ_0. We have $\mathrm{d}\tau_0 = \sqrt{g_{00}(\varrho_0)}\mathrm{d}t$, and the metric in these new coordinates becomes

$$\mathrm{d}s^2 = \left(\frac{1-\frac{GM}{2\varrho c^2}}{1+\frac{GM}{2\varrho c^2}}\right)^2 \left(\frac{1-\frac{GM}{2\varrho_0 c^2}}{1+\frac{GM}{2\varrho_0 c^2}}\right)^{-2} c^2\mathrm{d}\tau_0^2 - \left(1+\frac{GM}{2\varrho c^2}\right)^4 \left(\mathrm{d}\varrho^2+\varrho^2\mathrm{d}\Omega^2\right). \tag{2.10}$$

To further analyze the metric, we perform a post-Newtonian expansion by assuming that the distances ϱ and ϱ_0 are larger than GM/c^2 or, equivalently, that the dimensionless parameters $GM/\varrho c^2$ and $GM/\varrho_0 c^2$ are small. The resulting expansion is

$$\begin{aligned}\mathrm{d}s^2 \approx{}& \left(1-2\frac{GM}{\varrho c^2}+2\left(\frac{GM}{\varrho c^2}\right)^2\right)\left(1+2\frac{GM}{\varrho_0 c^2}+2\left(\frac{GM}{\varrho_0 c^2}\right)^2\right)c^2\mathrm{d}\tau_0^2 \\ &- \left(1+2\frac{GM}{\varrho c^2}+\frac{3}{2}\left(\frac{GM}{\varrho c^2}\right)^2\right)\left(\mathrm{d}\varrho^2+\varrho^2\mathrm{d}\Omega^2\right).\end{aligned} \tag{2.11}$$

This approximate form of the metric (2.86) will be used in our study.

2.2 Quantum time dilation in atomic spectra

The objective of this section is to provide the example supporting the hypothesis that quantum time dilation is a universal phenomenon that can be observed within the standard formulation of quantum mechanics without taking into account time operators and any others unorthodox physics. To achieve this, we propose considering the lifetime of an excited hydrogen-like atom as a clock [33] and demonstrate that when such an atom moves in a coherent superposition of momenta, its lifetime undergoes the same quantum time dilation as the clocks studied in [54]. This offers a spectroscopic signature of a clock experiencing a superposition of proper times, which serves as an alternative to previous interferometry proposals aiming to observe a decrease in interference visibility [52, 53, 74, 75].

Observations of spectroscopic signatures of classical time dilation have been made for atoms moving at speeds as low as 10 m/s [79]. Nonclassical effects in emission spectroscopy due to the coherent spreading of the atomic center-of-mass wave function were first investigated in the early 1990s[80–83], and the effect of center-of-mass superposition was recently studied in a scalar field model [84]. In our work, we demonstrate the exact quantum time dilation effect described in [54] by observing the spontaneous decay rate of an atom moving in a coherent superposition of relativistic momenta. This finding paves the way for a new class of spectroscopic measurements that are sensitive to relativistic effects arising from quantum coherence.

Additionally, we highlight a novel correction to the classical Doppler shift that modifies the shape of the atomic emission spectrum. This correction becomes prominent when measuring the spectrum along the direction of the atom's motion. Conversely, when the spectrum is measured perpendicular to the motion, first-order momentum-dependent effects vanish, and second-order relativistic corrections emerge. This is evident from the angular distributions of radiation emitted by moving atoms, which we present. These distributions indicate the emission directions most affected by motion and suggest the optimal approach for measuring quantum time dilation.

Moreover, we analyze potential experimental scenarios in which both the quantum Doppler and quantum time dilation effects can be measured. Based on the current state-of-the-art techniques involving atomic ion clocks and setups with large momentum exchanges, we argue that the required parameter regimes can be reached. Previous spectroscopic experiments have successfully observed classical time dilation in atoms moving at speeds as low as 10 m/s [79], and we anticipate further advancements in this field.

Subsequently, we provide evidence supporting the hypothesis that quantum time dilation is a universal phenomenon for clocks moving in superpositions of inertial trajectories. To achieve this, we introduce an alternative clock model based on the lifetime of an excited atom. Through our investigation, we demonstrate that this atom-based clock exhibits quantum time dilation

in accordance with (2.5). This finding brings quantum time dilation effects closer to experimental verification by showcasing their manifestation in a realistic clock model grounded in the phenomenon of spontaneous emission, which is the underlying mechanism behind atomic clocks.

2.2.1 Spectroscopy of moving atoms

Consider a two-level atom with mass m, where the ground state $|g\rangle$ and excited state $|e\rangle$ are separated by an energy difference $\hbar\Omega$ in the atom's rest frame. The dynamics of the atom, as well as the electromagnetic fields $\hat{\mathbf{E}}$ and $\hat{\mathbf{B}}$, are described by the Hamiltonian

$$\hat{H} = \hat{H}_{\text{atom}} + \hat{H}_{\text{field}} + \hat{H}_{\text{af}}, \tag{2.12}$$

where the free Hamiltonian of the atom to leading relativistic order in the atom's center-of-mass momentum $\hat{\boldsymbol{p}}/mc$ (e.g. [85]) is

$$\hat{H}_{\text{atom}} = \frac{\hat{\mathbf{p}}^2}{2m} - \frac{1}{8}\frac{\hat{\mathbf{p}}^4}{m^3c^2} + \hbar\Omega\left(1 - \frac{1}{2}\frac{\hat{\mathbf{p}}^2}{m^2c^2}\right)|e\rangle\langle e|\,, \tag{2.13}$$

and the electromagnetic field Hamiltonian is $\hat{H}_{\text{field}} = \sum_{\boldsymbol{k},\xi}\hbar\omega_k\hat{a}^\dagger_{\boldsymbol{k},\xi}\hat{a}_{\boldsymbol{k},\xi}$, which is a mode sum over the wave vector $\boldsymbol{k}$ and polarization index ξ with the corresponding eigenfrequencies $\omega_k = kc$ and annihilation operators $\hat{a}_{\boldsymbol{k},\xi}$. The atom interacts with the electromagnetic field through the interaction Hamiltonian [86–90]

$$\hat{H}_{\text{af}} = -\hat{\boldsymbol{d}}\cdot\hat{\boldsymbol{E}}^\perp - \frac{1}{2m}\left[\hat{\boldsymbol{p}}\cdot\left(\hat{\boldsymbol{B}}\times\hat{\boldsymbol{d}}\right) + \left(\hat{\boldsymbol{B}}\times\hat{\boldsymbol{d}}\right)\cdot\hat{\boldsymbol{p}}\right], \tag{2.14}$$

where the first term represents the dipole interaction given by the dipole operator $\hat{\boldsymbol{d}} = \boldsymbol{d}\left(|g\rangle\langle e| + |e\rangle\langle g|\right)$ in the laboratory frame, and the second term represents the Röntgen term, which takes into account the Lorentz-transformed electromagnetic field experienced by the atom in motion.[1] The Röntgen term is a consequence of the vectorial nature of the electromagnetic field, and thus would not appear in an analogous scalar field model [84, 99]. It is important to note that all the operators entering the Hamiltonian (2.12) are expressed in the laboratory

[1] This term, known as the Röntgen term, has been known since the 19th century [91]. However, it was initially omitted in early works on light-matter interactions. Its incorporation into the formalism dates back to the works of Babiker in the 1980s [92]. It was later rigorously shown in the early 2000s that this term is necessary to achieve agreement with special relativity [87, 93, 94]. Nowadays, it is routinely used in studies of atom-field interactions involving moving bodies [89, 95–98].

frame.[2] The electromagnetic fields appearing in (2.14) are given by

$$\hat{\boldsymbol{E}}^{\perp}(\boldsymbol{r}) = -i \sum_{\boldsymbol{k},\xi} \sqrt{\frac{\hbar\omega_k}{2\epsilon_0 V}} \boldsymbol{\epsilon}_{\boldsymbol{k},\xi} \hat{a}_{\boldsymbol{k},\xi} e^{i\boldsymbol{k}\cdot\hat{\boldsymbol{r}}} + \text{H.c.}, \tag{2.15}$$

$$\hat{\boldsymbol{B}}(\boldsymbol{r}) = i \sum_{\boldsymbol{k},\xi} \sqrt{\frac{\hbar}{2\epsilon_0 V \omega_k}} \left(\boldsymbol{k} \times \boldsymbol{\epsilon}_{\boldsymbol{k},\xi}\right) \hat{a}_{\boldsymbol{k},\xi} e^{i\boldsymbol{k}\cdot\hat{\boldsymbol{r}}} + \text{H.c.}, \tag{2.16}$$

where ϵ_0 is the vacuum permittivity and V the quantization volume, while $\boldsymbol{\epsilon}_{\boldsymbol{k},\xi}$ is the polarization vector perpendicular to the wave vector $\boldsymbol{k}$. By employing the rotating wave approximation [87, 89], the interaction Hamiltonian (2.14) can be expressed as

$$\hat{H}\text{af} = -i\hbar \sum_{\boldsymbol{k},\xi} \sqrt{\frac{\hbar\omega_k}{2\epsilon_0 V}} \hat{g}_{\boldsymbol{k},\xi} e^{i\boldsymbol{k}\cdot\hat{\boldsymbol{r}}} \left|e\right\rangle \left\langle g\right| \hat{a}_{\boldsymbol{k},\xi} + \text{H.c.}, \tag{2.17}$$

where the coupling constant depends on the momentum of the atom

$$\hat{g}_{\boldsymbol{k},\xi} = \boldsymbol{\epsilon}_{\boldsymbol{k},\xi} \cdot \boldsymbol{d} + \frac{1}{m\omega_k} \left(\hat{\boldsymbol{p}} - \frac{\hbar\boldsymbol{k}}{2}\right) \cdot \left[\left(\boldsymbol{k} \times \boldsymbol{\epsilon}_{\boldsymbol{k},\xi}\right) \times \boldsymbol{d}\right], \tag{2.18}$$

and is an operator itself with eigenvalues $g_{\boldsymbol{k},\xi}$.

It is important to mention that the Hamiltonian $\hat{H}_{\text{af}}$ in (2.17) explicitly depends on the center-of-mass position operator $\hat{\boldsymbol{r}}$, which is treated as a quantum degree of freedom. This Hamiltonian establishes a coupling between the internal energy levels of the atom and its center-of-mass motion, leading to a recoil effect when the atom undergoes decay. The presence of the second term in (2.18) arises directly from the Röntgen term in (2.14).

Let us now examine the energy scales associated with the system under consideration, specifically the energy of the atom's internal degree of freedom $\hbar\Omega$, its rest energy mc^2, and its kinetic energy $\langle\hat{\boldsymbol{p}}^2/2m\rangle$. In the subsequent analysis, we will focus on regimes where the internal energy of the atom is much smaller than both its rest energy and its kinetic energy. This condition allows for a valid first-order expansion in terms of both $\hbar\Omega/mc^2$ and $\hbar\Omega/\langle\hat{\boldsymbol{p}}^2/2m\rangle$.

Let's consider an atom initially prepared in an excited state, characterized by a center-of-mass wave function $\psi(\boldsymbol{p})$, while the electromagnetic field is in a vacuum state. We can represent the initial state of the system as $|\Psi(0)\rangle = \int \mathrm{d}\boldsymbol{p}, \psi(\boldsymbol{p}) \left|e, \boldsymbol{p}, 0\right\rangle$. The composite system undergoes an

[2] For example, the dipole moment is connected to its rest value $\boldsymbol{d}'$ by a Lorentz transformation $\boldsymbol{d} = \boldsymbol{d}' - \frac{\boldsymbol{d}'\cdot\boldsymbol{v}}{v^2}\boldsymbol{v} + \frac{\boldsymbol{d}'\cdot\boldsymbol{v}}{v^2}\boldsymbol{v}/\sqrt{1 - v^2/c^2}$, where $\boldsymbol{v}$ is the velocity of the moving atom.

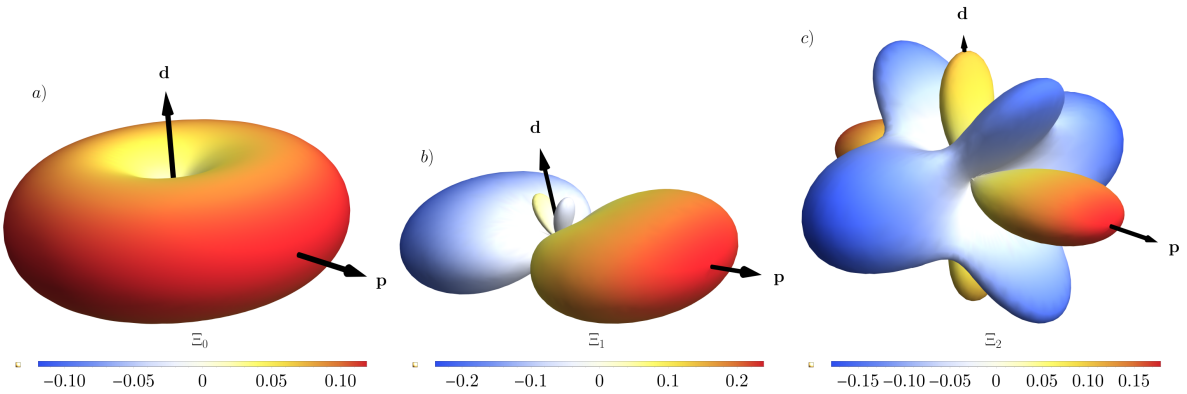

Figure 2.1: a) Angular dipole distribution of emitted photons from a decaying atom at rest ($\boldsymbol{p} = \boldsymbol{0}$) with respect to the center of mass momentum $\boldsymbol{p}$ and dipole momentum $\boldsymbol{d}$. b) Linear motion correction: Angular distribution modifications due to the linear momentum of the atom, c) Quadratic motion correction: Angular distribution modifications due to the quadratic momentum of the atom. Positive corrections are depicted in red, while negative corrections are shown in blue.

evolution over time, leading to the resulting state

$$|\Psi(t)\rangle = \int \mathrm{d}\boldsymbol{p}\, \alpha\left(\boldsymbol{p}, t\right) |e, \boldsymbol{p}, 0\rangle + \sum_{\boldsymbol{k},\xi} \int \mathrm{d}\boldsymbol{p}\, \beta_{\boldsymbol{k},\xi}\left(\boldsymbol{p}, t\right) |g, \boldsymbol{p} - \hbar\boldsymbol{k}, 1_{\boldsymbol{k},\xi}\rangle\,, \tag{2.19}$$

which has been expanded in the energy eigenstates $|e, \boldsymbol{p}, 0\rangle$ and $|g, \boldsymbol{p} - \hbar\boldsymbol{k}, 1_{\boldsymbol{k},\xi}\rangle$, associated respectively with the energies

$$\hbar\omega_e(\boldsymbol{p}) = \frac{\boldsymbol{p}^2}{2m} - \frac{\boldsymbol{p}^4}{8m^3c^2} + \hbar\Omega\left(1 - \frac{1}{2}\frac{\boldsymbol{p}^2}{m^2c^2}\right), \tag{2.20}$$

$$\hbar\omega_g(\boldsymbol{p}, \boldsymbol{k}) = \frac{(\boldsymbol{p} - \hbar\boldsymbol{k})^2}{2m} - \frac{(\boldsymbol{p} - \hbar\boldsymbol{k})^4}{8m^3c^2} + \hbar\omega_k. \tag{2.21}$$

The time-dependent coefficients in $|\Psi(t)\rangle$ can be determined by solving the corresponding Schrödinger equation using a Laplace transform, as commonly employed in Wigner-Weisskopf theory [100]. By employing a single pole approximation [81], we obtain the following expressions for the coefficients

$$\alpha\left(\mathbf{p}, t\right) = e^{-i\omega_e(\boldsymbol{p})t} e^{-\frac{\Gamma(\boldsymbol{p})}{2}t} \psi\left(\boldsymbol{p}\right), \tag{2.22}$$

$$\beta_{\boldsymbol{k},\xi}\left(\boldsymbol{p}, t\right) = \sqrt{\frac{\hbar\omega_k}{2\epsilon_0 V}} g_{\boldsymbol{k},\xi}(\boldsymbol{p}) \psi\left(\boldsymbol{p}\right) \frac{e^{-i\omega_e(\boldsymbol{p})t} e^{-\frac{\Gamma(\boldsymbol{p})}{2}t} - e^{-i\omega_g(\boldsymbol{p},\boldsymbol{k})t}}{i\left[\omega_e(\boldsymbol{p}) - \omega_g(\boldsymbol{p}, \boldsymbol{k})\right] + \frac{\Gamma(\boldsymbol{p})}{2}}, \tag{2.23}$$

where $\Gamma(\boldsymbol{p})$ is the total transition rate of the spontaneous decay of the atom moving with momentum $\boldsymbol{p}$

$$\Gamma(\boldsymbol{p}) = \sum_{\boldsymbol{k},\xi} \frac{\omega_k}{8\pi^2\hbar\epsilon_0 c^3} g^2_{\boldsymbol{k},\xi}(\boldsymbol{p})\delta\left[\omega_e(\boldsymbol{p}) - \omega_g(\boldsymbol{p},\boldsymbol{k})\right]. \tag{2.24}$$

Then, the total transition rate in the long-time limit is

$$\Gamma = \lim_{t\to\infty} \frac{\mathrm{d}}{\mathrm{d}t} \sum_{\boldsymbol{k},\xi} \int \mathrm{d}\boldsymbol{p}\ \left|\beta_{\boldsymbol{k},\xi}\left(\boldsymbol{p},t\right)\right|^2 = \int \mathrm{d}\boldsymbol{p}\ \left|\psi\left(\boldsymbol{p}\right)\right|^2 \Gamma(\boldsymbol{p}), \tag{2.25}$$

where the results of [93, 94] are recovered when $\psi\left(\boldsymbol{p}\right)$ is a momentum eigenstate.

As described in Appendix 2.6.2, the angular distribution of the emitted radiation can be obtained by omitting the angular integration in (2.25), resulting in the following expression

$$\frac{\Gamma(\Theta,\Phi)}{\Gamma_0} = \Xi_0(\Theta,\Phi)\left(1 - \frac{3}{2}\frac{\hbar\Omega}{mc^2}\right) + \frac{1}{mc}\Xi_1(\Theta,\Phi)\int \mathrm{d}p\ p|\psi(p)|^2 + \frac{1}{2m^2c^2}\Xi_2(\Theta,\Phi)\int \mathrm{d}p\ p^2|\psi(p)|^2, \tag{2.26}$$

where Θ and Φ are the azimuthal and polar angles of $\boldsymbol{k}$ vector relative to $\boldsymbol{p}$, respectively, $\Gamma_0 = \frac{\Omega^3 d'^2}{3\pi\epsilon_0\hbar c^3}$ is the total decay rate of a standing atom ignoring recoil effects (i.e., $\hbar\Omega \ll mc^2$), and we have assumed that the atom moves only along the z axis, perpendicular to the dipole moment vector $\boldsymbol{d}$.

Hence, $\psi(p)$ should be interpreted as a marginal distribution of a complete center-of-mass wave function, where $|\psi(p)|^2$ represents the integrated probability density over the x and y momentum directions, while being well localized along the z axis.

The term $\Xi_0(\Theta,\Phi)$ corresponds to the standard angular distribution of dipole radiation, and it depends on the polar angle Θ and azimuthal angle Φ

$$\Xi_0(\Theta,\Phi) = \frac{3}{8\pi}\left(1 - \sin^2\Theta\cos^2\Phi\right), \tag{2.27}$$

while

$$\Xi_1(\Theta,\Phi) = \frac{3}{4\pi}\cos\Theta\left(1 - 2\sin^2\Theta\cos^2\Phi\right), \tag{2.28}$$

$$\Xi_2(\Theta,\Phi) = \frac{3}{16\pi}\left[6\cos 2\Theta + 5\cos^2\Phi\left(\cos 4\Theta - \cos 2\Theta\right)\right], \tag{2.29}$$

are first and second order corrections in p/mc to the dipole distribution appearing due to the motion of the atom [87]. The motional corrections to the angular distribution of radiation are universal, meaning they occur regardless of the atom's motion, except when the atom is at rest. These corrections exhibit a consistent shape that is unaffected by the specific form of the

momentum wave function $\psi(p)$ (as shown in Fig. 2.1).

By integrating over the polar angle Θ and azimuthal angle Φ, the familiar formula [87, 89, 93, 94] can be recovered.

$$\Gamma = \Gamma_0 \left(1 - \frac{3\hbar\Omega}{2mc^2} - \frac{1}{2m^2c^2} \int \mathrm{d}p\; p^2 |\psi(p)|^2\right). \tag{2.30}$$

When the atom moves along a classical trajectory with momentum $\bar{p}$, the momentum wave function takes the form $|\psi(p)|^2 = \delta(p - \bar{p})$. In this case, the transition rate Γ is related to the transition rate in the atom's rest frame $\Gamma_0 \left(1 - \frac{3\hbar\Omega}{2mc^2}\right)$ through a Lorentz factor. Specifically, we have $\Gamma = \Gamma_0 \left(1 - \frac{3\hbar\Omega}{2mc^2}\right) \sqrt{1 - v^2/c^2} \approx \Gamma_0 \left(1 - \frac{3\hbar\Omega}{2mc^2} - \frac{\bar{p}^2}{2m^2c^2}\right)$. This expression agrees with (2.30) and ensures consistency with special relativity.

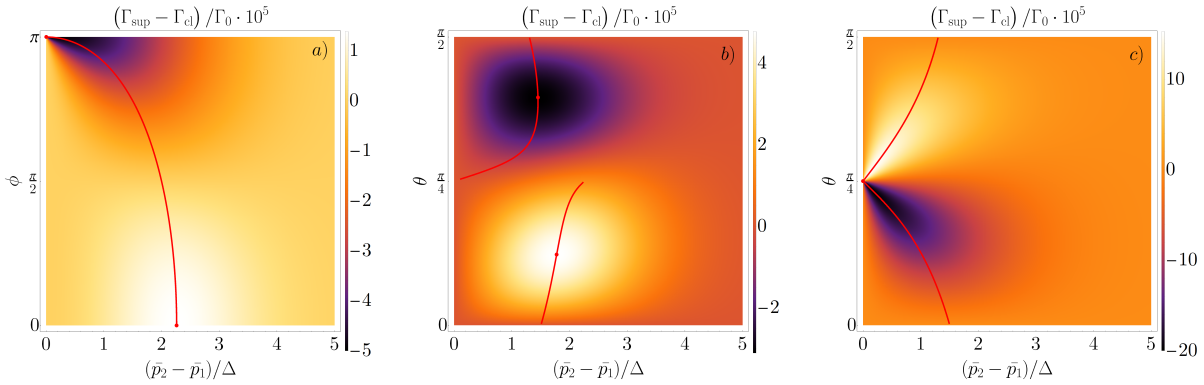

Figure 2.2: The plot depicts the difference in the total emission rate between a superposition and a classical mixture of two momentum wave packets of an atom. It shows how this difference depends on the momentum difference, relative phase, and weight of the wave packets. Panel a) corresponds to an equal-weighted superposition with $\theta = \pi/4$. Panels b) and c) represent fixed relative phases of $\phi = 0$ and $\phi = \pi$, respectively.
The red line indicates the maximum value of the effect for a given relative phase or weight, while the red circles mark the maximum and minimum values across the entire plot. A nonzero value for a finite momentum difference signifies the phenomenon of quantum time dilation.
Each panel assumes a momentum spread of $\Delta = 0.01mc$ for each wave packet, and the sum of their average momenta is $\bar{p}_1 + \bar{p}_2 = 0.05mc$.

Furthermore, by analyzing the expressions in (2.22), it is possible to derive the shape of an emission line. This emission line can then be easily converted to an absorption spectrum using the Einstein coefficients. The probability of an atom emitting a photon with momentum $\hbar\boldsymbol{k}$ can

be determined as follows

$$\mathcal{P}(\boldsymbol{k}) = \lim_{t\to\infty} \sum_{\xi} \int \mathrm{d}\boldsymbol{p}\, |\beta_{\boldsymbol{k},\xi}(\boldsymbol{p},t)|^2 . \tag{2.31}$$

Under the assumption of a large mass m, motion along the z axis, and a dipole moment perpendicular to the motion, we can deduce the specific characteristics of a transition line for photons emitted in the direction of motion (a detailed analysis of these characteristics is presented in Appendix 2.6.2)

$$\mathcal{P}_{\parallel}(\omega) = \frac{3}{8\pi} \int \mathrm{d}p\, |\psi(p)|^2 \frac{\left(1+3\frac{p}{mc}\right)\Gamma_0/2\pi}{\left[\omega - \Omega\left(1+\frac{p}{mc}\right)\right]^2 + \frac{\Gamma_0^2}{4}\left(1+2\frac{p}{mc}\right)}, \tag{2.32}$$

and perpendicular to both the dipole moment and to the direction of motion

$$\mathcal{P}_{\perp}(\omega) = \frac{3}{8\pi} \int \mathrm{d}p\, |\psi(p)|^2 \frac{\left(1-\frac{3}{2}\frac{p^2}{m^2c^2}\right)\Gamma_0/2\pi}{\left[\omega - \Omega\left(1-\frac{1}{2}\frac{p^2}{m^2c^2}\right)\right]^2 + \frac{\Gamma_0^2}{4}\left(1-\frac{p^2}{m^2c^2}\right)}. \tag{2.33}$$

It is important to note that both $\mathcal{P}_{\parallel}(\omega)$ and $\mathcal{P}_{\perp}(\omega)$ have been expanded up to the leading relativistic order, taking into account the center-of-mass momentum distribution $|\psi(p)|^2$ integrated against a Lorenz distribution. When observed in the direction of motion, the transition line experiences a Doppler shift, as the Lorenz distribution is linearly shifted in momentum by an amount $\Omega \to \Omega(1+p/mc)$. Conversely, for light emitted or absorbed perpendicular to the motion, the Doppler shift is absent, and the dominant relativistic corrections cause a shift in the center of the Lorenz distribution by an amount $\Omega \to \Omega(1-p^2/2m^2c^2)$, which is quadratic in momentum. These findings highlight the distinct effects of Doppler shift and relativistic corrections in the emission and absorption spectra of the system.

Each of the quantities of interest, namely the angular distribution of radiation, the total decay rate, and the shape of the emission line, are routinely measured in various experiments [101]. These experimental measurements provide valuable insights into the behavior of atoms and their interactions with electromagnetic fields. Having established how these observables depend on the center-of-mass momentum distribution, we are now equipped to utilize nonclassical center-of-mass motion in such experimental scenarios as a direct probe of quantum time dilation. This opens up exciting opportunities to experimentally investigate and verify the effects of quantum time dilation, providing further support for the universal nature of this phenomenon.

2.2.2 Spectroscopic signatures of quantum time dilation

To begin our analysis, we will investigate the transition rate Γ for atoms existing in coherent superpositions and incoherent classical mixtures of localized momentum wave packets. This allows us to examine the differences in the behavior of these two scenarios. Analogously to the quantum clock model described in 2.1.1, an atom is considered to be either in a superposition (2.2) with a momentum distribution given by

$$\psi_{\text{sup}}(\boldsymbol{p}) = \mathcal{N}\left(\cos\theta\,\langle\boldsymbol{p}|\varphi_{\bar{\boldsymbol{p}}_1}\rangle + e^{i\phi}\sin\theta\,\langle\boldsymbol{p}|\varphi_{\bar{\boldsymbol{p}}_2}\rangle\right), \tag{2.34}$$

where

$$\mathcal{N} \equiv \left[\sqrt{\pi}\Delta\left(1+\cos\phi\ \sin 2\theta\ e^{-\frac{(\bar{\boldsymbol{p}}_1-\bar{\boldsymbol{p}}_2)^2}{4\Delta^2}}\right)\right]^{-1/2} \tag{2.35}$$

or in a classical mixture such that

$$P_{cl}(\boldsymbol{p}) = \cos^2\theta\ \ |\langle\boldsymbol{p}|\varphi_{\bar{\boldsymbol{p}}_1}\rangle|^2 + \sin^2\theta\ \ |\langle\boldsymbol{p}|\varphi_{\bar{\boldsymbol{p}}_2}\rangle|^2 \tag{2.36}$$

of momentum wave packets.

For simplicity, let us assume that $\bar{\boldsymbol{p}}_1$ and $\bar{\boldsymbol{p}}_2$ are collinear. By evaluating equation (2.25), we obtain the relative difference in the total emission rates between these two scenarios

$$\frac{\Gamma_{\text{sup}}-\Gamma_{\text{cl}}}{\Gamma_0} = \frac{1}{2m^2c^2}\int \mathrm{d}\boldsymbol{p}\ p^2\left(|\psi_{\text{sup}}(\boldsymbol{p})|^2 - P_{cl}(\boldsymbol{p})\right)\gamma_Q^{-1}, \tag{2.37}$$

which corresponds to the quantum correction to the classical time dilation contribution, as specified in Equation (2.5) and derived in the work by Smith and Ahmadi [54]. It is remarkable to find that the clock model employed in this study, which is based on the spontaneous decay of an atom, exhibits the identical quantum time dilation effect as the quantum clock model investigated in [54] and discussed in Section 2.1.1. This observation lends support to the hypothesis that quantum time dilation, in the context of constant velocities, is universally applicable and impacts all clocks in a consistent manner.

The disparity γ_Q^{-1} in the transition rate between a coherent superposition and classical mixture of momentum wave packets can assume positive or negative values, contingent upon the relative phase ϕ and relative weight θ of the two wave packets (refer to Fig. 2.2). Specifically, for an equally weighted superposition, the expression in Equation (2.37) is independent of the sum of the wave packets' momenta. It takes on a positive value when the relative phase is less than $\phi = \pi/2$, and it becomes negative when the relative phase exceeds this threshold. Notably, the quantum contribution showcases a prominent peak at a specific relative phase ϕ. When $\phi = 0$,

this peak emerges at a finite momentum difference of $\bar{p}_2 - \bar{p}_1 \approx 2\Delta$. Conversely, when the relative phase is $\phi = \pi$, the position of the peak shifts closer to $\bar{p}_2 - \bar{p}_1 \approx 0$.

This behavior can be comprehended by examining the structure of the wave packets in momentum space. When the wave packets nearly completely overlap, their relative phase becomes crucial. In the limit where the separation between the wave packets in momentum space approaches zero, the distinction between the coherent superposition and incoherent classical mixture disappears since the two wave packets become indistinguishable. However, as the relative phase approaches π, the real part of the center-of-mass wave function approaches zero, highlighting the significance of the imaginary part, which is an antisymmetric function. This is in contrast to the classical mixture, where the density remains single-peaked.

Surprisingly, an equally weighted superposition does not maximize the effect of quantum time dilation, as it saturates at $-\Delta^2/2m^2c^2$ for a relative phase equal to $\phi = \pi$. The global maximum, on the other hand, is attained for $\phi = \pi$ with a slightly unbalanced superposition, $\theta \approx \pi/4 \pm (\bar{p}_2 - \bar{p}_1)/2\sqrt{2}\Delta$.

If the wave packets have average momenta much larger than their spreads, i.e., $(\bar{p}_1+\bar{p}_2)/\Delta \gg 1$, then the maximum becomes proportional to the sum of the momenta, $\pm\sqrt{2}\Delta|\bar{p}_1 + \bar{p}_2|/4m^2c^2$. This indicates that the effect of quantum coherence on the emission rate increases as the average momenta of the wave packets increase.

Note that the quantum correction γ_{Q}^{-1} to the observed time dilation through the atom's decay rate is a second-order effect in the atom's average momentum, as seen in (2.5) and (2.37), similar to the classical time dilation contribution governed by γ_{C}^{-1}. However, linear effects, such as the Doppler shift, can also be influenced by momentum coherence. These effects can be characterized by comparing the first moments of the momentum distributions associated with a coherent superposition and an incoherent classical mixture

$$\delta_Q \equiv \frac{1}{mc}\int \mathrm{d}\boldsymbol{p}\; p\left(|\psi_{\mathrm{sup}}(\boldsymbol{p})|^2 - P_{cl}(\boldsymbol{p})\right) = \frac{\cos\phi\;\sin 4\theta\,(\bar{p}_2 - \bar{p}_1)}{4mc\left[\cos\phi\sin 2\theta + e^{\frac{(\bar{p}_2-\bar{p}_1)^2}{4\Delta^2}}\right]}. \tag{2.38}$$

The behavior of δ_Q exhibits distinct characteristics compared to γ_Q^{-1}. Notably, δ_Q vanishes when the superposition of symmetric wave packets is equally weighted. However, due to its linear dependence on momentum, δ_Q is easier to measure as its absolute magnitude is inherently larger than the second-order quantum time dilation effect described by γ_Q^{-1}. Further analysis of δ_Q is presented in Appendix 2.6.1.

If one examines the angular distribution of emitted photons from the decaying atom, as given

by equation (2.26), the difference between the coherent and incoherent cases can be expressed as

$$\frac{\Gamma_{\mathrm{sup}}(\Theta,\Phi)-\Gamma_{\mathrm{cl}}(\Theta,\Phi)}{\Gamma_0} = \Xi_1(\Theta,\Phi)\ \delta_Q + \Xi_2(\Theta,\Phi)\ \gamma_Q^{-1}. \tag{2.39}$$

It is important to note that the angular distribution of radiation can be linearly affected by the atom's momentum coherence. In particular, the contribution stemming from momentum coherence is most pronounced for photons emitted in the direction of the atom's motion, as shown in Figure 2.1(b). However, it should be emphasized that this quantum correction will vanish if the atom's center-of-mass is prepared in an equally weighted superposition of momentum wave packets.

In contrast, the emission of photons perpendicular to both the dipole moment and the direction of motion is not linearly affected by the atom's momentum. Moreover, as depicted in Figure 2.1(c), the second-order contribution is largest in this direction, suggesting that detecting photons in this direction is optimal for measuring quantum time dilation.

Similar to the total emission rate and the angular distribution, the shape of a transition line is also affected by the nonclassicality of the center-of-mass state, as shown in (2.32) and(2.33). That is, the emission spectrum of an atom in a coherent momentum superposition is distinct from that of an incoherent classical mixture. As suggested by the analysis of the angular distribution of radiation, we will focus on two cases: photons emitted parallel and perpendicular to the atom's motion. Experimentally, both scenarios can be realized by emission and absorption spectroscopy, with the latter producing an absorption line shape that can be derived from the emission shape via the Einstein coefficients. To keep the discussion simpler, we will discuss only the emission line.

First, the photons emitted in the direction of motion experience the classical Doppler effect, which leads to a linear shift of the transition line center with respect to p/mc. This behavior is distinct from the relativistic effects, which result in quadratic shifts with respect to p/mc. Similar to quantum time dilation, the correction arising from momentum coherence to the Doppler shift can be referred to as the *quantum Doppler shift*.

It is important to highlight that the quantum Doppler effect does not alter the total emission rate, but rather modifies the shape of the emission spectrum. In contrast, the total emission rate is influenced by quantum time dilation. The quantum Doppler effect smoothens the contrast between the two transition rate peaks associated with the two different Doppler-shifted emission lines, as illustrated in Fig.2.3(a)-(b). The distinction between the quantum and classical Doppler shifts is most prominent between the emission peaks, indicating that postselection of the atom's final momentum may further enhance the effect. A detailed quantitative analysis elucidating how the quantum Doppler effect alters the shape of the emission line is provided in Appendices2.6.1

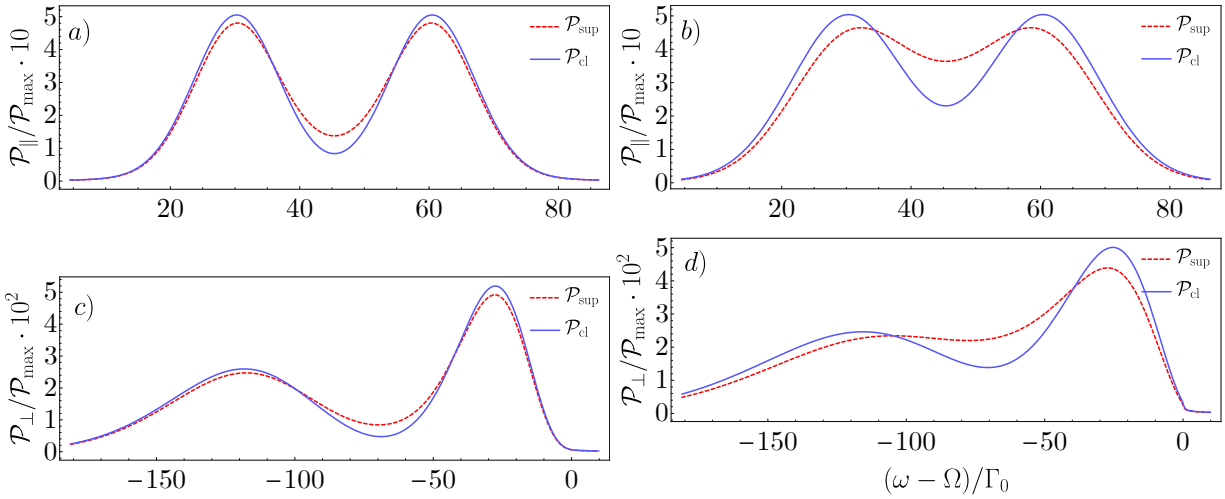

Figure 2.3: Emission line shape $\mathcal{P}(\omega)$ of the spontaneous decay of an atom that is initially prepared in a coherent superposition ($\mathcal{P}_{\rm sup}$) and in a classical mixture ($\mathcal{P}_{\rm cl}$) of two momentum wave packets sharply peaked at different momenta, $\bar{p}_1 = 2\cdot 10^{-8}mc$ and $\bar{p}_2 = 4\cdot 10^{-8}mc$ (velocities achievable for ion clocks [102] or momentum cat states [103]). The emission line is measured parallel, $\mathcal{P}_{\parallel}(\omega)$ or perpendicular, $\mathcal{P}_{\perp}(\omega)$ to the motion of the wave packets and is normalized to the maximum probability for a single stationary wave packet in a given case, $\mathcal{P}_{\rm max}$. In the former case, the dominant shift of the transition peak comes from the Doppler shift, while for the latter case—from the time dilation. Note that transverse emission in suppressed compared to parallel emission. Panels a) and b) are calculated for a broad transition, $\Omega/\Gamma_0 \approx 1.5\cdot 10^9$ (e.g. hydrogen $^2P - {}^1S$ transition), while panels c) and d) are associated with the extremely narrow $\Omega/\Gamma_0 \approx 1.5\cdot 10^{17}$ (e.g. aluminium $^1S_0 - {}^3P_0$ transition). It showcases the fact that quantum relativistic effects can be probed even for broad transitions, if the Doppler shift is affected. If the spread of the momentum wave packets is much smaller than their separation, $\Delta \ll |\bar{p}_2 - \bar{p}_1|$, coherent and incoherent cases are almost indistinguishable, with two sharp shifted peaks clearly visible (panels (a) and (c), $\Delta/mc = 6\cdot 10^{-9}$). Note the broadening of structures due to a finite spread of momentum (i.e., a homogeneous Doppler effect). If the momentum spread becomes larger and the overlap of the two wave packets increases (panels (b) and (d), $\Delta/mc = 8\cdot 10^{-9}$), interference effects become visible, manifesting direct confirmation of quantum relativistic effects in the atomic spectrum. (Both the plots and their captions are sourced from the work co-authored by the author of this dissertation [1]. This choice is made to maintain the readability and conciseness of the description.)

and 2.6.2.

In the scenario where emission occurs perpendicular to the direction of motion, the classical Doppler shift, which is linear in p/mc, is not present. Instead, the center of the transition line is shifted quadratically in p/mc, indicating the emergence of relativistic effects. These relativistic corrections, which can be measured in advanced experiments [79], are also influenced by momentum coherence in a similar fashion to the quantum Doppler shift, as depicted in Fig. 2.3(c)-(d).

2.2.3 Experimental considerations

Since de Broglie's initial prediction of wave-particle duality, atomic interferometry has made remarkable progress both conceptually and technologically [104]. Particularly, the development of large momentum beamsplitters has allowed for the creation of superpositions of atomic beams traveling along distinct trajectories [105–108]. This breakthrough has paved the way for quantum-based alternatives to classical gravimeters, gradiometers, and accelerometers [53, 109–113]. In these experimental setups, the main focus is typically on suppressing radiation losses as they can disrupt the phase relations between different arms of an interferometer [108].

In contrast to traditional approaches, our proposal aims to investigate the nonclassical behavior of center-of-mass motion through spectroscopic measurements. As demonstrated earlier, a coherent superposition of relativistic momenta has an impact on the spontaneous emission rate that goes beyond classical time dilation effects, providing a spectroscopic signature of quantum time dilation. Spectroscopic techniques offer a wide range of possibilities for observing similar quantum-relativistic effects, including stimulated absorption and emission spectroscopy, as well as methods involving the Mössbauer effect and Rydberg states [104]. Notably, atomic clocks serve as a natural testbed for relativistic theories due to their exceptional precision [102, 114, 115]. These clocks have already been utilized to observe classical time dilation at velocities as low as a few meters per second [79].

To effectively measure quantum time dilation, experimental setups must address the challenges associated with the interplay of different time scales. The lifetime of the excited atom needs to be sufficiently long to enable the creation of significant momentum separation and precise excitation of the atomic beam. However, it cannot exceed the coherence time of the center-of-mass superposition. Fortunately, advancements in phase imprinting techniques in atomic systems now allow for the engineering of initial states that maximize the quantum contribution [116, 117].

There are promising experimental configurations that offer the required level of accuracy to observe quantum-relativistic effects. Notably, quantum clocks based on aluminum ions have achieved remarkable precision surpassing leading relativistic corrections [79, 102, 115]. In these

setups, an aluminum ion is trapped in a quadrupole trap, creating an effective harmonic potential. Through advanced cooling techniques, the ion is prepared close to its zero-point motion energy. Perturbations are then applied to induce coherent-state-like oscillatory motion. Spectroscopic measurements allow for the resolution of frequency shifts due to the ion's motion at levels below $10^{-18}\Omega$, significantly surpassing the leading relativistic correction of $10^{-15}\Omega$ [102].

To observe quantum time dilation in an ion-based system, it is necessary to prepare a coherent momentum superposition, commonly referred to as a momentum Schrödinger cat state. This task itself represents a state-of-the-art challenge, but recent advancements have demonstrated significant progress in this direction [103, 109, 118, 119]. Notably, experiments have successfully prepared ytterbium ions in mesoscopic superpositions of motional states, showcasing the feasibility of creating coherent momentum superpositions in trapped ion systems [103].

In order to observe the quantum time dilation effect, it is crucial to work with an ion that exhibits a narrow transition line. This is necessary to resolve the associated frequency shift, which is second order in the average momenta of the wave packets. In practice, the mean velocity of a trapped ion, which can be easily resolved in an ion clock laboratory, is typically around $5m/s$. This corresponds to a coherent state $|\alpha\rangle$ with a magnitude of $|\alpha| \approx 12$. State-of-the-art techniques have achieved separations between coherent states of up to $|\alpha| \approx 24$ [103], demonstrating that coherent superpositions of momenta can be achieved within the spectroscopic resolution required for observing quantum time dilation effects.

In atomic clock experiments, the measurement of a transition line plays a central role. The observed difference in the shape of the transition line between a coherent superposition and an incoherent classical mixture of momentum wave packets, as illustrated in Figs. 2.3(c)-(d), would provide confirmation of the presence of quantum time dilation. This difference is most pronounced at a frequency corresponding to the average of the mean momenta of the superposed wave packets.

In optimized scenarios, the upshift of the transition probability due to momentum coherence at this specific frequency can reach up to 40%, as depicted in Fig.2.3(d). Such changes in transition line shape are routinely measured in state-of-the-art experiments involving ion clocks [79, 102].

In order to observe a clear signature of quantum time dilation, it is crucial to find the right balance between the ability to create a superposition of momentum wave packets and the precision of a given ion clock. While obstacles such as excess motion, secular motion, the quadratic Zeeman effect, and deviations from harmonic trapping [115] exist, they are typically well resolved in atomic clock experiments. However, further work is required to fully characterize these effects in the presence of relativistic momentum coherence and to determine the optimal experimental conditions for observing quantum time dilation.

Experiments involving large momentum transfer between light and atomic beams offer an

alternative approach for measuring quantum time dilation [106, 108, 120–122]. In these experiments, the limitations imposed by excited state decay can actually work to their advantage. While such experiments have not yet been realized for narrow transitions at the level of atomic clocks, there is ongoing research to develop this capability, as it is seen as a crucial component for gravitational wave detectors [121] and dark matter detectors [123]. Progress in this direction could enable the measurement of quantum time dilation in these setups, as the use of narrower transitions would enhance the spectroscopic precision.

The current momentum separation achieved in experiments involving large momentum transfer is approximately 140 $\hbar k$ for the strontium transition ${}^1S_0$ -${}^3P_1$, where k is the magnitude of the wave vector of the incident light [108]. This corresponds to a velocity difference of approximately $1m/s$ between two clouds of atoms. However, larger momentum transfers are expected in the future, with experimental proposals aiming for up to 1000 $\hbar k$ [108].

The widths of these momentum wave packets are relatively small for detecting quantum time dilation, with an rms Doppler width of 25 kHz, which corresponds to a velocity width of approximately $0.02m/s$ [108]. At present, the maximal value of quantum time dilation, which scales as $\frac{\Delta}{mc}\frac{p_2-p_1}{mc}\Gamma_0$, is still too small to be measured in these experiments. However, as the interest in large momentum transfer grows, particularly for the study of quantum gravitational effects at low energies, it may be possible to engineer a quantum time dilation experiment in the near future. This could be achieved either by increasing the momentum spread of a single wave packet or by increasing the momentum separation between different momentum wave packets.

In addition to the superposition of momentum wave packets, quantum effects can also manifest in atoms in spatial superpositions [81–84, 124]. Experimental studies in this area have been particularly useful for analyzing phase coherence in Bose-Einstein condensates interacting with light [124]. These systems provide a clean and controllable environment for studying atomic systems, allowing for fine-tuning of interactions and spatial geometry. Therefore, they offer potential platforms for experiments with coherent superpositions of momentum wave packets, such as studying non-equilibrium dynamics in double-well traps [125].

It is worth noting that, unlike ion clocks, experiments involving large momentum transfer or trapped ultracold gases have not yet achieved the necessary velocities to be sensitive to relativistic motion of particles. However, these experiments have the advantage of utilizing large ensembles of atoms, which leads to a stronger signal that scales proportionally to the number of particles involved. This can potentially compensate for the lower velocities and enable the detection of quantum-relativistic effects.

2.3 Quantum time dilation in a gravitational field

In this section, we will analyze the quantum effects in gravitational time dilation. As previously explained (see 2.1.1), relativistic quantum time dilation occurs when examining the behavior of a quantum clock experiencing time dilation. In the previous section, we studied kinematical time dilation. Now, we will focus on the impact of the superposition principle on gravitational time dilation using a simple clock: a decaying two-level atom. We aim to investigate how placing such an atom in a superposition of positions affects the quantum contributions to classical time dilation, with a particular emphasis on spontaneous emission. Our goal is to demonstrate that the emission rate of an atom in a coherent superposition of wave packets in a gravitational field significantly differs from that of an atom in a classical mixture of these packets. Moreover, we will analyze how this nonclassical effect manifests as a fractional frequency shift in the atom's internal energy. We aim to show that this quantum contribution is within the detectable range of current atomic clocks, opening up new possibilities for experimental verification of quantum effects in gravitational field. Additionally, we will investigate the influence of spatial coherence on the emission spectrum of the atom. By characterizing the spectral line shape of the emitted radiation, we aim to gain insights into how the nonclassical nature of the superposition impacts the overall dynamics of the system.

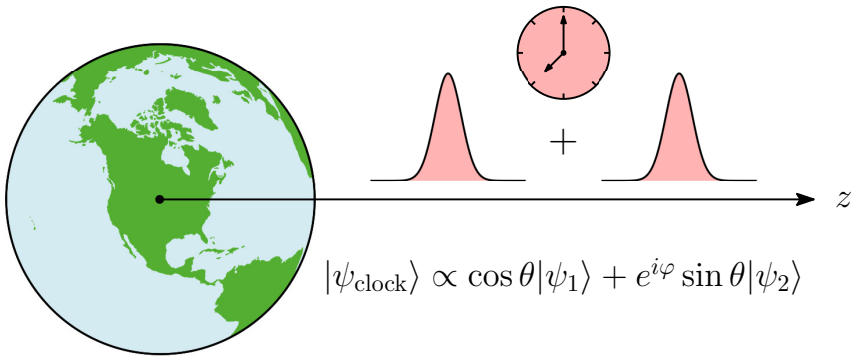

Figure 2.4: A visual depiction of the setup where a clock is positioned in a superposition of different heights within a gravitational field, as described in (2.41).

As it was shown in the previous section (see 2.2) the quantum time dilation effect arises for a clock model based on the spontaneous emission rate of an excited atom interacting with the electromagnetic field [1]. This effect leads to a frequency shift on the order of $\delta\nu/\nu_0 \sim 10^{-15}$ and is accompanied by modifications to the atomic spectrum due to the quantum coherence among the momentum wave packets. This raises the expectation that similar spectroscopic signatures would emerge when an atom is in a spatial superposition in a gravitational field, as depicted in

Fig. 2.4, experiencing a superposition of gravitational time dilation.

Indeed, an analogous nonclassical gravitational time dilation effect has been demonstrated for a quantum clock in a spatial superposition at different heights within a gravitational field [126], and has been interpreted within the formalism of quantum reference frames [127]. In particular, the average time measured by such a clock exhibits similarities to (2.3), but with γ_{Q}^{-1} representing quantum corrections arising from gravity. In a manner similar to (2.3), the average time observed by the quantum clock comprises two terms. The first term corresponds to a classical contribution associated with a statistical mixture of time dilation observed by clocks localized at the mean position of each wave packet forming the superposition. The second term represents a correction arising from the quantum nature of the clock's spatial degrees of freedom. These quantum corrections have been studied in various models, including scalar field theory [128, 129] and full quantum electromagnetism [1, 81], considering different contributions to the clock's Hamiltonian such as nonrelativistic kinetic energy [1, 54, 81, 126, 128, 129], special relativistic corrections [1, 54, 126, 128, 129], and general relativistic corrections [126]. These corrections have been shown to manifest in physically relevant observables, such as total transition rates [1, 81, 128, 129], emission line shapes [1, 81], and well-defined time observables [54, 126].

While reference [126] considers a superposition of wave packets in a gravitational field, it also incorporates additional contributions to the clock's Hamiltonian, such as nonrelativistic kinetic energy and a special relativistic correction. Consequently, quantum corrections beyond the anticipated gravitational quantum time dilation effect are observed. However, it is still possible to isolate and extract the gravitational quantum time dilation contribution (see Appendix 2.6.5). This allows us to determine the specific effect arising solely from the gravitational field, leading to the expected gravitational quantum time dilation

$$\gamma_{\mathrm{Q}}^{-1} = \frac{g}{4c^2} \frac{(z_2 - z_1)\cos\varphi \sin 4\theta}{\cos\varphi \sin 2\theta + \mathrm{e}^{\frac{(z_2-z_1)^2}{4\Delta^2}}}. \tag{2.40}$$

Here, g represents the local magnitude of the gravitational field at the reference height $z = 0$. The clock's external degrees of freedom are prepared in the state

$$|\psi_{clock}\rangle \propto \cos\theta\, |\psi_1\rangle + e^{i\varphi} \sin\theta\, |\psi_2\rangle\,, \tag{2.41}$$

where $|\psi_i\rangle$ denotes a Gaussian wave packet of width Δ localized around z_i.

The primary goal of this section is to illustrate that the quantum correction to the time observed by a clock in a spatial superposition within a gravitational field, represented as γ_{Q}^{-1}, also appears in the spontaneous emission rate of an excited atom. Additionally, we investigate the influence of spatial coherence on the atom's emission spectrum.

Our focus in this section is on the phenomenon of spontaneous emission as it serves as a suitable platform for demonstrating the quantum gravitational time dilation effect. This process exemplifies a quantum clock and provides a clean framework for analysis. However, it is important to note that the quantum gravitational time dilation effect is expected to manifest in various setups, including ions in Paul traps or many-particle systems in optical lattices.

We commence by examining the spontaneous emission rate of a two-level atom with quantized center-of-mass degrees of freedom that is placed in a spatial superposition in a gravitational field. We show that the spontaneous emission rate exhibits the nonclassical gravitational effect described in [126]. To achieve this, we quantize the electromagnetic field in an accelerating frame and use the equivalence between uniformly accelerating observers and those at rest in a gravitational field. By doing so, we establish the consistency of this nonclassical effect, characterized by γ_{Q}^{-1}, with the equivalence between the effects of a constant gravitational field and uniform acceleration. Furthermore, we provide an estimate of the magnitude of γ_{Q}^{-1} and conclude that this quantum time dilation effect is within the realm of observability with current technology. Additionally, we explore how spatial coherence in a gravitational field gives rise to distinct nonclassical features in the emission spectrum of the atom.

2.3.1 Model

The analysis of composite quantum systems in gravitational fields is of great theoretical interest, particularly as experimental investigations are entering regimes where a description based solely on adding a background Newtonian gravitational potential to the Schrödinger equation is insufficient [130, 131]. The coupling between internal and center-of-mass degrees of freedom in such systems lacks a classical analogue and gives rise to phenomena such as gravitationally induced quantum dephasing [132–134], interferometric gravitational wave detection [135], quantum tests of the classical equivalence principle [136], and proposals for quantum versions of the equivalence principle [65, 66, 137], as it was mentioned in the introduction.

In general, the inclusion of relativistic corrections in the description of light-matter interactions is typically achieved by incorporating classical physics effects, such as second-order Doppler shifts, velocity-dependent masses, and time dilation resulting from relative motion or gravitational effects. However, such approaches can be problematic as they do not guarantee self-consistency and often rely on classical concepts, such as worldlines or redshift. An example of the challenges arising in this context is the issue of spurious "friction" experienced by a moving and decaying atom [89], which was later resolved through a proper relativistic treatment [90].

For the case without gravity, the atom-field interaction has been rigorously derived up to leading relativistic order [90], while its extension to include gravity was initially accomplished

by Marzlin in 1995 [138]. However, the complete first-order post-Newtonian expansion was only recently presented by Schwartz and Giulini [139]. This derivation has also been extended to systems with non-zero total charge and used to obtain relativistic frequency shifts of ionic clocks in a rigorous manner [140].

These approaches assume that the atom is treated as a composite system and that the energy scales involved are below the threshold for pair production of any of the massive particles within the system. This assumption allows for a simplified relativistic analysis by performing quantization after placing the classical system in a fixed particle sector. For a simple atomic model consisting of two charged, massive, and moving particles interacting via Coulomb forces and embedded in electromagnetic and weak gravitational fields, the effective atomic Hamiltonian was derived in [139, 141]. Under the assumption of a heavy atom (or equivalently, that the effects due to the gravitational field dominate over the velocity spread of the atom), the Hamiltonian takes on the expected form

$$\hat{H} = Mc^2\left(1+\frac{\phi(\hat{\boldsymbol{R}})}{c^2}\right) + \hbar\Omega\left(1+\frac{\phi(\hat{\boldsymbol{R}})}{c^2}\right)|e\rangle\langle e| + \hat{H}_{\mathrm{L}} - \hat{\boldsymbol{d}}\cdot\hat{\boldsymbol{E}}, \tag{2.42}$$

where M is the mass of the atom, $\phi(\hat{\boldsymbol{R}})$ is the scalar gravitational potential in a post-Newtonian expansion, $\hat{\boldsymbol{R}}$ is the center-of-mass position of the atom, $\hbar\Omega$ is the energy gap of the relevant transition in the atom, $|e\rangle$ corresponds to the excited state of the atom, $\hat{H}_{\mathrm{L}}$ is the Hamiltonian of the electromagnetic light in the presence of the gravitational field, and the last term describes the dipole coupling between the atom and electric field $\hat{\boldsymbol{E}}$.

The dipole interaction term in the Hamiltonian retains its standard form when all the quantities involved (dipole moment $\hat{\boldsymbol{d}}$ and electric field $\hat{\boldsymbol{E}}$) are expressed as measured quantities with respect to the proper time of an observer at position $\boldsymbol{R}$ [138, 139, 142]. The second term in Equation (2.42) can be interpreted as the Hamiltonian of mass defect, which describes the relativistic coupling between the center of mass and the internal degrees of freedom [132, 133, 137, 140, 141]. Consequently, it can be absorbed into the Hamiltonian of the center of mass (the first term in Equation (2.42)), effectively correcting the mass by accounting for the mass defect.

In the case of a homogeneous gravitational field, it is advantageous to describe the system in a uniformly accelerated frame known as Rindler coordinates. This coordinate system allows us to analyze a spectroscopic measurement that is performed close to the Earth's surface, with the atomic cloud coherently delocalized in a gravitational field. By expressing the total Hamiltonian in these Rindler coordinates, we simplify the calculations and interpretation of the results. Based on the Rindler transformation introduced in 2.1.2 here we present a heuristic derivation of the total Hamiltonian in this frame.

2.3.2 The Hamiltonian

We are now set to formulate the Hamiltonian that represents a two-level atom interacting with the electromagnetic field in the context of Rindler coordinates, effectively simulating a constant gravitational field. Initially, devoid of gravitational considerations, the Hamiltonian pertaining to an atomic entity of mass M, distinguished by a ground state $|g\rangle$ and an exctited state $|e\rangle$, separated by an energy interval quantified as $\hbar\Omega$, is defined as

$$\hat{H}^{(0)} = \hat{H}^{(0)}_{\text{atom}} + \hat{H}^{(0)}_{\text{field}} + \hat{H}^{(0)}_{\text{af}}, \tag{2.43}$$

The components in this formula represent the atomic Hamiltonian, the Hamiltonian of the electromagnetic field, and the coupling between the atom and the field. These elements are all precisely defined within the framework of the Jaynes-Cummings model, as referenced in the cited literature [81, 143–145]

$$\begin{aligned} \hat{H}^{(0)}_{\text{atom}} &= Mc^2 + \hbar\Omega \left|e\right\rangle \left\langle e\right|, \\ \hat{H}^{(0)}_{\text{field}} &= \sum_{\boldsymbol{k},\lambda} \hbar\omega_{\boldsymbol{k}} \hat{a}^{\dagger}_{\boldsymbol{k},\lambda} \hat{a}_{\boldsymbol{k},\lambda}, \\ \hat{H}^{(0)}_{\text{af}} &= -\hat{\boldsymbol{d}} \cdot \hat{\boldsymbol{E}}. \end{aligned} \tag{2.44}$$

Here $\hat{a}^{\dagger}_{\boldsymbol{k},\lambda}$ and $\hat{a}_{\boldsymbol{k},\lambda}$ symbolize the creation and anihilation operators for a photon carrying a wave vector $\boldsymbol{k}$ (the eigenfrequency $\omega_{\boldsymbol{k}}$) and polarization λ. The atom's dipole operator is denoted as $\hat{\boldsymbol{d}} = \boldsymbol{d}(|e\rangle\langle g| + |g\rangle\langle e|)$, while $\hat{\boldsymbol{E}}$ represents the electric field operator. The atomic Hamiltonian has been recalibrated to include the rest mass energy of the atom.

Next, we aim to identify the corresponding terms translated into Rindler coordinates. Initially, we focus on the atom's rest energy (denoted as the $\hat{H}^{(0)}_{\text{atom}}$ term). Owing to the adoption of Rindler coordinates, the metric tensor $g_{\mu\nu}$ exhibits a diagonal structure, with the g_{00} component being the only significant element. Given coordinates $\left(x^0, x^i\right)$ and the proposed metric tensor $g_{\mu\nu} = g_{00}\delta_{\mu 0}\delta_{\nu 0} - \delta_{\mu i}\delta_{\nu j}\delta^{ij}$, we can express the Lagrangian of a free particle in classical terms as follows

$$\mathcal{L} = -H^{(0)}_{\text{atom}} \sqrt{g_{\mu\nu}\dot{x}^{\mu}\dot{x}^{\nu}} = -H^{(0)}_{\text{atom}} \sqrt{g_{00} - \dot{\bar{x}}^2}, \tag{2.45}$$

where $H^{(0)}_{\text{atom}}$ is the classical counterpart of $\hat{H}^{(0)}_{\text{atom}}$, $\dot{x}^{\mu} = \frac{dx^{\mu}}{dx^0}$, and $\dot{\bar{x}}^2 = \delta_{ij}\frac{dx^i}{dx^0}\frac{dx^j}{dx^0}$. It's important to note here that $\dot{\bar{x}}$ is not actually the velocity of the particle; rather, it represents the velocity divided by c, as the coordinate x^0 is expressed in terms of length. In the case of a static metric, namely when g_{00} is independent of x^0 (as is the case with the Rindler metric, for instance), the following quantity, which is the Hamiltonian, remains conserved, as outlined in the referenced

literature [141]

$$H_{\text{atom}} = \frac{\partial \mathcal{L}}{\partial \dot{x}^i}\dot{x}^i - \mathcal{L} = \frac{H^{(0)}_{\text{atom}} g_{00}}{\sqrt{g_{00} - \dot{\tilde{x}}^2}}. \tag{2.46}$$

In this context, $\dot{x}^i$ are treated as functions of the canonical momenta, defined as $p_i = \frac{\partial \mathcal{L}}{\partial \dot{x}^i}$. Ultimately, if the particle is stationary, its energy is defined by $H_{\text{atom}} = H^{(0)}_{\text{atom}}\sqrt{g_{00}}$. We can derive a quantum analogue of this equality by replacing the classical Hamiltonians on both sides with their respective operators, yielding $\hat{H}_{\text{atom}} = \hat{H}^{(0)}_{\text{atom}}\sqrt{g_{00}}$. In further considerations, we restrict our calculations to the stationary case.

Returning to the exploration of the Rindler metric, which is defined by $g_{00} = \left(\frac{g\chi}{c^2}\right)^2$, we incorporate a new parameter, z. This parameter represents the distance between the particle and the reference hyperbola, determined by $\chi = \frac{c^2}{g} + z$. Given this, the conserved Hamiltonian can be rewritten in the following way

$$\hat{H}_{\text{atom}} = \hat{H}^{(0)}_{\text{atom}} \frac{g\chi}{c^2} = \hat{H}^{(0)}_{\text{atom}} \left(1 + \frac{\phi(z)}{c^2}\right), \tag{2.47}$$

where $\phi(z) = gz$ is the linear gravitational potential. Consequently, the atomic energy scales by a factor of $1 + \frac{\phi(z)}{c^2}$. It is important to note that this result aligns with [140], supporting the validity of our simplified approach, which treats gravity purely kinematically using a Rindler frame of reference. We draw attention to the fact that this scaling factor emerges organically within our computations, requiring no supplemental logic. One observes that the inclusion of this factor links the internal clock degrees of freedom with the motional degrees of the atom through the term $\hat{H}^{(0)}_{\text{atom}}\phi(z)/c^2$, which accounts for the gravitational time dilation experienced by the clock [132, 133, 137, 141].

Emphasizing the general structure of the atomic Hamiltonian, it should contain a kinetic term $\boldsymbol{P}^2/2M$, where $\boldsymbol{P}$ represents the total momentum of the atom [54, 133]. Nevertheless, we posit that the atom carries considerable mass, rendering the kinetic energy pertaining to both the system's total momentum and its dispersion negligible when compared to other energy forms encapsulated by the Hamiltonian. This infers that we will dismiss any movement of the center of mass. Thus, we will discard all terms dependent on either the velocity or its derived dispersion as per [126]. We further justify this exclusion by approximating the magnitude of individual time dilation effects drawn from [126]. We undertake such an approximation in Appendix 2.6.5, demonstrating that, for the parameter range considered, corrections due to motion are indeed significantly smaller than the purely gravitational one, hence validating our simplifying assumptions.

The Hamiltonian of the electromagnetic field in curved spacetime was deduced in [78]. We only consider one (right) Rindler wedge in this context, consequently omitting all terms containing ladder operators from the left Rindler wedge. Hence, we will use the following Hamiltonian

$$\hat{H}_{\text{field}} = \sum_{\lambda=1,2} \int_{-\infty}^{\infty} \mathrm{d}k\, \hbar\omega_k \hat{b}^{\dagger R}_{k,\lambda} \hat{b}^{R}_{k,\lambda}, \tag{2.48}$$

where $\hat{b}^{\dagger R}_{k,\lambda}$ and $\hat{b}^{R}_{k,\lambda}$ are, respectively, the raising and lowering operators in the right Rindler wedge, and $k = |\boldsymbol{k}|$ is the wavenumber.

We'll proceed under the assumption that the atom is situated within an optical cavity, which permits photons to propagate solely in the direction of the gravitational field. As a result, we confine our problem to a single spatial dimension, simplifying the quantization scheme considerably, as detailed in [78].

To recast the atom-field interaction term in Rindler coordinates, we only need to express the electric field in these coordinates. The absence of the $\sqrt{g_{00}}$ term in this interaction Hamiltonian results from our use of the so-called coordinate components of the electric field [139]. To facilitate this, we define the electric field as [78]

$$\hat{\boldsymbol{E}} = i \sum_{\lambda=1,2} \int_{-\infty}^{\infty} \mathrm{d}k \sqrt{\frac{\hbar\omega_k}{4\pi\varepsilon_0}} \left[\mathrm{e}^{ik\xi} \hat{b}^{R}_{k,\lambda} + \text{ H.c. } \right] \hat{\boldsymbol{e}}_\lambda. \tag{2.49}$$

Once more, we have omitted the terms incorporating ladder operators from the left Rindler wedge. Observe that, in contrast to [78], we operate within the Schrödinger picture, resulting in the electric field operator having no explicit time dependence. By applying the rotating wave approximation, the interaction term can be simplified as follows

$$\hat{H}_{\text{af}} = -\hat{\boldsymbol{d}} \cdot \hat{\boldsymbol{E}} = -i\hbar \sum_{\lambda=1,2} g_{k,\lambda} \int_{-\infty}^{\infty} \mathrm{d}k \left(\mathrm{e}^{ik\xi} \hat{b}^{R}_{k,\lambda} |e\rangle\langle g| + \text{H.c.} \right), \tag{2.50}$$

where

$$g_{k,\lambda} = \sqrt{\frac{\omega_k}{4\pi\hbar\varepsilon_0}} (\boldsymbol{d} \cdot \hat{\boldsymbol{e}}_\lambda) \tag{2.51}$$

is the coupling constant governing the strength of the atom-light interaction.

Comparing the final Hamiltonian in Rindler coordinates

$$\hat{H} = \hat{H}_{\text{atom}} + \hat{H}_{\text{field}} + \hat{H}_{\text{af}} \tag{2.52}$$

with the simplified version of the Hamiltonian in post-Newtonian gravity (2.42), one concludes

that they are essentially the same.

As a result, our investigation focuses on spontaneous emission within a uniformly accelerating reference frame. We anticipate that the findings derived from this study will be in alignment with the outcomes from a post-Newtonian gravitational analysis.

2.3.3 Spontaneous emission in the gravitational field

Our analysis focuses on a context where a two-level atom remains stationary at a specific altitude above the ground level $z = 0$ ($\chi = \frac{c^2}{g}$), subjected to a gravitational field. By applying Rindler coordinates, the reference hyperbola is selected to be at ground level, suggesting that the time coordinate τ is equivalent to the proper time experienced by an observer at $z = 0$. We propose that the phenomena occur strictly within a single (right) Rindler wedge, a substantial distance away from the Rindler horizon.

The state of the system will be represented by a state vector that contains information about the atom's position (z), its internal state (either the ground state $|g\rangle$ or the excited state $|e\rangle$), and the number of photons in mode k with polarization λ ($n_{k,\lambda}$) within the specific Rindler wedge under consideration. Initially, the atom is in an excited state and exists in an electromagnetic vacuum

$$|\Psi(0)\rangle = \int \mathrm{d}z\, \psi(z)\, |z, e, 0\rangle\,. \tag{2.53}$$

Since the deexcitation of the atom can yield only a single photon, the overall state of the system at the Rindler time τ can be expressed as follows

$$|\Psi(\tau)\rangle = \int \mathrm{d}z\, \alpha(z,\tau)\, |z, e, 0\rangle + \sum_{\lambda=1,2} \int\int \mathrm{d}k\, \mathrm{d}z\, \beta_{k,\lambda}(z,\tau)\, |z, g, 1_{k,\lambda}\rangle\,, \tag{2.54}$$

which has been expanded in the energy eigenstates $|z, e, 0\rangle$ and $|z, g, 1_{k,\lambda}\rangle$, associated respectively with energies

$$\begin{aligned} \hbar\omega_g(z) &= Mc^2 \left(1 + \frac{gz}{c^2}\right) \\ \hbar\omega_e(z) &= \left(Mc^2 + \hbar\Omega\right) \left(1 + \frac{gz}{c^2}\right). \end{aligned} \tag{2.55}$$

The integrals over z in (2.53) and (2.54) are originally defined to range from $z = -\frac{c^2}{g}$ (where the position $\chi = 0$ corresponds to the event horizon) to $z = \infty$. However, due to the assumption that the atom is situated far from the Rindler horizon, we can extend these integrals to $z = -\infty$. It is important to note that by omitting the kinetic term $\boldsymbol{P}^2/2M$ in the Hamiltonian (2.52), we eliminate any momentum-dependent terms, allowing us to focus exclusively on the position

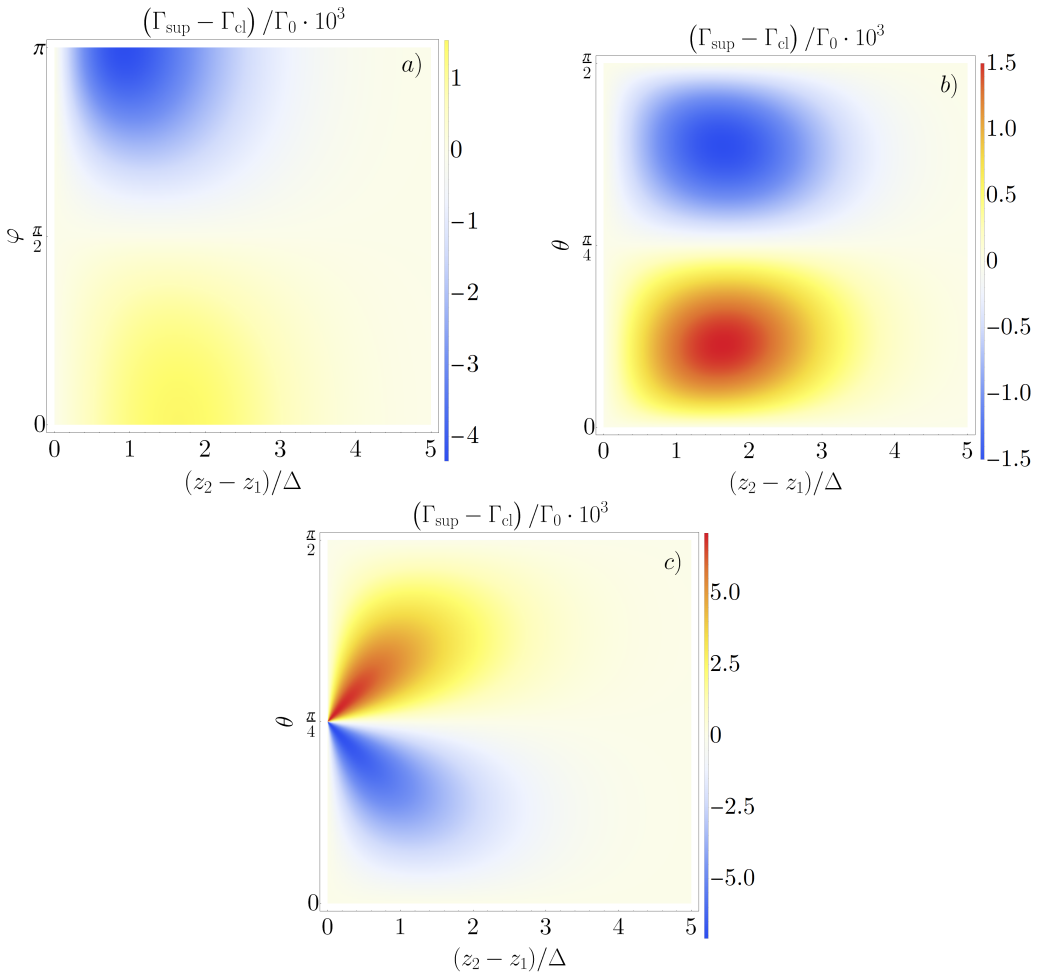

Figure 2.5: The deviation in the total emission rate between a superposition and a classical mixture of two Gaussian wave packets, centered around z_1 and z_2, as a function of the difference $z_2 - z_1$, the relative phase φ, and weight θ: (a) the wave packets have unequal weights ($\theta = \pi/8$), (b) the relative phase remains constant at $\varphi = 0$, (c) the relative phase remains constant at $\varphi = \pi$. In every graph, the dispersion of position along the z axis remains fixed at $\Delta = 0.01c^2/g$.

representation. This simplifies the analysis significantly.

The lifetime of the atom is expected to be influenced by gravitational time dilation, leading to a dependence on the initial state's distribution along the z direction. This should be reflected in the dependence of the transition rate

$$\Gamma = -\frac{\mathrm{d}}{\mathrm{d}\tau} \int \mathrm{d}z \, |\alpha(z, \tau)|^2 \tag{2.56}$$

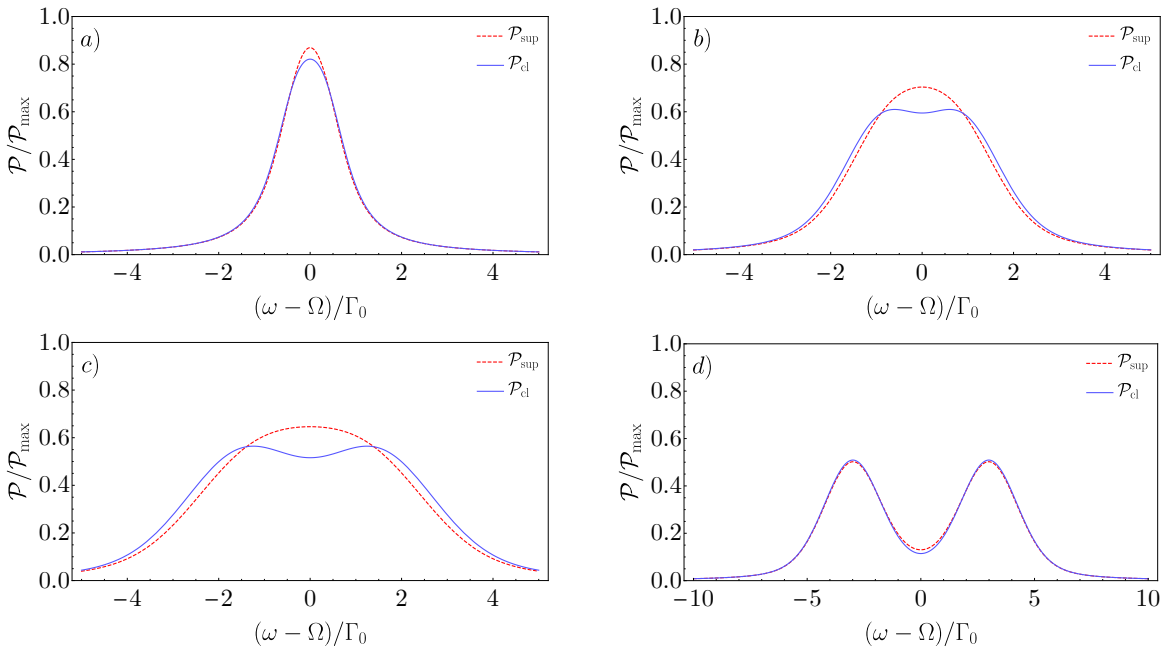

Figure 2.6: Comparison of the emission line shape, $\mathcal{P}(\omega)$, for an atom initially in a coherent superposition ($\mathcal{P}_{\rm sup}$) and in a classical mixture ($\mathcal{P}_{\rm cl}$) of wave packets situated at different heights z_1 and z_2. The transition is extremely narrow $\Omega/\Gamma_0 \approx 1.5\times10^{17}$ (as in the aluminium ${}^1S_0 - {}^1P_0$ transition). Graph (a) is calculated for $z_1 = -z_2 = -2\times10^{-18}c^2/g$, (b) for $z_1 = -z_2 = -6\times10^{-18}c^2/g$, and (c) for $z_1 = -z_2 = -10^{-17}c^2/g$. In these scenarios, the wave packets' spread equals $\Delta = (z_2 - z_1)/2$. For graph (d), with $z_1 = -z_2 = -10^{-17}c^2/g$, the spread is $\Delta = (z_2 - z_1)/4$.

on the initial wave function $\psi(z)$.

In Appendix 2.6.3, the coefficients $\alpha(z,\tau)$ and $\beta_{k,\lambda}(z,\tau)$ are determined by solving the Schrödinger equation using the Hamiltonian (2.52). The obtained expressions are as follows

$$\alpha(z,\tau) = \psi(z)\exp\left[\left(-i\omega_e(z) - \frac{\Gamma(z)}{2}\right)\tau\right], \tag{2.57}$$

$$\beta_{k,\lambda}(z,\tau) = \frac{g_{k,\lambda}\psi(z)\mathrm{e}^{-i(\omega_g(z)+k\xi)}}{\frac{1}{2}\Gamma(z) + i\left(\Omega\left(1+\frac{gz}{c^2}\right)-\omega_k\right)}\left[\mathrm{e}^{-\left(i\Omega\left(1+\frac{gz}{c^2}\right)+\frac{1}{2}\Gamma(z)\right)\tau} - \mathrm{e}^{i\omega_k\tau}\right], \tag{2.58}$$

where $\Gamma(z) = \left(1+\frac{gz}{c^2}\right)\frac{\Omega \boldsymbol{d}^2}{2\hbar c\varepsilon_0} \equiv \left(1+\frac{gz}{c^2}\right)\Gamma_0$ represents the transition rate of the atom localized at height z. Then, the overall transition rate for $\Gamma_0\tau \ll 1$ is given by (see Appendix 2.6.4)

$$\Gamma = \int \mathrm{d}z, |\psi(z)|^2\Gamma(z), \tag{2.59}$$

which represents a weighted average of transition rates at various heights. Furthermore, as demonstrated in Appendix 2.6.4, the normalized standard deviation of the transition rate related to the spatial extent is

$$\frac{\sigma_\Gamma}{\Gamma} = \frac{g\sigma_z}{c^2}, \tag{2.60}$$

where σ_z is the standard deviation of the wave function $\psi(z)$ in position space. By comparing the values of Γ for specific initial states, we can examine whether there exist any distinctions in the observed gravitational time dilation between atoms in coherent superpositions and those in classical mixtures of position wave packets. In the former case, the initial wave function is defined as follows

$$\psi_{\text{sup}}(z) = \mathcal{N}\left[\cos\theta \mathrm{e}^{-\frac{(z-z_1)^2}{2\Delta^2}} + \mathrm{e}^{i\varphi}\sin\theta \mathrm{e}^{-\frac{(z-z_2)^2}{2\Delta^2}}\right], \tag{2.61}$$

where

$$\mathcal{N} = \left[\sqrt{\pi}\Delta\left(1+\cos\varphi\sin 2\theta \mathrm{e}^{-(z_1-z_2)^2/4\Delta^2}\right)\right]^{-1/2}, \tag{2.62}$$

whereas in the second case, the probability distribution reads

$$P_{\text{cl}}(z) = \frac{1}{\sqrt{\pi}\Delta}\left[\cos^2\theta \mathrm{e}^{-\frac{(z-z_1)^2}{\Delta^2}} + \sin^2\theta \mathrm{e}^{-\frac{(z-z_2)^2}{\Delta^2}}\right]. \tag{2.63}$$

We evaluate equation (2.59) and derive the following formula for the relative difference in the total emission rate between these two cases

$$\frac{\Gamma_{\text{sup}}-\Gamma_{\text{cl}}}{\Gamma_0} = \int \mathrm{d}z\left(1+\frac{gz}{c^2}\right)\left(|\psi_{\text{sup}}(z)|^2 - P_{\text{cl}}(z)\right) = \frac{g}{4c^2}\frac{\cos\varphi\sin 4\theta(z_2-z_1)}{\cos\varphi\sin 2\theta + \mathrm{e}^{\frac{(z_2-z_1)^2}{4\Delta^2}}} = \gamma_{\text{Q}}^{-1}. \tag{2.64}$$

We now establish the universality of the obtained result. As an illustration, the work by [140] scrutinized an ion clock setup, investigating fractional frequency shifts of internal energy levels that encompassed both relativistic and gravitational effects. Following their rationale (refer to (37) in [140]), the operator representing the fractional frequency shift $\frac{\delta\hat{\nu}}{\nu_0}$ for a two-level system in a gravitational field comprises two components: the center-of-mass kinetic energy and a contribution originating from gravity. Under the approximation adopted in our study, wherein the atom's rest mass energy vastly surpasses its center-of-mass kinetic energy, this operator can be expressed as follows

$$\frac{\delta\hat{\nu}}{\nu_0} = \frac{g\hat{z}}{c^2}. \tag{2.65}$$

Consequently, the discrepancy between the anticipated fractional frequency shifts in the coherent

and incoherent scenarios is determined by the following expression

$$\left\langle \frac{\delta\hat{\nu}}{\nu_0} \right\rangle_{\text{sup}} - \left\langle \frac{\delta\hat{\nu}}{\nu_0} \right\rangle_{\text{cl}} = \gamma_{\text{Q}}^{-1}, \tag{2.66}$$

which precisely represents the contribution to the quantum gravitational time dilation effect.

It is important to note that the analysis of any specific system would involve a comprehensive examination of all experimental frequency shifts, dynamics leading to different effective conditional states, and other relevant factors. Such an analysis goes beyond the scope of this work, which primarily aims to provide a proof-of-principle description of the quantum gravitational time dilation effect.

Let us now discuss some fundamental properties of this result. Firstly, γ_{Q}^{-1} vanishes when $\theta = 0$, $\frac{\pi}{4}$, or $\frac{\pi}{2}$. If $\theta = 0$ or $\theta = \frac{\pi}{2}$, there is no difference between the coherent superposition and the classical mixture, so it is expected for (2.64) to vanish. Secondly, the quantity (2.64) also vanishes for $\varphi = \frac{\pi}{2}$. In this case, the probability distribution corresponding to the coherent superposition matches the probability distribution of the classical mixture. Finally, (2.64) also vanishes for $|z_2 - z_1| \gg \Delta$, indicating that the states are placed far apart compared to their spread, rendering the interference effects in the coherent superposition negligible. The correction (2.64) is depicted in Fig. 2.5 for fixed values of θ and φ. It is noteworthy that γ_{Q}^{-1} can be either positive or negative, depending on the relative phase φ and relative weight θ.

The quantity (2.64) may appear extremely small due to the factor $\frac{g}{c^2}(z_2 - z_1)$, which is on the order of $\sim 10^{-18}$ for a height difference of the wave packets $z_2 - z_1 \sim 1$cm. However, it is worth noting that the same factor appears in classical gravitational time dilation—the difference in time measured by two clocks situated at heights z_2 and z_1 is also proportional to $\frac{g}{c^2}(z_2 - z_1)$. Therefore, if the spread of the wave packets is comparable to the distance between them, the effect of quantum time dilation can be of the same magnitude as classical gravitational time dilation. The spatial extent of a non-Gaussian wave function introduces an additional source of uncertainty in estimating the transition rate (or fractional frequency shift) compared to the scenario of a well-localized atom. This correction to the overall uncertainty can be approximated to leading order using (2.60) and is typically reduced in common experimental setups through multiple interrogations N, making its contribution scale as $\sim \sigma_\Gamma/\sqrt{N}$. Generally, the total uncertainty depends on the specific experimental implementation and includes various contributions, such as projection noise. For instance, a detailed analysis in [140] for trapped-ion optical clocks demonstrated that the spatial extent of the Gaussian wave packet has a subleading effect on overall precision.

In the case we consider here, the variance in the spatial probability distribution of a superpo-

sition of two Gaussian wave packets is given by

$$\sigma_z^2 = \frac{1}{4}(z_2 - z_1)^2 + \frac{1}{2}\Delta^2 + \sigma_{\mathrm{Q}}^2, \tag{2.67}$$

where

$$\sigma_{\mathrm{Q}}^2 = -\frac{(z_2 - z_1)^2}{4} \frac{\cos\varphi \sin 2\theta}{e^{\frac{(z_2-z_1)^2}{4\Delta^2}} + \cos\varphi \sin 2\theta} \tag{2.68}$$

is an additional quantum correction due to the coherent superposition. As discussed earlier, the regime $|z_2 - z_1| \sim \Delta$ provides a favorable setting for observing the effect, leading to $\sigma_z \sim \Delta$ overall, and more generally,

$$\sigma_\Gamma/\Gamma \sim \gamma_{\mathrm{Q}}^{-1}. \tag{2.69}$$

This implies that if experimental accuracy allows resolving γ_{Q}^{-1}, the effect of the spatial spread of the wave function will remain a subleading factor in the total uncertainty.

Additionally, from (2.58), we can extract information about the shape of the emission line. The probability of the atom emitting a photon with energy $\omega_{\boldsymbol{k}}$ is given by

$$\mathcal{P}(\omega_k) = \lim_{\tau\to\infty} \sum_{\lambda=1,2} \int \mathrm{d}z |\beta_{k,\lambda}(z,\tau)|^2. \tag{2.70}$$

Under the assumption $\Omega/\Gamma_0 \ll 1$, we obtain the following expression for the transition line, as outlined in Appendix 2.6.4

$$\mathcal{P}(\omega_k) = \int \mathrm{d}z \frac{1}{2\pi} \frac{\left(1 + \frac{gz}{c^2}\right) |\psi(z)|^2 \Gamma_0}{\frac{1}{4}\Gamma_0^2 \left(1 + \frac{gz}{c^2}\right)^2 + \left(\Omega\left(1 + \frac{gz}{c^2}\right) - \omega_k\right)^2}. \tag{2.71}$$

Thus, $\mathcal{P}(\omega_k)$ is proportional to the height distribution $|\psi(z)|^2$ integrated with a Lorentz distribution. The transition line is gravitationally blue- or red-shifted depending on the position of the atom, as the Lorentz distribution is shifted by $\Omega \to \Omega\left(1 + \frac{gz}{c^2}\right)$. For double-peaked wave functions with peaks at significant distances from each other, the transition line splits into two. The difference in the emission line shape between a coherent superposition, (2.146), and a classical mixture, (2.148), of wave packets is shown for specific configurations of $\psi_{\mathrm{sup}}(z)$ and $P_{\mathrm{cl}}(z)$ in Fig. 2.6.

Note that the difference in the spectrum shape gradually diminishes as the difference in heights $z_2 - z_1$ decreases for a given Ω/Γ_0, and when the ratio $|z_2 - z_1|/\Delta$ increases. This behavior is consistent with the previously described behavior of γ_{Q}^{-1}, where the quantum time dilation effect vanishes when the spatial separation of the wave packets becomes significantly larger than their spatial extent.

2.4 Universality of quantum time dilation

In previous sections, we examined various approaches to the problem of quantum time dilation. We referenced the definition proposed by Smith and Ahmadi [70], which describes the effect in relation to the properties of the time operator. Then, in section 2.2 and 2.3, we demonstrated that the same effect can be observed in a real-life example of an atom interacting with an electromagnetic field. Now in this section, we will undertake a comprehensive exploration of the phenomenon of quantum time dilation and our main goal is to show to what extent quantum time dilation is a universal effect and what this concept actually means.
First let us recall the basic properties of the classical time dilation known from the theory of relativity. Classical time dilation is usually defined as the difference in measured time between two clocks that either exhibit different velocities or are exposed to varying gravitational potentials. Such effects are typically correlated with classically delineated trajectories, marked by parameters of position, momentum, and acceleration.

Nonetheless, we venture into scenarios where spatial degrees of freedom are handled through a quantum perspective, enabling the clock to exist in a coherent superposition of either two momenta or two heights. This manipulation introduces quantum amendments to the classical time dilation, known as kinematic and gravitational quantum time dilations, correspondingly.

We aim to demonstrate that akin to its classical version, kinematic quantum time dilation maintains universality across all clock mechanisms. Conversely, gravitational quantum time dilation does not uphold this trait. Our examination also intends to show that, despite both effects boiling down to the incoherent averaging of diverse classical time dilation contributions, there is an existence of an additional quantum time dilation effect, absent in the classical realm. This quantum peculiarity can be derived from higher-order corrections to the system's Hamiltonian.

In this section, we delve into the concept of universal time dilation experienced by all types of clocks - be it pendulum clocks, atomic clocks, or otherwise - when they move at a steady velocity. By "universal," we refer to the notion that the time dilation effect is independent of the unique construction of a given clock. This universality is a direct implication of the principle of relativity, stating that motion at a consistent velocity is relative. It logically follows that a situation involving two diverse clocks moving at the same speed relative to an observer is equivalent to a situation where both clocks remain stationary while the observer moves in the opposite direction. In the latter scenario, both clocks must undergo identical effects as neither holds precedence, leading to a universal time dilation independent of the clock mechanism.

However, this reasoning does not apply to motion with non-uniform velocities, resulting in non-universal time dilation effects [77]. For example, the impact of acceleration on different

types of clocks varies based on their mechanisms. A pendulum clock's reaction to acceleration differs from that of an atomic clock. Moreover, it has been shown [146–148] that no physical clock can remain unaffected by acceleration due to the Unruh effect [149], which implies the non-existence of ideal clocks. An ideal clock, as defined by the postulates of special relativity, would accurately measure proper time, which depends solely on instantaneous velocity and is not influenced by factors such as acceleration.

The study and use of an idealized clock as a theoretical model continue to be important in physics. Additionally, the relational formulation of quantum mechanics [150], particularly the investigation of the properties of quantum clocks [70, 132, 151–159], is emerging as one of the most promising approaches for understanding the nature of time.

2.4.1 Universality of kinematic quantum time dilation

In this section, we will derive the connection between the energy, denoted by E, and momentum, symbolized by $\boldsymbol{p}$, of a classical particle with point-like characteristics. The particle of mass m is positioned at $\boldsymbol{r}$ in a gravitational field $g_{\mu\nu}$ that remains stationary, and for which $g_{0i} = 0$. The expression delineating this relationship is as follows

$$E = \sqrt{g_{00}(\boldsymbol{r})}\sqrt{(mc^2)^2 - g^{ij}(\boldsymbol{r})p_i p_j c^2}. \tag{2.72}$$

To bring quantum mechanics into our classical system, we look at a general setup characterized by the Hilbert space $\mathcal{H}_{\text{cm}} \otimes \mathcal{H}_{\text{clock}}$ that includes the center-of-mass movements of the clock ($\mathcal{H}_{\text{cm}}$), and its internal parts ($\mathcal{H}_{\text{clock}}$) that are responsible for actual timekeeping. When these elements interact, it can cause the clock's "ticking" speed to change due to motion or the effect of gravity.

To get a quantum version of our model, we need to change the Hamiltonian, which describes the system's energy, into an operator based on the classical energy expression. Also, we need to link the internal degrees of freedom of our system, or "clock," with its external motion. So, instead of just the mass of the clock, we consider the energy of the clock's internal structure, thanks to the idea from relativity theory that energy and mass are equivalent.

So, if we let $\hat{H}_{\text{clock}}$ stand for the Hamiltonian of the clock's internal structure and $\hat{H}$ represent the total Hamiltonian, the first step in "quantizing" the relation (2.72) gives us this expression for the total Hamiltonian

$$\hat{H} = \sqrt{g_{00}(\hat{\boldsymbol{r}})}\sqrt{\left(mc^2 + \hat{H}_{\text{clock}}\right)^2 - g^{ij}(\hat{\boldsymbol{r}})\hat{p}_i\hat{p}_j c^2}, \tag{2.73}$$

Throughout this paper, we will employ the Weyl symmetric ordering for the position and mo-

mentum operators $\hat{\boldsymbol{r}}$ and $\hat{\boldsymbol{p}}$, which function in the Hilbert space $\mathcal{H}_{\text{cm}}$. This is symbolized by $\overset{\text{W}}{:}\cdot\overset{\text{W}}{:}$ in our discussions. Nevertheless, other methodologies for ordering are also viable. For instance, by using an order parameter, denoted as λ, we can define this alternative ordering as $:\hat{p}\hat{x}:\equiv\lambda\hat{p}\hat{x}+(1-\lambda)\hat{x}\hat{p}$. In the quantum description of physical systems, determining the precise sequence of non-commuting operators is not predetermined. While the practice of using Weyl's ordering is widespread, it's important to stress that this choice is arbitrary and lacks a concrete physical justification. Consequently, we have initiated an investigation to ascertain whether a different definition would uphold consistent results within the context of our model.

In the subsequent section, we will be addressing the more general scenario where both kinematic and gravitational effects are significant. However, in this section, we focus on the kinematic time dilation where the gravitational field is absent, allowing us to substitute $g_{00}(\hat{\boldsymbol{r}})\to 1$ and $g^{ij}(\hat{\boldsymbol{r}})\to-\delta^{ij}$ into equation (2.73). Our investigation will be centered on determining if quantum time dilation is a universal phenomenon. Universality, in the context of classical clocks, implies that the magnitude of time dilation is independent of the clock's underlying mechanism. When considering quantum clocks, this universality is defined by the independence of the time dilation effect from the Hilbert space $\mathcal{H}_{\text{clock}}$ or the clock's internal Hamiltonian $\hat{H}_{\text{clock}}$.

In the subsequent discussion, we will solely consider the interaction part of the dynamics, since local terms are not relevant for discussing time-dilation effects and can always be effectively eliminated by shifting to the interaction picture description. Let's consider the clock prepared in the initial state as follows

$$|\Psi(0)\rangle=\int \mathrm{d}^3\boldsymbol{p},\psi(\boldsymbol{p})\,|\boldsymbol{p}\rangle\otimes|0\rangle\,, \tag{2.74}$$

where $|\boldsymbol{p}\rangle\in\mathcal{H}_{\text{cm}}$ denotes a well-defined momentum state, $\psi(\boldsymbol{p})$ represents the momentum representation of the normalized wave function, and $|0\rangle\in\mathcal{H}_{\text{clock}}$ is an initial internal state of the clock. When relativistic effects are considered as corrections to nonrelativistic dynamics, and $\langle\hat{H}_{\text{clock}}\rangle,|\langle c\hat{p}\rangle|\ll mc^2$ [139], the expanded Hamiltonian (2.73) can be approximated as

$$\hat{H}\approx\frac{\hat{\boldsymbol{p}}^2}{2m}-\frac{\hat{\boldsymbol{p}}^4}{8m^3c^2}+\hat{H}_{\text{clock}}\left(1-\frac{\hat{\boldsymbol{p}}^2}{2m^2c^2}\right), \tag{2.75}$$

where the term multiplying $\hat{H}_{\text{clock}}$ is the leading term of the Lorentz factor responsible for classical time dilation. The dynamics are governed by the Schrödinger equation, $i\hbar\partial_t\,|\Psi(t)\rangle=\hat{H}\,|\Psi(t)\rangle$, without explicitly requiring the covariant Tomonaga-Schwinger equation [160]. The wave function can be expressed as

$$|\Psi(t)\rangle=\int \mathrm{d}^3\boldsymbol{p}\,\psi(\boldsymbol{p})\,|\boldsymbol{p}\rangle\otimes|\phi(\boldsymbol{p},t)\rangle\,, \tag{2.76}$$

where all time dependence is absorbed into $|\phi(\boldsymbol{p},t)\rangle$, which is the evolved internal state of the clock associated with the motional state $|\boldsymbol{p}\rangle$. The parameter t represents the physical time governing the system's evolution. However, our interest lies in the operational definition of time, corresponding to the measurement outcome τ performed on the clock's internal degrees of freedom.

The distinction between physical time and clock-measured time is crucial, as the aim of this work is to investigate the relativistic properties of time in quantum systems that act as clocks. Due to the Pauli objection [161, 162], constructing a time operator within quantum mechanics is not feasible. Thus, the authors adopt an operational definition of time, essentially positing that time is what can be measured by a clock—a physical system undergoing some form of evolution.

Consequently, the clock undergoes an evolution described by the passage of time t, which remains inaccessible to an observer who can only measure time through a quantum clock. The measurement of the quantum clock is the focus of our investigation. Let us denote the set of measurement operators providing the time readout τ as $\{\hat{E}(\tau)\}$. This measurement is performed on a clock system to estimate the value of time according to the operational definition, which seeks to determine the time value without directly relying on any quantum measurement form.

The goal is to achieve the most accurate time estimation using the operational definition, without explicit reference to a specific quantum measurement. However, the distribution $\langle\phi(\boldsymbol{p},t)|\,\hat{E}(\tau)\,|\phi(\boldsymbol{p},t)\rangle$ should be peaked at τ and serve as an unbiased estimator for classical time dilation

$$\int \langle\phi(\boldsymbol{p},t)|\,\hat{E}(\tau)\,|\phi(\boldsymbol{p},t)\rangle\ \mathrm{d}\tau \approx t\left(1-\frac{\boldsymbol{p}^2}{2m^2c^2}\right). \tag{2.77}$$

Constructing such operators in the context of quantum metrology has been an ongoing research topic [70, 163–169]. As the measurement is performed solely on the internal degrees of freedom, we can trace out the center-of-mass degrees of freedom and use the reduced density matrix $\hat{\rho}_{\mathrm{clock}}(t) \equiv \mathrm{Tr}_{\mathrm{cm}}\hat{\rho}(t)$, representing the clock's internal state

$$\hat{\rho}_{\mathrm{clock}}(t) = \int \mathrm{d}^3\boldsymbol{p}\,|\psi(\boldsymbol{p})|^2\,|\phi(\boldsymbol{p},t)\rangle\,\langle\phi(\boldsymbol{p},t)|\,. \tag{2.78}$$

Thus, the probability $\mathcal{P}(\tau)$ to obtain the measurement result τ is given by

$$\begin{aligned}\mathcal{P}(\tau) &= \mathrm{Tr}\left(\hat{E}(\tau)\hat{\rho}_{\mathrm{clock}}(t)\right)\\ &= \int \mathrm{d}^3\boldsymbol{p}\,|\psi(\boldsymbol{p})|^2\,\langle\phi(\boldsymbol{p},t)|\,\hat{E}(\tau)\,|\phi(\boldsymbol{p},t)\rangle\,.\end{aligned} \tag{2.79}$$

From this expression, it is clear that the phase of the momentum representation wave function $\psi(\boldsymbol{p})$ does not influence the clock's readouts. Only the probability density of the wave function

matters. Therefore, instead of using the initial state of the system given by (2.74), we could use a density matrix involving a classical mixture of definite momentum states

$$\hat{\rho}(0) = \int \mathrm{d}^3\boldsymbol{p}\, |\psi(\boldsymbol{p})|^2\, |\boldsymbol{p}\rangle \langle \boldsymbol{p}| \otimes |0\rangle \langle 0|\,, \tag{2.80}$$

which is a state with erased coherences between different momentum eigenstates in (2.74), and the result (2.79) would remain identical. In other words, the effective time dilation of the clock is equal to a weighted average, with weights $|\psi(\boldsymbol{p})|^2$, of time dilations of clocks characterized by well-defined momenta. These classical time dilations are universal, i.e., independent of the clock mechanism, so the weighted average (2.79) of universal time dilations must also be universal. This argument completes the proof of the universality of kinematic quantum time dilation for the case of an arbitrary quantum state of the clock $\psi(\boldsymbol{p})$.

2.4.2 Quantum time dilation for classical states

Throughout the preceding section, we presented an analysis of time measurement employing a quantum clock for a given quantum state described by a wave function. This provides an excellent opportunity to delve into the fundamental aspects of the quantum time dilation effect and contemplate whether it can be generalized in a manner that cannot be mimicked by classical states alone.

Our elementary analysis offers a fresh perspective on the interpretation of quantum time dilation studied in previous works [1, 54]. It is important to note that the result (2.79), which characterizes quantum time dilation, can be obtained using the state (2.80). This state represents a classical mixture of definite momentum states, implying that it can be considered completely classical. This raises a question regarding the nature of the "quantum" time dilation described by (2.79) and explored in [1, 54]. To gain a better understanding, let us revisit the reasoning presented in those works.

Consider two different motional states of the clock, $|\psi_1\rangle$ and $|\psi_2\rangle \in \mathcal{H}_{\mathrm{cm}}$, represented by Gaussian wave packets that correspond to the clock traveling at two distinct average speeds. Now, let the initial clock state be a coherent superposition given by

$$|\psi\rangle = \mathcal{N}\left(\cos\theta\, |\psi_1\rangle + \sin\theta e^{i\varphi}\, |\psi_2\rangle\right) \in \mathcal{H}_{\mathrm{cm}}, \tag{2.81}$$

where θ represents the respective weights and φ is the relative phase between the superposed states. It is important to introduce the normalization factor $\mathcal{N}$ when dealing with nonorthogonal superposed states.

The momentum representation wave function $\psi(\boldsymbol{p}) \equiv \langle \boldsymbol{p} | \psi \rangle$ for the state (2.81) can be expressed as

$$\psi(\boldsymbol{p}) = \mathcal{N}\left(\cos\theta, \psi_1(\boldsymbol{p}) + \sin\theta e^{i\varphi}, \psi_2(\boldsymbol{p})\right), \tag{2.82}$$

If $\psi_1(\boldsymbol{p})$ and $\psi_2(\boldsymbol{p})$ are nonorthogonal, it is clear that variations in the phase φ will impact the corresponding momentum density distribution $|\psi(\boldsymbol{p})|^2$ appearing in (2.79). As a result, the effective time dilation will depend on the phase φ. This dependence on the relative phase φ is considered a signature of the quantum nature of the observed time dilation effect.

To quantify the magnitude of the effect, the authors of [1, 54] compute the difference between the clock rate evaluated for the initial superposed state $|\psi\rangle \otimes |0\rangle$ and its classical counterpart, which is evaluated for a classical mixture of the two wave packets $|\psi_1\rangle$ and $|\psi_2\rangle$

$$\hat{\rho}(0) = \mathcal{N}'\left(\cos^2\theta\, |\psi_1\rangle\langle\psi_1| + \sin^2\theta\, |\psi_2\rangle\langle\psi_2|\right) \otimes |0\rangle\langle 0|. \tag{2.83}$$

The resulting difference quantifies the amount of quantum time dilation. Therefore, this quantum time dilation can be viewed as an effect of state discrimination procedure between a quantum-superposed clock state (2.81) and a classical mixture (2.83).

It is worth noting that an alternative approach would be to consider the classical counterpart as (2.80) instead of (2.83). In this case, the difference in clock rates would always be zero. This is because the expression (2.79) depends solely on the diagonal elements of the density matrix in momentum space. Such a construction would result in no quantum contribution to classical time dilation. Therefore, the magnitude of quantum time dilation relies on an arbitrary convention regarding which classical state should be chosen as a reference.

This ambiguity arises from the nonorthogonality of the wave packets $\psi_1(\boldsymbol{p})$ and $\psi_2(\boldsymbol{p})$. This ambiguity could be eliminated by using orthogonal wave packets. However, in that case, no quantum time dilation would be observed. Unlike the double-slit experiment, which reveals the quantum nature of interference between orthogonal states, quantum time dilation crucially depends on the nonorthogonality of the modes $\psi_1(\boldsymbol{p})$ and $\psi_2(\boldsymbol{p})$. It is evident that one can decompose the initial state (2.81) in such a way that the two terms in the decomposition correspond to overlapping wave functions. Therefore, adding a relative phase between these terms leads to a change in the momentum distribution appearing in (2.79). However, this should be viewed more as an artifact resulting from choosing a specific decomposition of the state rather than a manifestation of a fundamental effect.

Let us delve deeper and explore a discrimination procedure that involves a superposition and a mixture of two states, resulting in quantum time dilation, but with an alternative pair of states. To illustrate this, consider the example of two coherent states $|\alpha\rangle$, $|\beta\rangle \in \mathcal{H}_{\text{cm}}$ of the

center-of-mass degree of freedom. Decompose $|\alpha\rangle$ in a basis $\frac{1}{\sqrt{2}}(|\alpha\rangle \pm |\beta\rangle)$ as follows

$$|\alpha\rangle = \frac{1}{2}(|\alpha\rangle + |\beta\rangle) + \frac{1}{2}(|\alpha\rangle - |\beta\rangle). \tag{2.84}$$

According to the aforementioned discrimination procedure, the classical counterpart of the state (2.84) in this case is defined as the following classical mixture

$$\hat{\varrho} \equiv \frac{\mathcal{N}}{2}(|\alpha\rangle + |\beta\rangle)(\langle\alpha| + \langle\beta|) + \frac{\mathcal{N}}{2}(|\alpha\rangle - |\beta\rangle)(\langle\alpha| - \langle\beta|) = \mathcal{N}(|\alpha\rangle\langle\alpha| + |\beta\rangle\langle\beta|). \tag{2.85}$$

In general, both states have different momentum distributions, and therefore, the measure used to quantify the amount of quantum time dilation for the state (2.81) yields a nonzero value for the classical state (2.84).

2.4.3 Combined kinematic and gravitational quantum time dilation

In previous sections, we explored how kinematic time dilation affects a clock moving along a superposition of trajectories. Our analysis was extensive, made possible by the straightforward form of the interaction Hamiltonian. This simplicity highlighted the momentum eigenbasis within the $\mathcal{H}_{\text{cm}}$ space, resulting in the clock's reduced density matrix becoming a mixed state of different clock states. Each state corresponded to a distinct momentum of the center-of-mass degree of freedom (2.78). Our current endeavor is to adjust our perspective and evaluate a situation that includes both kinematic and gravitational time dilation. In this situation, the interaction Hamiltonian does not distinguish a specific basis in the $\mathcal{H}_{\text{cm}}$ space.

Consider a scenario with a point-like clock positioned in a Schwarzschild gravitational field at a specific position $\boldsymbol{r}_0$. Near the clock, the Schwarzschild metric, expressed through the local proper time at the position $\boldsymbol{r}_0$ and the proper length $\boldsymbol{r}$, can be approximated in a post-Newtonian framework as derived in 2.1.3

$$\begin{aligned} g_{00}(\boldsymbol{r}) &\approx \left(1 + \frac{2GM}{r_0c^2} + \frac{2G^2M^2}{r_0^2c^4}\right)\left(1 - \frac{2GM}{rc^2} + \frac{2G^2M^2}{r^2c^4}\right), \\ g_{ij}(\boldsymbol{r}) &\approx -\delta_{ij}\left(1 + \frac{2GM}{rc^2} + \frac{3G^2M^2}{2r^2c^4}\right). \end{aligned} \tag{2.86}$$

The expansions (2.86) are now incorporated into the Hamiltonian (2.73), and we choose the x axis to align with the local gravitational field at $\boldsymbol{r}_0$. This leads us to the subsequent approximation of the total Hamiltonian of the clock (2.73)

$$\hat{H} \approx \hat{H}_{\text{clock}} + \hat{H}_{\text{cm}}(\hat{\boldsymbol{r}}, \hat{\boldsymbol{p}}) + \hat{H}_{\text{int}}. \tag{2.87}$$

Here, the individual terms are derived by dismissing higher-order contributions to the total energy, which are significantly smaller than the rest energy mc^2.
More specifically, $\langle \hat{H}_{\text{clock}} \rangle, |\langle c\hat{p} \rangle|, |\langle mg\hat{x} \rangle|, mgr_0, \frac{GMm}{r_0} \ll mc^2$. We find

$$\hat{H}_{\text{cm}} \equiv mc^2 + \frac{\hat{p}^2}{2m} + mg\hat{x} + \frac{3g}{2mc^2} \overset{\text{W}}{:} \hat{p}^2\hat{x} \overset{\text{W}}{:}, \hat{H}_{\text{int}} \equiv \hat{H}_{\text{clock}} \underbrace{\left(-\frac{\hat{p}^2}{2m^2c^2} + \frac{g\hat{x}}{c^2} - \frac{3g}{2m^2c^4} \overset{\text{W}}{:} \hat{p}^2\hat{x} \overset{\text{W}}{:} \right)}_{\hat{V}_1}$$
$$+ \hat{H}^2_{\text{clock}} \underbrace{\left(\frac{\hat{p}^2}{2m^3c^4} + \frac{3g}{2m^3c^6} \overset{\text{W}}{:} \hat{p}^2\hat{x} \overset{\text{W}}{:} \right)}_{\hat{V}_2}, \tag{2.88}$$

where $g \equiv GM/r_0^2$ denotes the gravitational acceleration at $\boldsymbol{r}_0$, $\hat{x}$ is the position operator in the direction of the gravitational field at $\boldsymbol{r}_0$ measuring the proper distance from that point, and the symbol $\overset{\text{W}}{:} \cdot \overset{\text{W}}{:}$ signifies Weyl's symmetric ordering. In relation to the parameter λ introduced in the prior section, for the most general form of the ordering operator, it can be stated that Weyl's ordering is consistent with $\lambda = 1/2$.

In order to understand the evolution of the system, we apply the von Neumann equation for the density matrix $\hat{\rho}^I(t)$ of the total system in the interaction picture (represented by the I superscript), wherein the interaction Hamiltonian is expressed by
$\hat{H}^I_{\text{int}}(t) \equiv e^{\frac{i}{\hbar}(\hat{H}_{\text{clock}} + \hat{H}_{\text{cm}})t} \hat{H}_{\text{int}} e^{-\frac{i}{\hbar}(\hat{H}_{\text{clock}} + \hat{H}_{\text{cm}})t}$

$$i\hbar \frac{\partial}{\partial t} \hat{\rho}^I(t) = \left[\hat{H}^I_{\text{int}}(t), \hat{\rho}^I(t) \right]. \tag{2.89}$$

The approximate solution to (2.89) can be found in the first order of the Dyson series by assuming that the initial state of the system shows no correlations between the kinematic and internal degrees of freedom: $\hat{\rho}(0) \equiv \hat{\rho}_{\text{cm}}(0) \otimes \hat{\rho}_{\text{clock}}(0)$. After reverting to the Schrödinger picture we can compute the reduced density matrix of the clock's internal state by tracing out the kinematic degrees of freedom $\hat{\rho}_{\text{clock}}(t) \equiv \text{Tr}_{\text{cm}}\, \hat{\rho}(t)$. The calculations are detailed in Appendix 2.6.6, and the final result is given by

$$\hat{\rho}_{\text{clock}}(t) \approx \hat{\rho}^0_{\text{clock}}(t) - \frac{i}{\hbar} \left(\left[\hat{H}_{\text{clock}}, \hat{\rho}^0_{\text{clock}}(t) \right] \text{Tr} \left(\hat{V}1 \hat{\rho}_{\text{cm}}(0) \right) + \left[\hat{H}^2_{\text{clock}}, \hat{\rho}^0_{\text{clock}}(t) \right] \text{Tr} \left(\hat{V}2 \hat{\rho}_{\text{cm}}(0) \right) \right) t. \tag{2.90}$$

Here, $\hat{\rho}^0_{\text{clock}}(t) \equiv e^{-\frac{i}{\hbar}\hat{H}_{\text{clock}}t} \hat{\rho}_{\text{clock}}(0) e^{\frac{i}{\hbar}\hat{H}_{\text{clock}}t}$ describes the evolution of the clock's internal degrees of freedom in the absence of coupling with the kinematic degrees of freedom. Let us compare (2.90) with the previously obtained special case (2.78) involving only the kinematic time dilation.

In that specific case, we could express the result as a classical mixture of final states corresponding to definite values of momentum. Similarly, for purely gravitational time dilation without kinematic effects, the result (2.94) involves a mixture of final states corresponding to definite positions of the clock. Our general result (2.90) surpasses that. Note that the terms involving the operator $\hat{V}_1$ contain elements that mix up position and momentum operators $\frac{3g}{2m^2c^4} \overset{\text{W}}{:} \hat{p}^2\hat{x} \overset{\text{W}}{:}$, as seen in (2.88). For this reason, our general result (2.90) cannot be replicated using a classical mixture of definite position or momentum final states. The terms appearing in (2.90) have the form

$$\begin{aligned} \mathrm{Tr}\left[\overset{\text{W}}{:} \hat{p}^2\hat{x} \overset{\text{W}}{:} \hat{\rho}_{\text{cm}}(0)\right] &= \frac{1}{3}\,\mathrm{Tr}\left[\left(\hat{p}^2\hat{x} + \hat{p}\hat{x}\hat{p} + \hat{x}\hat{p}^2\right)\hat{\rho}_{\text{cm}}(0)\right] \\ &= \int \mathrm{d}p\mathrm{d}x\mathrm{d}x' \; \frac{3xp^2 - i\hbar p}{6\pi\hbar} e^{-\frac{i}{\hbar}p(x-x')} \langle x|\hat{\rho}_{\text{cm}}(0)|x'\rangle. \end{aligned} \tag{2.91}$$

The introduction of more advanced terms in our calculations has led to the discovery of a relativistic modification in the evolution of a clock. This modification is associated with the combined distributions of position and momentum operators, which makes our results more encompassing than those presented in the earlier sections. In general, there is no classical equivalent to the state referenced as (2.80) that could generate non-classical components of the form (2.91). These components depend on both position and momentum, which do not commute, meaning a straightforward substitution of quantum averaging with classical weighted averaging over states with well-defined positions and momentum is not feasible.

Importantly, the result expressed in (2.91) is influenced by the type of ordering applied in the Hamiltonian (2.88). Different orderings, other than Weyl's ordering, may result in varying outcomes. Consequently, making direct measurements of these higher-order terms can be a method to validate the types of ordering employed in specific physical systems.

This novel contribution of ours is not yet documented in the existing literature on quantum effects due to gravitational time dilation [2, 126, 159, 170–172]. We achieved it by transcending the limitations of second-order perturbation theory and delving into more complex, higher-order terms as seen in (2.90). The term proportional to (2.91) has no classical parallel and can thus be recognized as a uniquely quantum effect.

Finally, this work demonstrates that the inclusion of both kinematic and gravitational degrees of freedom can reveal new quantum effects that do not hinge on a particular discrimination procedure. This underscores the significance of the noncommutative nature of the position and momentum operators in these phenomena.

2.4.4 Nonuniversality of gravitational quantum time dilation

Let us now consider a scheme involving gravitational time dilation only. For this purpose, we will utilize the expansion (2.88) in the limit of high values of m, where the kinematic degrees of freedom become negligible, resulting in the omission of momentum-dependent terms

$$\hat{H}_{\mathrm{cm}} \approx mc^2 + mg\hat{x}, \tag{2.92}$$

$$\hat{H}_{\mathrm{int}} \approx \hat{H}_{\mathrm{clock}} \frac{g\hat{x}}{c^2}. \tag{2.93}$$

This approach leads to a gravitational analog of (2.78), where the momentum $\hat{\boldsymbol{p}}$ is replaced by the position $\hat{\boldsymbol{r}}$ of the clock in a gravitational field

$$\hat{\rho}'_{\mathrm{clock}}(t) = \int \mathrm{d}^3\boldsymbol{r}\, |\psi'(\boldsymbol{r})|^2 \left|\phi'(\boldsymbol{r},t)\right\rangle \left\langle\phi'(\boldsymbol{r},t)\right|, \tag{2.94}$$

where $\psi'(\boldsymbol{r}) \equiv \langle \boldsymbol{r}|\psi\rangle$. This suggests that the effective time dilation is equivalent to the classical weighted average of time dilations measured by clocks distributed in space according to the probability distribution $|\psi'(\boldsymbol{r})|^2$. At first glance, the analogy between (2.78) and (2.94), and thus between kinematic and gravitational time dilation, appears complete, implying that gravitational quantum time dilation should also be universal. However, this conclusion is incorrect. A critical assumption in our derivation is that the clock Hamiltonian $\hat{H}_{\mathrm{clock}}$ in (2.87) does not depend on $\hat{\boldsymbol{p}}$ and $\hat{\boldsymbol{r}}$. The independence of $\hat{\boldsymbol{p}}$ follows directly from the Lorentz invariance of the theory, as the clock's Hamiltonian must be identical in all inertial frames. However, the independence from $\hat{\boldsymbol{r}}$, implying that the clock's mechanism is unaffected by the gravitational field's strength, is not valid.

Specifically, it is established that every physical system responds differently to proper acceleration: for example, a pendulum clock and an atomic clock will be affected differently by acceleration. It has been shown that no "ideal clock," which is entirely insensitive to proper acceleration, can exist [146–148]. Similarly, due to the equivalence principle, where the effects of proper acceleration are indistinguishable from gravitational effects, no realistic clock can measure proper time accurately in a gravitational field. Therefore, deviations from the standard gravitational time dilation formula (based on $\sqrt{g_{00}}$ for a static field) can be expected for any realistic system. The rate of a pendulum clock or any other time-measuring device thus depends on the gravitational field's strength, reflecting that the clock's design inherently depends on proper acceleration. This effect has been demonstrated even for the most robust clocks in existence: unstable elementary particles [146–148]. Consequently, even classical gravitational time dilation cannot be universal, let alone its quantum-superposed counterpart. The fundamental reason for

this is that only motion with constant velocity is relative; acceleration is absolute, not relative, and the principle of relativity does not apply to accelerated motions. Therefore, the effect of acceleration or gravity on a clock's rate must fundamentally depend on the clock's mechanism.

2.5 Conlusions of the chapter

In the section 2.2, we presented a spectroscopic signature of quantum time dilation, observed in the spontaneous emission rate or lifetime of an excited atom moving in a superposition of relativistic momentum wave packets. Our analysis shows that the total transition rate is significantly influenced by the momentum coherence in the atom's center-of-mass state. Interestingly, the quantum contribution to the observed time dilation can be either positive or negative, depending on the relative phase between the superposed momentum states. Importantly, these quantum effects are within the reach of existing experimental setups, such as optical clocks [79, 105–108].

Furthermore, we observed a notable correspondence between quantum time dilation in the atomic lifetime, as described by (2.37), and quantum time dilation observed by an ideal clock in a different physical system [54, 157]. This result indicates the universality of quantum time dilation, suggesting that it affects all clocks similarly, regardless of their underlying mechanisms.

The effects of quantum time dilation on atomic spectra complement the growing body of research on relativistic clock interferometry. While clock interferometry explores the effects of clock superpositions experiencing different proper times due to relativistic effects, our spectroscopic approach focuses on the role of coherence across relativistic momentum wave packets. By probing proper time superpositions in this regime, our proposal offers a unique perspective on the interplay between quantum theory and relativity.

We further investigated the presence of a quantum Doppler effect arising when an atom's center-of-mass is in a superposition of momentum wave packets. This effect manifests in the shape of the emission spectrum, resulting in a modification of its structure. Specifically, the quantum Doppler effect smooths the contrast between the characteristic Doppler-shifted peaks typically observed in the spectrum.

In the following section 2.3, we have presented an example of a realistic scenario where quantum time dilation in a gravitational field is expected to occur. By analyzing the spontaneous emission process of a two-level atom at rest in an external gravitational field, modeled as an accelerated frame of reference according to the equivalence principle, we demonstrated that the atom's spontaneous emission rate depends on its wave function in position space. Specifically, this rate is nontrivially influenced by the presence of spatial coherence in the atom's center-of-mass state. Our findings align with those of [126] for a realistic clock model, further demonstrating that quantum time dilation occurs in practical scenarios. This provides additional evidence that quantum time dilation is not merely a theoretical construct but can be observed in real-world situations. Moreover, by utilizing the equivalence principle to describe the effect of gravity on the clock, we arrived at the same conclusions as would be expected from a post-Newtonian analysis.

This suggests that our findings can be interpreted as a confirmation of the equivalence principle applied to quantum systems.

Our analysis leads to a method for detecting the effect of quantum time dilation: placing a decaying particle in a superposition of heights and monitoring the dependence of the decay rate on the particle's initial state. Similarly, a spectroscopic method for detecting quantum time dilation involves setting a clock (either ionic or atomic) in a superposition of heights and measuring either the spontaneous decay or, more commonly, the fractional frequency shift. According to our results, the coherence effect should become noticeable when the spread of two position wave packets is comparable to the distance between them. The quantum correction to classical time dilation can be of the same order of magnitude as the classical gravitational time dilation factor for appropriately chosen state parameters. Therefore, if gravitational time dilation can be detected for such distances, the quantum time dilation effect should also be observable.

Typically, experimental measurements of gravitational time dilation involve comparing two clocks at different heights, as demonstrated in tabletop experiments [173], flight-based clocks [174], or clocks separated by hundreds of meters [175]. For these approaches, future advancements are already planned: satellite-based experiments that will improve accuracy by orders of magnitude [176, 177]. Recent developments with optical lattice clocks have also shown that resolving the gravitational redshift within a single sample on a sub-millimeter scale is possible [178, 179]. Specifically, a frequency change consistent with the linear gravitational field was measured along a system consisting of 100,000 strontium atoms [178], where the atoms were uncorrelated to suppress corrections due to quantum coherence across the sample.

We have shown that for an optimally prepared state in the simplest spectroscopic system, the gravitational quantum time dilation effect is comparable to the gravitational redshift induced by a millimeter-sized height difference near Earth's surface. In the most favorable setup with two overlapping wave packets of opposite relative phase, the change in the total emission rate scales as $\frac{g\Delta}{4c^2}\Gamma_0$, where Δ is the spatial spread of the wave packets. In the case of micrometer-scale superpositions [180–183], this results in a 10^{-23} change in the total emission rate, or equivalently, the same change in the fractional frequency shift. Although current measurements of atomic lifetimes and emission rates lack the precision to detect such a correction—they are typically determined up to tenths of a percent [184–186]—the correction to the fractional frequency shift is just below the precision of state-of-the-art measurements, which are sensitive to gravitational time dilation on millimeter scales [178, 179, 187, 188]. Increasing the scale of the spatial superposition of the atomic species from micrometers to millimeters would result in a correction of the order of 10^{-20}, which is within the reach of current technology. Given recent experimental progress with optical clocks, the natural next step is to devise a scheme to prepare the optimal superposition state in this setting and examine how to unambiguously observe quantum time di-

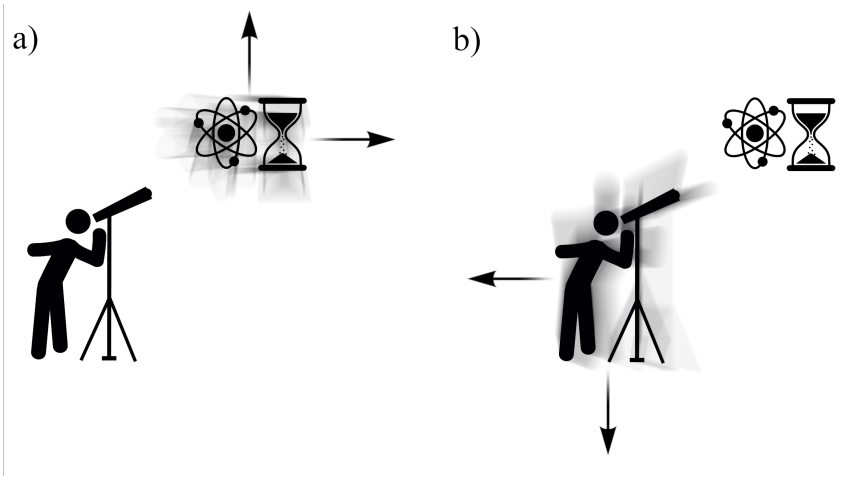

Figure 2.7: a) A pair of arbitrary clocks moving together along a superposition of two different trajectories, observed from a classical inertial frame; b) a pair of resting clocks observed from a quantum reference frame moving at a superposition of two different velocities.

lation with present-day technology, as the magnitude of the effect is within current experimental precision.

Finally, in the section 2.4, we demonstrated that while kinematic quantum time dilation is universal, gravitational quantum time dilation is not. Our proof of universality provides a necessary condition for quantum reference frames to be well-defined [189]. Consider the scheme presented in Fig. 2.7a) where a pair of arbitrary clocks moving along a superposition of two different trajectories is observed from a classical inertial frame. In Fig. 2.7b), we show an analogous scheme, where the pair of clocks is at rest, but they are observed from a quantum reference frame moving at a superposition of velocities. In the latter case, both clocks must experience time dilation in exactly the same way. Therefore, if both schemes a) and b) are to be equivalent, then the quantum time dilation observed in case a) must be universal.

We also argued that the definition of quantum time dilation relies on an arbitrary choice of the classical reference state, and for other, equally justified choices, the effect vanishes. However, we derived an alternative quantum time dilation effect that manifests itself with higher-order coupling terms between translational and internal degrees of freedom. In this case, the quantum noncommutativity of the involved position and momentum operators guarantees that the effect has no classical analog. Our findings clarify the current understanding of quantum time dilation, providing statements about its universality and underlying nature.

2.6 Appendices

2.6.1 Momentum wave packets and signatures of coherence

Here, explicit forms of momentum wave packets from the main text are presented. It is assumed that the atom in consideration moves along the z-direction with its momentum distribution in perpendicular directions well localized around $p_x = p_y = 0$. Moreover, we consider the atom to be either in a coherent superposition of two Gaussian wave packets

$$\psi_{\text{sup}}(p) = \mathcal{N}\left[\cos\theta e^{-\frac{(p-\bar{p}_1)^2}{2\Delta^2}} + e^{i\phi}\sin\theta e^{-\frac{(p-\bar{p}_2)^2}{2\Delta^2}}\right], \tag{2.95}$$

where $\mathcal{N} = [\sqrt{\pi}\Delta(1+\cos\phi\sin 2\theta e^{-(\bar{p}_1-\bar{p}_2)^2/4\Delta^2})]^{-1/2}$, or in an incoherent mixture described by the momentum distribution

$$P_{\text{cl}} = \frac{1}{\sqrt{\pi}\Delta}\left[\cos^2\theta e^{-\frac{(p-\bar{p}_1)^2}{\Delta^2}} + \sin^2\theta e^{-\frac{(p-\bar{p}_2)^2}{\Delta^2}}\right]. \tag{2.96}$$

The difference between coherent superpositions and classical mixtures of momentum wave packets can be characterized by the difference in moments associated with their respective momenta distributions

$$K_j \equiv \frac{1}{j!m^j c^j}\int \mathrm{d}p\; p^j\left[|\psi_{\text{sup}}(p)|^2 - P_{cl}(p)\right]. \tag{2.97}$$

In case of Gaussian wave packets considered above, K_1 and K_2 take the explicit form

$$\begin{aligned} K_1 &= \frac{\cos\phi\sin 4\theta\,(\bar{p}_2-\bar{p}_1)}{4mc\left[\cos\phi\sin 2\theta + e^{\frac{(\bar{p}_2-\bar{p}_1)^2}{4\Delta^2}}\right]} = \delta_Q, \\ K_2 &= \frac{\cos\phi\sin 2\theta\left[(\bar{p}_2-\bar{p}_1)^2 - 2\left(\bar{p}_2^2-\bar{p}_1^2\right)\cos 2\theta\right]}{8m^2c^2\left[\cos\phi\sin 2\theta + e^{\frac{(\bar{p}_2-\bar{p}_1)^2}{4\Delta^2}}\right]} = \gamma_Q^{-1}. \end{aligned} \tag{2.98}$$

Analysis of K_2 is presented in Fig. 2.8 and of K_1 in Fig. 2.9.

Note that K_1 vanishes for an equally weighted superposition $\theta = \pi/4$. Let us show that this feature is a common feature of all symmetric wave packets. Let $\varphi(p)$ be a normalized wave packet symmetric with respect to $p = 0$. Then, we can write an equally weighted, coherent superposition of two momentum wave packets as

$$\varphi_{\text{sup}}(p) = \frac{\mathcal{N}}{\sqrt{2}}\left[\varphi(p-p_1) + e^{i\phi}\varphi(p-p_2)\right], \tag{2.99}$$

with $\mathcal{N}^2 = \left[1 + \cos\phi \int \mathrm{d}p\ \varphi(p-p_1)\varphi(p-p_2)\right]^{-1}$. For the corresponding classical mixture, the momentum distribution takes the form

$$P_{\mathrm{cl}} = \frac{1}{2}\left(\varphi^2(p-p_1) + \varphi^2(p-p_2)\right). \tag{2.100}$$

Then, by an explicit evaluation, one finds that

$$\begin{aligned}\frac{2mc}{\mathcal{N}^2}K_1 &= \frac{2}{\mathcal{N}^2}\int \mathrm{d}p\ p\left[|\varphi_{\mathrm{sup}}(p)|^2 - P_{cl}(p)\right] \\ &= -\cos\phi\Big[\left(\int \mathrm{d}p\ \varphi(p-p_1)\varphi(p-p_2)\right)\left(\int \mathrm{d}p\ p\left(\varphi^2(p-p_1)+\varphi^2(p-p_2)\right)\right) \\ &\quad - 2\int \mathrm{d}p\ p\,\varphi(p-p_1)\varphi(p-p_2)\Big].\end{aligned} \tag{2.101}$$

The term in the third row of (2.101) equals p_1+p_2, because $\varphi(p-p_{1,2})$ are normalized and well localized around $p_{1,2}$. By substituting $p \to p-(p_1+p_2)/2$ and utilizing the fact that expression $\varphi(p-p')\varphi(p+p')$ is an even function of p, one finds that

$$2\int \mathrm{d}p\ p\ \varphi(p-p_1)\varphi(p-p_2) = (p_1+p_2)\int \mathrm{d}p\ \varphi(p-p_1)\varphi(p-p_2). \tag{2.102}$$

Substituting these two results into (2.101) it is seen that that $K_1 = 0$. The only necessary condition is for $\varphi(p)$ to be an even function with respect to $p=0$.

2.6.2 Derivation of the emission rate and spectrum shape

Let us focus on the angular distribution of the emitted radiation. The angular distribution can be obtained by omitting angular integration in (2.25). Note that such an approach does not explicitly utilize the photon distribution that comes from an integration over the probabilities $|\beta_{\boldsymbol{k},\xi}|^2$. However, as shown in [87] this approach is consistent with the special relativity, reproducing dipole pattern of radiation in the comoving frame. Writing explicitly (2.25) gives (see (9)-(11) in [89] for a derivation)

$$\begin{aligned}\Gamma &= \lim_{t\to\infty}\frac{\mathrm{d}}{\mathrm{d}t}\sum_{\boldsymbol{k},\xi}\int \mathrm{d}\boldsymbol{p}\ |\beta_{\boldsymbol{k},\xi}(\boldsymbol{p},t)|^2 \\ &= 2\pi\int \mathrm{d}\boldsymbol{p}\,|\psi(\boldsymbol{p})|^2\sum_{\boldsymbol{k},\xi}\frac{\omega_k}{2\hbar\epsilon_0(2\pi c)^3}g^2_{\boldsymbol{k},\xi}(\boldsymbol{p})\delta\left(\Omega-\omega_k+\frac{1}{m}\boldsymbol{k}\cdot(\boldsymbol{p}-\hbar\boldsymbol{k}/2)\right).\end{aligned} \tag{2.103}$$

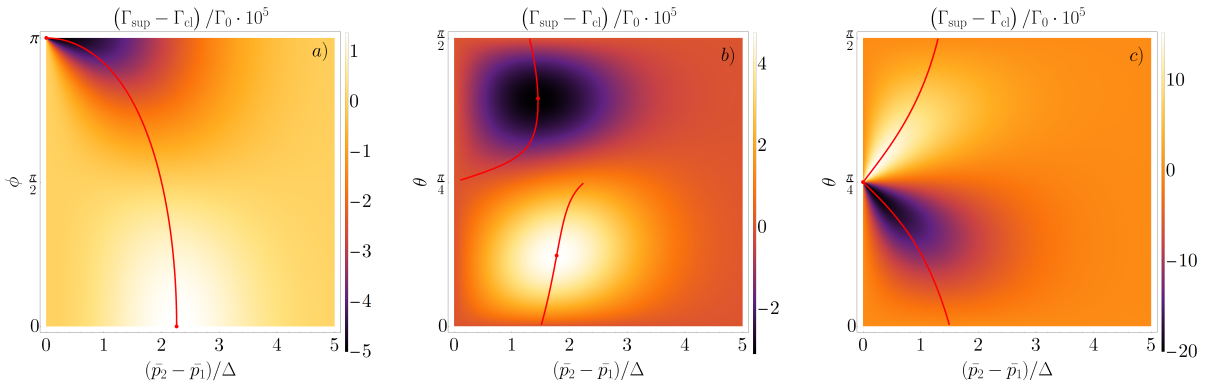

Figure 2.8: Fig. 2.2 from the main text; shown in Appendix for a purpose of comparison with Fig. 2.9. The difference in total emission rates between a superposition and a classical mixture of two momentum wave packets of an atom as a function of the wave packets' momentum difference and their relative phase and weight. The red line marks the maximum value of the effect for a given relative phase or relative weight, while the red circles signify maximum and minimum values across the given subplot. a) equal weighted superposition of momentum wave packets, $\theta = \pi/4$. b) Relative phase fixed at $\phi = 0$. The red line is not continuous at the point $\theta = \pi/4$, and it sharply ends at $(\bar{p}_2 - \bar{p}_1)/\Delta = 2\sqrt{1 + W_0(1/e)} \approx 2.261$, where W_0 is the principal branch of the Lambert W function. c) Relative phase fixed at $\phi = \pi$. It can be seen that two extrema exist for small values of $(\bar{p}_1 - \bar{p}_2)/\Delta$ and $\theta \approx \pi/4$. One can show that these extrema are placed at $\theta = \frac{\pi}{4} - \frac{1}{4}\frac{\bar{p}_2 - \bar{p}_1}{\bar{p}_2 + \bar{p}_1}(1 \pm \sqrt{1 + 2(\bar{p}_2 + \bar{p}_1)^2/\Delta^2})$ and their corresponding values are $\pm\Delta^2(\sqrt{1 + 2(\bar{p}_1 + \bar{p}_2)^2/\Delta^2} - 1)/4m^2c^2$. Nonzero value for a finite momentum difference signifies the phenomenon of quantum time dilation. In each of the panels, the momentum spread of each of wave packets is $\Delta = 0.01mc$ and the sum of their average momenta is equal to $\bar{p}_1 + \bar{p}_2 = 0.05mc$.

By taking a continuous limit of the summation over $\boldsymbol{k}$,

$$\sum_k \to \int \mathrm{d}\boldsymbol{\kappa} \int \mathrm{d}\omega\ \omega^2 \sin\theta, \tag{2.104}$$

where $\boldsymbol{\kappa} = \frac{\boldsymbol{k}c}{\omega} = (\sin\Theta\cos\Phi, \sin\Theta\sin\Phi, \cos\Theta)$ and $\int \mathrm{d}\boldsymbol{\kappa} = \int_0^{\pi} \mathrm{d}\Theta \int_0^{2\pi} \mathrm{d}\Phi$, we can omit the integral over direction $\boldsymbol{\kappa}$ to get the angular distribution

$$\Gamma(\Theta, \Phi) = \frac{\pi}{\hbar\epsilon_0(2\pi c)^3} \int \mathrm{d}\boldsymbol{p}\, |\psi(\boldsymbol{p})|^2 \sum_\xi \int_0^\infty \mathrm{d}\omega\, \omega^3 \sin\Theta g^2_{\boldsymbol{k},\xi}(\boldsymbol{p})\, \delta\left(\Omega - \omega + \frac{1}{m}\boldsymbol{k}\cdot(\boldsymbol{p} - \hbar\boldsymbol{k}/2)\right). \tag{2.105}$$

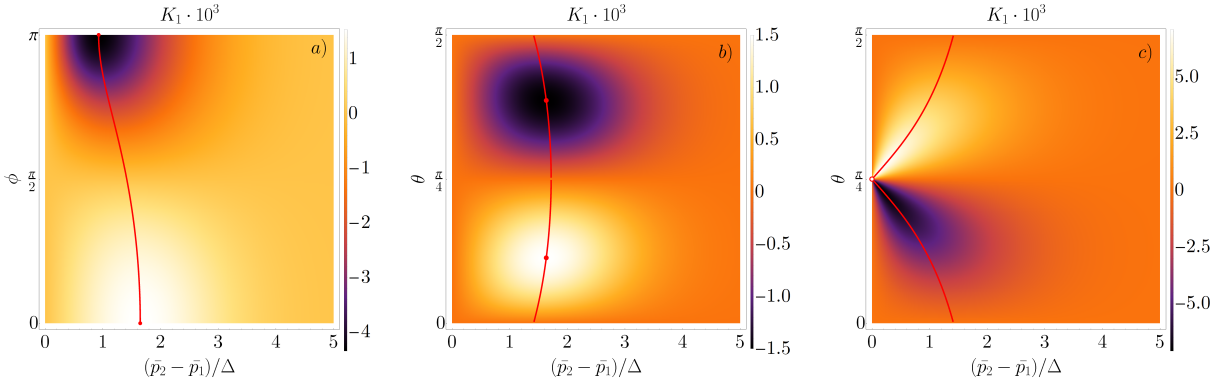

Figure 2.9: The difference in first moments $K_1 = \delta_Q$ of the momentum distributions associated with a superposition and a classical mixture of two momentum wave packets as a function of the wave packets' momentum difference and their relative phase and weight, which quantifies the difference in magnitude of angular distribution of emission: a) unequal weighted superposition of momentum wave packets, $\theta = \pi/8$, b) Relative phase fixed at $\phi = 0$, c) Relative phase fixed at $\phi = \pi$. The red line marks the maximum value of the effect for a given relative phase or a relative weight, while the red circles signify maximum and minimum values across the whole plot. Nonzero values for a finite momentum difference signifies the phenomenon of quantum time dilation. In each of the panels, the momentum spread of each of the wave packets is $\Delta = 0.01mc$ and the sum of their average momenta is equal to $\bar{p}_1 + \bar{p}_2 = 0.05mc$.

Note we are now working in the continuous limit and so the sum over ω_k has been replaced with an integral over ω.

Under the assumption that the atom is heavy the coupling constant $g^2_{\boldsymbol{k},\xi}(\boldsymbol{p})$ can be expanded to first order in $\hbar\Omega/mc^2$ and to second order in p^2/m^2c^2

$$g^2_{\boldsymbol{k},\xi}(\boldsymbol{p}) \approx (\boldsymbol{d}\cdot\boldsymbol{\epsilon}_{\boldsymbol{k},\xi})^2 + \frac{2}{mc}(\boldsymbol{d}\cdot\boldsymbol{\epsilon}_{\boldsymbol{k},\xi})\left(\boldsymbol{p} - \frac{\hbar\omega_k\boldsymbol{\kappa}}{2c}\right)\cdot[(\boldsymbol{\kappa}\times\boldsymbol{\epsilon}_{\boldsymbol{k},\xi})\times\boldsymbol{d}] + \frac{1}{m^2c^2}(\boldsymbol{p}\cdot[(\boldsymbol{\kappa}\times\boldsymbol{\epsilon}_{\boldsymbol{k},\xi})\times\boldsymbol{d}])^2 . \tag{2.106}$$

Making use of the vector equalities

$$\sum_\xi (\boldsymbol{d}\cdot\boldsymbol{\epsilon}_{\boldsymbol{k},\xi})^2 = d^2 - (\boldsymbol{d}\cdot\boldsymbol{\kappa})^2 , \tag{2.107}$$

$$\sum_\xi (\boldsymbol{d}\cdot\boldsymbol{\epsilon}_{\boldsymbol{k},\xi})\,\boldsymbol{A}\cdot[(\boldsymbol{\kappa}\times\boldsymbol{\epsilon}_{\boldsymbol{k},\xi})\times\boldsymbol{d}] = (\boldsymbol{d}\cdot\boldsymbol{\kappa})(\boldsymbol{A}\cdot\boldsymbol{d}) - d^2(\boldsymbol{A}\cdot\boldsymbol{\kappa}) , \tag{2.108}$$

$$\sum_\xi (\boldsymbol{A}\cdot[(\boldsymbol{\kappa}\times\boldsymbol{\epsilon}_{\boldsymbol{k},\xi})\times\boldsymbol{d}])^2 = d^2(\boldsymbol{A}\cdot\boldsymbol{\kappa})^2 + A^2(\boldsymbol{d}\cdot\boldsymbol{\kappa})^2 - 2(\boldsymbol{A}\cdot\boldsymbol{\kappa})(\boldsymbol{d}\cdot\boldsymbol{\kappa})(\boldsymbol{A}\cdot\boldsymbol{d}) , \tag{2.109}$$

with $\boldsymbol{A} = \frac{2}{mc}\boldsymbol{p} - \frac{\hbar}{mc}\boldsymbol{k}$, it follows that

$$\sum_{\xi} g^2_{\boldsymbol{k},\xi}(\boldsymbol{p}) \approx d^2\Big[\kappa_\perp^2\left(1+\frac{\hbar\omega_k}{mc^2}\right) - \frac{2}{mc}\boldsymbol{p}\cdot\boldsymbol{\kappa}_\perp + \frac{1}{m^2c^2}\left(\boldsymbol{p}\cdot\boldsymbol{\kappa}\right)^2 - \frac{2}{m^2c^2}\left(\boldsymbol{p}\cdot\boldsymbol{\kappa}\right)\kappa_\parallel p_\parallel + \frac{1}{m^2c^2}p^2\kappa_\parallel^2\Big], \tag{2.110}$$

where $\perp$ and $\parallel$ indicate projections perpendicular and parallel to the vector $\boldsymbol{d}$.

We now go back to the angular distribution, in which we have to compute the following integral

$$\sum_{\xi}\int_0^\infty \mathrm{d}\omega\,\omega^3\sin\Theta\, g^2_{\boldsymbol{k},\xi}(\boldsymbol{p})\,\delta\Big(\Omega-\omega+\frac{1}{m}\boldsymbol{k}\cdot(\boldsymbol{p}-\hbar\boldsymbol{k}/2)\Big). \tag{2.111}$$

Again, supposing that the atom moves in the z-direction with its momentum distribution in the perpendicular directions given by delta functions centered at $p_x = p_y = 0$. Thus we can consider $\boldsymbol{p} = (0,0,p)$. We will also suppose that $\boldsymbol{d} = (d,0,0)$ points in a direction perpendicular to $\boldsymbol{p}$. Then, (2.111) simplifies to

$$d^2\int_0^\infty \mathrm{d}\omega\;\eta(\omega)\delta\left(\lambda(\omega)\right) = d^2\frac{\eta(\omega_0)}{|\lambda'(\omega_0)|}, \tag{2.112}$$

where

$$\begin{aligned}
\eta(\omega) &\equiv \omega^3\sin\Theta\left[\left(1-\sin^2\Theta\cos^2\Phi\right)\left(1+\frac{\hbar\omega}{mc^2}\right) - \frac{2p}{mc}\cos\Theta + \frac{p^2}{m^2c^2}\left(\cos^2\Theta\sin^2\Phi+\cos^2\Phi\right)\right],\\
\lambda(\omega) &\equiv \Omega-\omega+\omega\frac{p}{mc}\cos\Theta - \frac{\omega^2\hbar}{2mc^2},\\
\omega_0 &\equiv \Omega\left(1+\frac{p}{mc}\cos\Theta+\frac{p^2}{2m^2c^2}\cos 2\Theta - \frac{\hbar\Omega}{2mc^2}\right).
\end{aligned} \tag{2.113}$$

The denominator can be expanded up to first order in $\hbar\Omega/mc^2$ and up to the second order in p^2/m^2c^2 yielding

$$\frac{1}{|\lambda'(\omega_0)|} \approx 1+\frac{p}{mc}\cos\Theta+\frac{p^2}{m^2c^2}\cos^2\Theta - \frac{\hbar\Omega}{mc^2}, \tag{2.114}$$

and finally

$$\frac{\eta(\omega_0)}{|\lambda'(\omega_0)|} \approx \frac{8\pi}{3}\sin\Theta\Big[\;\Xi_0(\Theta,\Phi)\left(1-\frac{3}{2}\frac{\hbar\Omega}{2mc^2}\right) + \Xi_1(\Theta,\Phi)\frac{p}{mc} + \Xi_2(\Theta,\Phi)\frac{p^2}{2m^2c^2}\Big], \tag{2.115}$$

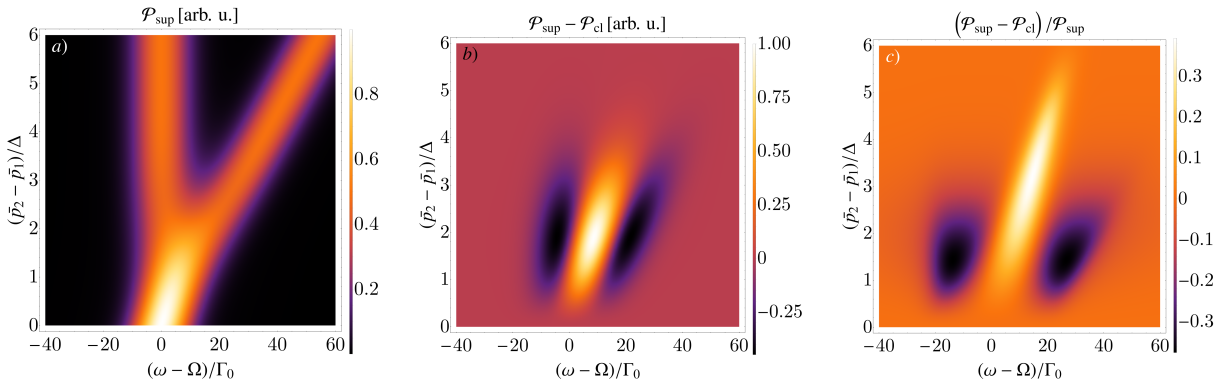

Figure 2.10: A comparison between shapes of the emission spectrum $\mathcal{P}_{\parallel}(\omega)$ associated with a coherent superposition ($\mathcal{P}_{\rm sup}$) and an incoherent classical mixture ($\mathcal{P}_{\rm cl}$) of momentum wave packets a) The transition line for an atom initially prepared in a superposition of two momentum wave packets as a function of emitted photon's frequency and difference between wave packets' momenta. The two-peak structure stemming from two distinct Doppler shifts is clearly visible. b) Absolute difference of emission probabilities between a superposition and a classical mixture of momentum wave packets as a function of the frequency of the emitted photon and difference between wave packets' momenta. The difference is most pronounced in regimes where wave packets overlap. c) Relative difference of emission probabilities between a superposition and a classical mixture of momentum wave packets as a function of the frequency of emitted photon and difference between the wave packets' momenta. It can be seen that the quantum contribution is largest in between the two transition peaks. This suggests that a postselection of final measured states of center-of-mass motion may increase the general visibility of the quantum Doppler effect.

where

$$\Xi_0(\Theta,\Phi) \equiv \frac{3}{8\pi}\left(1-\sin^2\Theta\cos^2\Phi\right), \tag{2.116}$$

$$\Xi_1(\Theta,\Phi) \equiv \frac{3}{4\pi}\cos\Theta\left(1-2\sin^2\Theta\cos^2\Phi\right), \tag{2.117}$$

$$\Xi_2(\Theta,\Phi) \equiv \frac{3}{16\pi}\left[6\cos 2\Theta + 5\cos^2\Phi\left(\cos 4\Theta - \cos 2\Theta\right)\right]. \tag{2.118}$$

Substituting this expression into (2.105) yields the angular distribution

$$\begin{aligned}\frac{\Gamma(\Theta,\Phi)}{\Gamma_0} &= \Xi_0(\Theta,\Phi)\left(1-\frac{3}{2}\frac{\hbar\Omega}{mc^2}\right)\\ &+\frac{1}{mc}\Xi_1(\Theta,\Phi)\int \mathrm{d}p\; p|\psi(p)|^2\\ &+\frac{1}{2m^2c^2}\Xi_2(\Theta,\Phi)\int \mathrm{d}p\; p^2|\psi(p)|^2.\end{aligned} \tag{2.119}$$

The difference between coherent and incoherent cases is then given by

$$\frac{\Gamma_{\mathrm{sup}}(\Theta,\Phi)-\Gamma_{\mathrm{cl}}(\Theta,\Phi)}{\Gamma_0} = \Xi_1(\Theta,\Phi)\;\delta_Q+\Xi_2(\Theta,\Phi)\;\gamma_Q^{-1}. \tag{2.120}$$

Integrating $\Gamma(\Theta,\Phi)$ over Θ and Φ yields the total transition rate

$$\Gamma=\Gamma_0\left(1-\frac{3\hbar\Omega}{2mc^2}-\frac{1}{2m^2c^2}\int \mathrm{d}p\; p^2|\psi(p)|^2\right). \tag{2.121}$$

If $\psi(p)$ is a wave packet well localized at p_0, then

$$\Gamma=\Gamma_0\left(1-\frac{3\hbar\Omega}{2mc^2}-\frac{p_0^2}{2m^2c^2}\right). \tag{2.122}$$

One can also immediately see that the quantum time dilation manifests in the total transition rate

$$\frac{\Gamma_{\mathrm{sup}}-\Gamma_{\mathrm{cl}}}{\Gamma_0}=\gamma_Q^{-1}. \tag{2.123}$$

The first term in (2.119) corresponds to the distribution of dipole radiation for an atom at rest which when integrated over Θ and Φ gives the transition rate Γ_0. The second term is a correction linear in p that associated with a Doppler shift. This term vanishes when integrated over Θ and Φ, ensuring consistency with special relativity as the total transition rate is $\Gamma=\Gamma_0/\gamma(p)$, which when expanded in p is seen to have zero contribution linear in momentum.

However, terms linear in momentum modify the angular distribution of radiation, manifesting as a pattern distinctively different than that of the dipole radiation distribution. The magnitude of this quantum correction depends on K_1 (i.e. δ_Q), which is an explicit function of the parameters characterizing the atomic wave functions and surprisingly vanishes if the atom moves in an equally weighted superposition.

Also of interest is how momentum coherence affects the shape of the atomic emission line, which can be probed through spectroscopic methods. For a plane wave characterized by a wave

vector $\boldsymbol{k}$, the probability of emission is given by

$$\mathcal{P}(\boldsymbol{k}) = \lim_{t\to\infty} \sum_{\xi} \int \mathrm{d}\boldsymbol{p} \ \left|\beta_{\boldsymbol{k},\xi}(\boldsymbol{p},t)\right|^2, \tag{2.124}$$

which utilizing (2.113) can be cast into form

$$\mathcal{P}(\boldsymbol{k}) = \frac{3\Gamma_0}{16\pi^2} \int \mathrm{d}\boldsymbol{p} \left|\psi(\boldsymbol{p})\right|^2 \sum_{\xi} \frac{g^2_{\boldsymbol{k},\xi}(\boldsymbol{p})/d^2}{\lambda^2(\omega) + \Gamma^2(\boldsymbol{p})/4}. \tag{2.125}$$

By expanding $\lambda(\omega)$, $g^2_{\boldsymbol{k},\xi}(\boldsymbol{p})/d^2$ and $\Gamma^2(\boldsymbol{p})$ up to second order in momentum, under the assumption that the emission line is measured perpendicular to the direction of motion, one finds

$$\mathcal{P}_{\perp}(\omega) = \frac{3}{8\pi} \int \mathrm{d}p \ |\psi(p)|^2 \frac{\left(1 - \frac{3}{2}\frac{p^2}{m^2c^2}\right)\Gamma_0/2\pi}{\left[\omega - \Omega\left(1 - \frac{1}{2}\frac{p^2}{m^2c^2}\right)\right]^2 + \frac{\Gamma_0^2}{4}\left(1 - \frac{p^2}{m^2c^2}\right)}. \tag{2.126}$$

On the other hand, in the case of photons measured parallel to the direction of motion, one obtains

$$\mathcal{P}_{\parallel}(\omega) = \frac{3}{8\pi} \int \mathrm{d}p \ |\psi(p)|^2 \frac{\left(1 + 3\frac{p}{mc}\right)\Gamma_0/2\pi}{\left[\omega - \Omega\left(1 + \frac{p}{mc}\right)\right]^2 + \frac{\Gamma_0^2}{4}\left(1 + 2\frac{p}{mc}\right)}. \tag{2.127}$$

In Fig. 2.10 we compare the parallel emission spectrum $\mathcal{P}_{\parallel}(\omega)$ for coherent superposition and incoherent classical mixtures of momentum wave packets.

2.6.3 Evolution of the system

In this Appendix we analyze the evolution of the atomic system in Rindler coordinates making use of the Hamiltonian

$$\hat{H} = \hat{H}_{\text{atom}} + \hat{H}_{\text{field}} + \hat{H}_{\text{af}}. \tag{2.128}$$

We need to solve the Schrödinger equation with the above Hamiltonian and the state (2.54)

$$\begin{aligned} & i\hbar \left(\int \mathrm{d}z\, \dot{\alpha}(z,\tau)\, |z,e,0\rangle + \sum_{\lambda=1,2} \int\int \mathrm{d}k\, \mathrm{d}z\, \dot{\beta}_{k,\lambda}(z,\tau)\, |z,g,1_{k,\lambda}\rangle \right) \\ & = \int \mathrm{d}z \left(\left(Mc^2 + \hbar\Omega\right) \left(1 + \frac{gz}{c^2}\right) \alpha(z,\tau) - i\hbar \sum_{\lambda=1,2} \int \mathrm{d}k\, g_{k,\lambda} \mathrm{e}^{ik\xi} \beta_{k,\lambda}(z,\tau) \right) |z,e,0\rangle \\ & + \sum_{\lambda=1,2} \int\int \mathrm{d}k\, \mathrm{d}z \left(\left(Mc^2 \left(1 + \frac{gz}{c^2}\right) + \hbar\omega_k \right) \beta_{k,\lambda}(z,\tau) - i\hbar g_{k,\lambda} \mathrm{e}^{-ik\xi} \alpha(z,\tau) \right) |z,g,1_{k,\lambda}\rangle \,. \end{aligned} \tag{2.129}$$

Here, the dot denotes the derivative with respect to the coordinate time τ. The infinite set of equations implied by this Schrödinger equation reads

$$\begin{aligned} \dot{\alpha}(z,\tau) &= -\, i\omega_e(z)\alpha(z,\tau) - \sum_{\lambda=1,2} \int \mathrm{d}k\, g_{k,\lambda} \mathrm{e}^{ik\xi} \beta_{k,\lambda}(z,\tau), \\ \dot{\beta}_{k,\lambda}(z,\tau) &= -\, i\left(\omega_g(z) + \omega_k\right) \beta_{k,\lambda}(z,\tau) - g_{k,\lambda} \mathrm{e}^{-ik\xi} \alpha(z,\tau), \end{aligned} \tag{2.130}$$

with

$$\omega_g(z) = \frac{Mc^2}{\hbar}\left(1 + \frac{gz}{c^2}\right) \qquad \text{and} \qquad \omega_e(z) = \left(\frac{Mc^2}{\hbar} + \Omega\right)\left(1 + \frac{gz}{c^2}\right). \tag{2.131}$$

The initial conditions are the following

$$\alpha(z,0) = \psi(z), \qquad \beta_{k,\lambda}(z,0) = 0. \tag{2.132}$$

We perform the Laplace transform and find

$$\begin{aligned} \omega\tilde{\alpha}(z,\omega) - \psi(z) &= -\, i\omega_e(z)\tilde{\alpha}(z,\omega) - \sum_{\lambda=1,2} \int \mathrm{d}k\, g_{k,\lambda} \mathrm{e}^{ik\xi} \tilde{\beta}_{k,\lambda}(z,\omega), \\ \omega\tilde{\beta}_{k,\lambda}(z,\omega) &= -\, i\left(\omega_g(z) + \omega_k\right) \tilde{\beta}_{k,\lambda}(z,\omega) - g_{k,\lambda} \mathrm{e}^{-ik\xi} \tilde{\alpha}(z,\omega). \end{aligned} \tag{2.133}$$

These equations lead to the following formulas for $\tilde{\alpha}(z,\tau)$ and $\tilde{\beta}_{k,\lambda}$

$$\tilde{\alpha}(z,\omega) = \frac{\psi(z)}{\mathfrak{H}(\omega)}, \qquad \tilde{\beta}_{k,\lambda}(z,\omega) = \frac{-g_{k,\lambda} \mathrm{e}^{-ik\xi} \tilde{\alpha}(z,\omega)}{\omega + i\left(\omega_g(z) + \omega_k\right)}, \tag{2.134}$$

where

$$\mathfrak{H}(\omega) = \omega + i\omega_e(z) - \sum_{\lambda=1,2} \int \mathrm{d}k \, \frac{g_{k,\lambda}^2}{\omega + i\left(\omega_g(z) + \omega_k\right)}. \tag{2.135}$$

We return to the time domain using an inverse Laplace transform with integration contour Υ going from negative imaginary infinity to positive imaginary infinity, closed by a large semicircle to the left of the imaginary axis

$$\alpha(z,\tau) = \frac{1}{2\pi i} \int_{\Upsilon} \mathrm{d}\omega \, \frac{\mathrm{e}^{\omega\tau}\psi(z)}{\mathfrak{H}(\omega)}, \tag{2.136}$$

and use the single pole approximation $\mathfrak{H}(\omega) = \omega - \omega_0$ with

$$\omega_0 = -i\omega_e(z) + \delta, \qquad \delta = \sum_{\lambda=1,2} \int \mathrm{d}k \, \frac{i g_{k,\lambda}^2}{\left(\omega_k - \Omega\left(1 + \frac{gz}{c^2}\right)\right) - i\varepsilon}. \tag{2.137}$$

Using the Sochocki-Plemelj formula

$$\lim_{\epsilon \to 0^+} \frac{1}{x - i\varepsilon} = i\pi\delta(x) + \mathcal{P}\left(\frac{1}{x}\right), \tag{2.138}$$

we transform it to

$$\omega_0 = -i\omega_e(z) - \frac{\Gamma(z)}{2}, \qquad \Gamma(z) = 2\pi \sum_{\lambda=1,2} \int \mathrm{d}k \, g_{k,\lambda}^2 \delta\left(\Omega\left(1 + \frac{gz}{c^2}\right) - \omega_k\right). \tag{2.139}$$

We note that

$$\sum_{\lambda=1,2} \hat{\boldsymbol{e}}_{\lambda,i} \hat{\boldsymbol{e}}_{\lambda,j} = \delta_{i,j} - \frac{k_i k_j}{k^2}, \tag{2.140}$$

and assume that the dipole moment of the atom is perpendicular to the direction of light propagation (direction of the gravitational field), to finally compute $\Gamma(z)$

$$\Gamma(z) = \int \mathrm{d}\omega_k \, \frac{\omega_k \boldsymbol{d}^2}{2\hbar c \varepsilon_0} \delta\left(\Omega\left(1 + \frac{gz}{c^2}\right) - \omega_k\right) = \left(1 + \frac{gz}{c^2}\right) \frac{\Omega \boldsymbol{d}^2}{2\hbar c \varepsilon_0} = \left(1 + \frac{gz}{c^2}\right) \Gamma_0. \tag{2.141}$$

Here $\Gamma_0 = \frac{\Omega \boldsymbol{d}^2}{2\hbar c \varepsilon_0}$ is the transition rate of the atom in absence of gravity, whereas $\Gamma(z)$ is the transition rate of a particle localized at height z in a gravitational field.

With (2.141) in hand, we can calculate the amplitude $\alpha(z,\tau)$ in the single pole approximation

$$\alpha(z,\tau) = \psi(z)\exp(\omega_0\tau) = \psi(z)\exp\left[\left(-i\omega_e(z) - \frac{\Gamma(z)}{2}\right)\tau\right]. \tag{2.142}$$

Now we substitute $\frac{\psi(z)}{\omega-\omega_0}$ for $\tilde{\alpha}(z,\omega)$ in the formula for $\tilde{\beta}_{k,\lambda}(z)$ (2.134), and perform the inverse Laplace transform to obtain

$$\beta_{k,\lambda}(z,\tau) = \frac{g_{k,\lambda}\psi(z)\mathrm{e}^{-i(\omega_g(z)+k\xi)}}{\frac{1}{2}\Gamma(z) + i\left(\Omega\left(1+\frac{gz}{c^2}\right)-\omega_k\right)}\left[\mathrm{e}^{-\left(i\Omega\left(1+\frac{gz}{c^2}\right)+\frac{1}{2}\Gamma(z)\right)\tau} - \mathrm{e}^{i\omega_k\tau}\right]. \tag{2.143}$$

2.6.4 Derivation of the emission rate and spectrum shape

Using the results from Appendix 2.6.3, one can compute the probability that the atom stays in the excited state until coordinate time τ

$$\int \mathrm{d}z|\alpha(z,\tau)|^2 = \int \mathrm{d}z|\psi(z)|^2 \exp\left(-\Gamma(z)\tau\right). \tag{2.144}$$

The transition rate is defined as the time derivative of this probability

$$\Gamma = -\frac{\mathrm{d}}{\mathrm{d}\tau}\int \mathrm{d}z|\psi(z)|^2\exp\left[-\Gamma(z)\tau\right] = \int \mathrm{d}z|\psi(z)|^2\Gamma(z)\exp\left[-\Gamma(z)\tau\right] \approx \int \mathrm{d}z|\psi(z)|^2\Gamma(z). \tag{2.145}$$

Here in the last line we made an assumption that the time τ is much shorter than the lifetime of the excited state in the absence of gravity $\tau \ll (\Gamma_0)^{-1}$, and we consider only the cases with $gz/c^2 \ll 1$ in the range of non-vanishing $\psi(z)$.

We are interested in computing the transition rate of an atom in a coherent superposition of two wave packets, Γ_{sup}, and comparing it with the transition rate of an atom in a probabilistic mixture of these wave packets, Γ_{cl}. We assume that in the first case the initial wave function is given by

$$\psi_{\mathrm{sup}}(z) = \mathcal{N}\left[\cos\theta\mathrm{e}^{-\frac{(z-z_1)^2}{2\Delta^2}} + \mathrm{e}^{i\varphi}\sin\theta\mathrm{e}^{-\frac{(z-z_2)^2}{2\Delta^2}}\right], \tag{2.146}$$

with

$$\mathcal{N} = \left[\sqrt{\pi}\Delta\left(1+\cos\varphi\sin 2\theta\mathrm{e}^{-(z_1-z_2)^2/4\Delta^2}\right)\right]^{-1/2}, \tag{2.147}$$

whereas in the second case the probability density reads

$$P_{\mathrm{cl}}(z) = \frac{1}{\sqrt{\pi}\Delta}\left[\cos^2\theta\mathrm{e}^{-\frac{(z-z_1)^2}{\Delta^2}} + \sin^2\theta\mathrm{e}^{-\frac{(z-z_2)^2}{\Delta^2}}\right]. \tag{2.148}$$

In order to compare these two transition rates we compute the ratio

$$\frac{\Gamma_{\mathrm{sup}}-\Gamma_{\mathrm{cl}}}{\Gamma_0} = \int \mathrm{d}z\left(1+\frac{gz}{c^2}\right)\left(|\psi_{\mathrm{sup}}(z)|^2 - P_{\mathrm{cl}}(z)\right) = \frac{g\cos\varphi\sin 4\theta(z_2-z_1)}{4c^2\left[\cos\varphi\sin 2\theta + \mathrm{e}^{\frac{(z_2-z_1)^2}{4\Delta^2}}\right]}. \tag{2.149}$$

The quantum superposition (2.146) and classical mixture (2.148) differ not only in the total transition rate but also in the shape of the associated emission spectrum. In order to check this we must compute the probability that the atom ultimately emits a photon with energy $\hbar\omega_k$

$$\mathcal{P}(\omega_k) = \lim_{\tau\to\infty} \sum_{\lambda=1,2} \int \mathrm{d}z |\beta_{k,\lambda}(z,\tau)|^2 = \sum_{\lambda=1,2} \int \mathrm{d}z \frac{g_{k,\lambda}^2 |\psi(z)|^2}{\frac{1}{4}\Gamma(z)^2 + \left(\Omega\left(1+\frac{gz}{c^2}\right) - \omega_k\right)^2}. \tag{2.150}$$

Substituting $g_{k,\lambda}^2 = \frac{\omega_k}{4\pi\hbar\varepsilon_0}(\boldsymbol{d}\cdot\hat{\boldsymbol{e}}_\lambda)^2$, and performing the sum over the polarizations, we obtain

$$\mathcal{P}(\omega_k) = \int \mathrm{d}z \frac{\omega_k}{2\pi\Omega} \frac{|\psi(z)|^2\Gamma_0}{\frac{1}{4}\Gamma_0^2\left(1+\frac{gz}{c^2}\right)^2 + \left(\Omega\left(1+\frac{gz}{c^2}\right) - \omega_k\right)^2}. \tag{2.151}$$

Usually the transition rate Γ_0 is several orders of magnitude smaller than the resonant light frequency Ω. Therefore, the integrand vanishes when the value of ω_k differs significantly from $\Omega\left(1+\frac{gz}{c^2}\right)$, and we can replace ω_k in the numerator of the integrand by $\Omega\left(1+\frac{gz}{c^2}\right)$. The expression we are left with reads

$$\mathcal{P}(\omega_k) = \int \mathrm{d}z \frac{1}{2\pi} \frac{\left(1+\frac{gz}{c^2}\right)|\psi(z)|^2\Gamma_0}{\frac{1}{4}\Gamma_0^2\left(1+\frac{gz}{c^2}\right)^2 + \left(\Omega\left(1+\frac{gz}{c^2}\right) - \omega_k\right)^2}, \tag{2.152}$$

which, plotted for the quantum superposition and mixed state (see Fig. 2.6), reveals the difference between these two cases.

2.6.5 Approximated results from [Khandelwal *et al.*, Quantum 4, 309 (2020)]

In [126] it was shown that a quantum clock moving with mean velocity v_0 and described by a superposition of two Gaussian wave packets with different mean heights, i.e.,

$$|\psi\rangle = \frac{1}{\sqrt{N}}\left(\sqrt{\alpha}\,|\psi_1\rangle + \mathrm{e}^{i\varphi}\sqrt{1-\alpha}\,|\psi_2\rangle\right), \tag{2.153}$$

where $|\psi_1\rangle$ and $|\psi_2\rangle$ are Gaussian states differing only in the value of mean height $\langle\hat{z}\rangle$ (the first one is localized around z_1, and the second one around z_2), reads the average time

$$\langle\hat{T}\rangle_{\mathrm{sup}}(t) = \langle\hat{T}\rangle_{\mathrm{mix}}(t) + T_{\mathrm{coh}}(t), \tag{2.154}$$

where t is the proper time of an observer at rest at the ground level $z=0$, $\langle\hat{T}\rangle_{\mathrm{mix}}$ is the average time read by the clock described by the classical mixture of the same two Gaussian states $|\psi_1\rangle$ and $|\psi_2\rangle$, and $\hat{T}_{\mathrm{coh}}$ is the contribution due to coherence between these two states. According to

[126], this second contribution is equal to

$$T_{\mathrm{coh}}(t)=\frac{N-1}{2N}\left[\left(\frac{z_2-z_1}{2\sigma_z}\right)^2\frac{\sigma_v^2}{c^2}-\frac{g(z_2-z_1)}{c^2}(1-2\alpha)-\frac{2}{\hbar}\frac{\sigma_v^2}{c^2}(z_2-z_1)(\bar{\boldsymbol{p}}-mgt)\tan\varphi\right]t. \tag{2.155}$$

Here σ_z and σ_v are the standard deviations in position and velocity of $|\psi_1\rangle$ and $|\psi_2\rangle$, respectively, $\bar{\boldsymbol{p}}$ is the mean momentum, and the normalization factor N is equal to

$$N=1+2\cos\varphi\sqrt{\alpha(1-\alpha)}\mathrm{e}^{-\left(\frac{z_2-z_1}{2\sigma_z}\right)^2}, \tag{2.156}$$

(notice that with such a normalization factor, the state is normalized to $\langle\psi|\psi\rangle=\sqrt{\pi}\Delta$). Let us estimate the order of magnitude of individual terms from (2.155) for parameters used to plot Fig. 2.6. For instance, if we take the difference of heights $z_2-z_1\sim 10^{-18}c^2/g$, the height dispersion $\sigma_z\sim 10^{-18}c^2/g$, the mass of the atom $m\sim 1\mathrm{u}\sim 10^{-27}\mathrm{kg}$, use the fact that $\sigma_z\sigma_p\sim\hbar$, and recall that $\sigma_p=m\sigma_v$, we get

$$\frac{\sigma_v^2}{c^2}\sim\frac{\hbar^2}{m^2c^2\sigma_z^2}\sim 10^{-26}. \tag{2.157}$$

The first term in the bracket in (2.155) is then of the order $\sim 10^{-26}$, whereas the second one is $\sim 10^{-18}$. To estimate the third term we recall that we consider a resting atom, i.e., $\bar{\boldsymbol{p}}=0$, and we compute the transition rate at times much smaller than a spontaneous emission lifetime of the excited state in the absence of gravitational field $t\ll\Gamma_0^{-1}$. Typically we have $\Gamma_0^{-1}\sim 10^{-8}s$, which means that the factor multiplying $\tan\varphi$ in the third term cannot be greater than $\sim 10^{-26}$. We should stress that the tangent function appearing in the last term do not lead to any infinities for $\varphi\to\pi/2$, because for such φ the factor multiplying the whole bracket vanishes, and the overall result is finite and relatively small (compared to the value at $\varphi=0$ or $\varphi=\pi$). Therefore we can neglect both the first and the third term to obtain

$$T_{\mathrm{coh}}(t)=\frac{N-1}{2N}\frac{g(z_2-z_1)}{c^2}(2\alpha-1)t=\frac{g\cos\varphi\sqrt{\alpha(1-\alpha)}(2\alpha-1)(z_2-z_1)}{c^2\left(2\cos\varphi\sqrt{\alpha(1-\alpha)}+\mathrm{e}^{\left(\frac{z_2-z_1}{2\sigma_z}\right)^2}\right)}t\equiv\gamma_{\mathrm{Q}}^{-1}t. \tag{2.158}$$

The omission of the terms proportional to σ_v^2/c^2 in this paper can be traced back to the fact that we omitted all the kinetic terms in the atomic Hamiltonian (2.47), so that we completely neglect any motion of the atom, and concentrate on the purely gravitational effect. The estimation presented above can be treated as a justification of this omission for considered range of

parameters.

Let us rewrite (2.158) in a slightly different notation, as used in the present paper. We substitute $\alpha \to \cos^2\theta$, and $\sigma_z \to \Delta$, to get

$$\gamma_{\mathrm{Q}}^{-1} = \frac{g\sqrt{\cos^2\theta(1-\cos^2\theta)}(2\cos^2\theta-1)(z_2-z_1)}{c^2\left(\mathrm{e}^{\left(\frac{z_2-z_1}{2\Delta}\right)^2}+2\cos\varphi\sqrt{\cos^2\theta(1-\cos^2\theta)}\right)} = \frac{g}{4c^2}\frac{\cos\varphi\sin 4\theta(z_2-z_1)}{\cos\varphi\sin 2\theta+\mathrm{e}^{\frac{(z_2-z_1)^2}{4\Delta^2}}}. \tag{2.159}$$

This is the same expression that appears in (2.64).

2.6.6 Evolution of the density matrix

The approximate solution to (2.89) can be obtained in the first order of the Dyson series

$$\hat{\rho}^I(t) \approx \hat{\rho}(0) - \frac{i}{\hbar}\int_0^t \mathrm{d}t'\left[\hat{H}^I_{\mathrm{int}}(t'),\hat{\rho}(0)\right]. \tag{2.160}$$

Returning to the Schrödinger picture, where $\hat{\rho}(t) \equiv e^{-\frac{i}{\hbar}(\hat{H}_{\mathrm{clock}}+\hat{H}_{\mathrm{cm}})t}\hat{\rho}^I(t)e^{\frac{i}{\hbar}(\hat{H}_{\mathrm{clock}}+\hat{H}_{\mathrm{cm}})t}$, we can compute the reduced density matrix of the clock's internal state by tracing out the kinematic degrees of freedom $\hat{\rho}_{\mathrm{clock}}(t) \equiv \mathrm{Tr}_{\mathrm{cm}}\,\hat{\rho}(t)$

$$\hat{\rho}_{\mathrm{clock}}(t) \approx e^{-i\hat{H}_{\mathrm{clock}}t}\hat{\rho}_{\mathrm{clock}}(0)e^{i\hat{H}_{\mathrm{clock}}t} - \frac{i}{\hbar}\int_0^t \mathrm{d}t'\,\mathrm{Tr}_{\mathrm{cm}}\left(e^{-i(\hat{H}_{\mathrm{clock}}+\hat{H}_{\mathrm{cm}})t}\left[\hat{H}^I_{\mathrm{int}}(t'),\hat{\rho}(0)\right]e^{i(\hat{H}_{\mathrm{clock}}+\hat{H}_{\mathrm{cm}})t}\right). \tag{2.161}$$

The first term in (2.161), $e^{-\frac{i}{\hbar}\hat{H}_{\mathrm{clock}}t}\hat{\rho}_{\mathrm{clock}}(0)e^{\frac{i}{\hbar}\hat{H}_{\mathrm{clock}}t}$, describes the evolution of the internal degrees of freedom of the clock in the absence of coupling with the kinematic degrees of freedom. We will denote this term as $\hat{\rho}^0_{\mathrm{clock}}(t)$. To evaluate the second term, we assume that the initial state of the system exhibits no correlations between the kinematic and internal degrees of freedom: $\hat{\rho}(0) \equiv \hat{\rho}_{\mathrm{cm}}(0)\otimes\hat{\rho}_{\mathrm{clock}}(0)$. The relation between the interaction picture and the Schr"odinger picture for the interaction Hamiltonian (2.88) is given by

$$\hat{H}^I_{\mathrm{int}}(t') = e^{\frac{i}{\hbar}(\hat{H}_{\mathrm{clock}}+\hat{H}_{\mathrm{cm}})t'}\left(\hat{H}_{\mathrm{clock}}\hat{V}_1+\hat{H}^2_{\mathrm{clock}}\hat{V}_2\right)e^{-\frac{i}{\hbar}(\hat{H}_{\mathrm{clock}}+\hat{H}_{\mathrm{cm}})t'}. \tag{2.162}$$

By substituting Equation (2.162) into Equation (2.161) and utilizing the fact that $\left[\hat{H}_{\mathrm{clock}},\hat{H}_{\mathrm{cm}}\right]=0$, we can rephrase Equation (2.161) as follows

$$\hat{\rho}_{\text{clock}}(t) \approx \hat{\rho}^0_{\text{clock}}(t) - \frac{i}{\hbar}\Big[\hat{H}_{\text{clock}}, \hat{\rho}^0_{\text{clock}}(t)\Big] \int_0^t \mathrm{d}t' \, \mathrm{Tr}_{\text{cm}} \left(e^{\frac{i}{\hbar}\hat{H}_{\text{cm}}t'} \hat{V} 1 e^{-\frac{i}{\hbar}\hat{H}_{\text{cm}}t'} \hat{\rho}_{\text{cm}}(0) \right) \\ - \frac{i}{\hbar}\Big[\hat{H}^2_{\text{clock}}, \hat{\rho}^0_{\text{clock}}(t)\Big] \int_0^t \mathrm{d}t' \, \mathrm{Tr}_{\text{cm}} \left(e^{\frac{i}{\hbar}\hat{H}_{\text{cm}}t'} \hat{V} 2 e^{-\frac{i}{\hbar}\hat{H}_{\text{cm}}t'} \hat{\rho}_{\text{cm}}(0) \right). \tag{2.163}$$

Next, we can employ the Baker–Campbell–Hausdorff formula, $e^{\hat{X}}\hat{Y}e^{-\hat{X}} = \hat{Y} + \Big[\hat{X}, \hat{Y}\Big] + \ldots$, to determine the exact form of the operators present in the trace from Equation (2.163)

$$e^{\frac{i}{\hbar}\hat{H}_{\text{cm}}t'} \hat{V} 1 e^{-\frac{i}{\hbar}\hat{H}_{\text{cm}}t'} \approx \hat{V}_1 \frac{i}{\hbar} t' \Big[\hat{H}_{\text{cm}}, \hat{V}_1\Big], e^{\frac{i}{\hbar}\hat{H}_{\text{cm}}t'} \hat{V}_2 e^{-\frac{i}{\hbar}\hat{H}_{\text{cm}}t'} \approx \hat{V}_2 + \frac{i}{\hbar} t' \Big[\hat{H}_{\text{cm}}, \hat{V}_2\Big], \tag{2.164}$$

where we neglect quadratic contributions in t' that are irrelevant in the short-time limit considered in this section. Substituting the result from Equation (2.164) into Equation (2.163) ultimately yields Equation (2.90).

3 Indefinite temporal order without gravity

Time, space and causality are only metaphors of the knowledge by which we interpret all things

(Friedrich Nietzsche [190])

According to the general theory of relativity, the flow of time can vary depending on the configuration of massive objects, thereby influencing the temporal order of events. When combined with quantum theory, this gravitational effect can lead to events with an indefinite temporal order if a massive object is prepared in an appropriate quantum state. It has been proposed that this could enable a theory-independent test of non-classical order of events by violating Bell-type inequalities for temporal order. However, we demonstrate that the theory-independence of this protocol is problematic: one of the auxiliary assumptions in the aforementioned approach is crucial and explicitly theory-dependent.
To illustrate this issue, we construct a comprehensive scenario where accelerating particles interacting with optical cavities result in a violation of temporal Bell inequalities. Due to the Equivalence Principle, the same issue arises in the gravitational context, necessitating theory-dependent additional assumptions to interpret a violation of Bell inequalities for temporal order as evidence of indefinite temporal order.

Contents

3.1 Useful tools

In this section, we will introduce the fundamental concepts used in this chapter. These theories and ideas serve as an introduction to the topic of further considerations that are the focus of this work.

3.1.1 Indefinite temporal order and Bell-type inequalities for time

The task of integrating two different theories, namely quantum mechanics and the theory of relativity, presents an additional problem when it comes to the concept of time. In quantum mechanics, time is treated in a classic way, meaning events happen in a fixed, predictable order. However, in the general theory of relativity, the order of events in time can be affected by how matter is distributed. The interesting part arises when we try to merge these two theories. If we ask for a quantum-level explanation of matter, we end up with a situation where there can be a mix - or superposition - of different matter distributions. This combination of theories suggests that the order of events in time, as understood in quantum mechanics, could also be affected. As a result, a successful merger of quantum mechanics and the theory of relativity might result in a time structure that is non-classical, or *indefinite* [191, 192].

The physical implications of an indefinite causal structure are still not well understood. Many quantum gravity theories aim to create a comprehensive theoretical framework [193, 194]. However, these theories often fail to clearly explain the non-classical causal relationships they describe.

A recent study introduced a thought experiment aiming to directly elucidate the physical implications of the non-classicality of temporal order, without relying on the specifics of a comprehensive quantum theory of gravity [71]. The central premise posits that a superposition of mass configurations will induce a non-classical time dilation on any system that might serve as a "clock" to identify spacetime events, effectively generating a superposition of time-like event sequences.

By using a specific protocol, it is possible to accomplish tasks like violating a Bell inequality, which would be impossible with a classical causal structure. This allows us to certify the non-classical nature of causal structures without relying on a particular theory, showing how the superposition principle applies to general relativity. The authors of [71] have developed new ways to test theories that combine relativity and quantum mechanics. This is similar to how Bell inequalities provided a method to test fundamental assumptions of quantum mechanics. It is now well-established that Bell inequalities can be violated within quantum mechanics [195, 196], and many recent experiments have confirmed these violations [197–200].

In our investigation, we plan to make a slight modification to the main premise from [71]. Therefore, we will explain the core concept of Bell inequalities for temporal order in the following sections of this dissertation.

The foundations of quantum theory and general relativity are fundamentally different. In quantum theory, systems generally do not have definite physical properties until they are measured. However, operations occur within a fixed background spacetime where causal relations between events—whether space-like or time-like—are determined independently of any operation or physical process. In contrast, general relativity does not have preset causal relations, as the geometry depends on the distribution of mass-energy. Therefore, it is expected that combining these two theories will result in a non-classical or indefinite causal structure [191, 192].

The physical interpretation of such an indefinite causal structure, however, remains elusive. The quantum switch, introduced in [201], provided the first instance of an indefinite causal structure. This demonstrated that quantum degrees of freedom, which govern the sequence of operations, can facilitate evolution that cannot be represented within a conventional quantum circuit.

While many quantum gravity strategies endeavor to formulate a comprehensive theoretical framework—including, among other aspects, the depiction of non-classical spacetimes and their origins [193, 194]—they typically do not offer a direct physical interpretation of such non-classical causal structure.

A recent study proposed a thought experiment to directly interpret the physical implications of non-classical temporal order, without relying on the complex details of a full quantum theory of gravity [71]. The key idea is that a superposition of mass configurations would cause non-classical time dilation in any system used as a "clock" to mark spacetime events. This would create, for example, a superposition of different sequences of time-like events. It was argued that, using a specific protocol, one could achieve something—violating a Bell inequality—that would be impossible if the temporal order of events were classical. This protocol is claimed to provide a theory-independent proof of the non-classical nature of the temporal order among a set of events.

Gravitational implementation of an indefinite temporal order

Recent methods for studying causal structures are based on gravitational time dilation [71]. However, Bell's theorem on temporal order considers time dilation more broadly. This leads to the question: can a similar experiment be done using only special relativity? We propose to delve into a scenario where the mass back-action on spacetime is minimal, but the relative motion induces clock desynchronization among moving clocks. Additionally, we hypothesize that a special relativistic execution of the experiment could be less stringent, offering a potential direction for future laboratory implementations.

In our research, we aim to employ a strategy where accelerating particles, represented as Unruh-DeWitt detectors, interact with optical cavities at specified times dictated by their internal clock degrees of freedom (DoFs). By allowing the particles to evolve in superposition along suitable accelerating trajectories, we plan to demonstrate that the interaction events recreate the "entanglement in time order" identical to that observed in the gravitational scenario.

Ultimately, we aim to use measurements on the particles to violate the "Bell inequalities for temporal order" as detailed in [71]. This research would constitute a significant stride towards the potential of testing the indefinite temporal order of events. We aim to demonstrate that indefinite temporal order can not only be achieved but also theoretically scrutinized in experiments that incorporate effects familiar from special relativity.

This outcome could pave a potential path for testing indefinite temporal order, without the need to grapple with gravity at the quantum level.

In our research, we plan to expand upon the theory discussed in [71]. The original theory was designed for large objects that can influence the order of events. However, in our research, we aim to use a quantum system to control the order of these events. To do this, it makes sense—and is easier—to use a fully quantum-based approach where each part of the process uses quantum measurements. To present our original idea let us firstly summarise the idea of Bell inequalities for temporal order introduced in [71].

For future reference, we will briefly review the key aspects of the protocol introduced in [71]. The protocol aims to create four events, A_1, B_1, A_2, B_2, with pair-wise orders that are 'entangled': A_1 is in the causal past/past lightcone of B_1, denoted $A_1 \prec B_1$, when $A_2 \prec B_2$, and A_1 is in the causal future/future lightcone of B_1, denoted $A_1 \succ B_1$ when $A_2 \succ B_2$. An exemplary depiction of two events A and B being in the relation $A \prec B$ or $A \succ B$ can be seen in Fig. 3.1. The full scenario is designed such that this entanglement leads to correlations that cannot be explained by a local classical framework, analogous to Bell-like scenarios for local classical properties. Importantly, an "event" here is operationally understood as "something that happens at a particular time and place" and is thus defined by some physical reference system. Similarly, for a fixed event A, the

relation $A \prec B$ operationally defines future events B that are reachable by a photon or a massive particle sent at event A.

In the proposed protocol, the reference systems are four clocks, a_1, b_1, a_2, b_2, while the events are associated with quantum operations performed on an additional system when the corresponding clock reaches a specified proper time: A_1 occurs (an operation is performed) when a_1 reaches time τ^*, B_1 occurs when b_1 reaches time τ^*, and so on.

In flat spacetime, if the clocks are initially synchronized (in an arbitrarily chosen reference frame), all events are space-like separated. However, introducing a massive body closer to some clocks than others causes differential time dilation, which can 'push' some events into the future light-cone of other events. Thus, the position of the mass provides control over the time order of events, see Fig. 3.1.

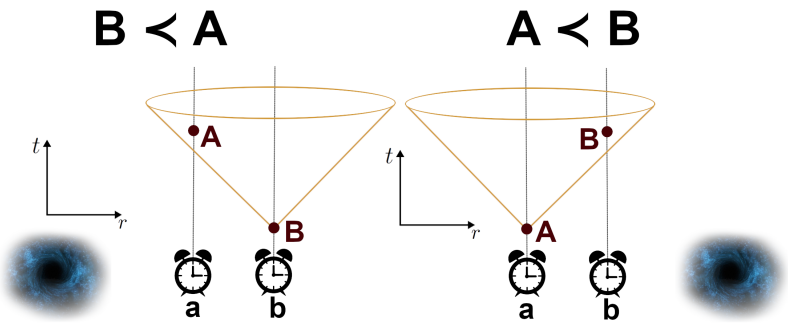

Figure 3.1: **Position of a mass as a control of time order.** Two identical clocks, a, b, are synchronized (with any source-mass sufficiently far away). Events A, B are defined by the location and fixed proper time τ^* of the corresponding clock. In the absence of any source mass, events A, B are space-like. However, if a massive object is initially (just after synchronization) placed closer to clock a than to b, event A can be in the future light cone of B (for sufficiently large τ^*), denoted $B \prec A$. Conversely, if the mass is closer to b, event A can be in the past light cone of B, denoted $A \prec B$.

If the control mass is prepared in a semiclassical configuration denoted K_A, event A_j, $j = 1, 2$ is in the past of B_j, while in a different configuration, K_B, event B_j is in the past of A_j. Thus, A_j is time-like from B_j for each mass configuration, but their order is interchanged. Moreover, for both mass configurations, the pair A_1, B_1 is space-like separated from A_2, B_2.

The full protocol also includes two additional systems on which the operations are performed, S_1 and S_2, referred to as 'targets'. The operations at events A_1 and B_1 are applied only to the target system S_1, while those at A_2 and B_2 are applied only to S_2. The two target systems are initially in a product state, $|\psi\rangle^{S_1} |\psi\rangle^{S_2}$, and the considered operations are unitary: $\hat{U}^{A_1}$ is

applied to S_1 at event A_1, and so on. Operations applied to the target systems S_1 and S_2 are referred to as 'wing' 1 and 2, respectively, of the experiment. By preparing the control mass in a superposition state, $|K\rangle = \frac{1}{\sqrt{2}}(|K_A\rangle + |K_B\rangle)$, the final state is

$$\left|\Psi^{\text{fin}}\right\rangle = \frac{1}{\sqrt{2}}\left(|K_A\rangle\,\hat{U}^{B_1}\hat{U}^{A_1}\,|\psi\rangle^{S_1}\,\hat{U}^{B_2}\hat{U}^{A_2}\,|\psi\rangle^{S_2} + |K_B\rangle\,\hat{U}^{A_1}\hat{U}^{B_1}\,|\psi\rangle^{S_1}\,\hat{U}^{A_2}\hat{U}^{B_2}\,|\psi\rangle^{S_2}\right). \quad (3.1)$$

Next, the control mass is measured in the basis $|\pm\rangle = \frac{1}{\sqrt{2}}(|K_A\rangle \pm |K_B\rangle)$, leaving the target system in

$$\left|\Psi^{\text{post}}\right\rangle = \frac{1}{\sqrt{2}}\left(|\psi_A\rangle^{S_1}\,|\psi_A\rangle^{S_2} \pm |\psi_B\rangle^{S_1}\,|\psi_B\rangle^{S_2}\right), \quad (3.2)$$

where $|\psi_A\rangle = \hat{U}^B\hat{U}^A\,|\psi\rangle$, $|\psi_B\rangle = \hat{U}^A\hat{U}^B\,|\psi\rangle$. We use the same unitaries in the two 'wings', i.e., for A_1 and A_2: $\hat{U}^{A_1} = \hat{U}^{A_2} \equiv \hat{U}^A$, and for B_1 and B_2: $\hat{U}^{B_1} = \hat{U}^{B_2} \equiv \hat{U}^B$.

In general, $\left|\Psi^{\text{post}}\right\rangle$ is an entangled state unless $|\psi_A\rangle = |\psi_B\rangle$ (and it is straightforward to find examples of unitaries $\hat{U}^A$, $\hat{U}^B$ where this is not the case). In the final step of the protocol, the entangled state is measured in appropriate bases, leading to a violation of a Bell inequality.

Assumption	Explanation
Local state	The initial state of the whole system is separable
Local operations	All transformations performed on the systems are local
Classical order	The events at which operations (transformations and measurements) are performed are classically ordered
Space-like separation	Events (A_1, B_1) are space-like separated from events (A_2, B_2). Additionally, the measurement of a control mass is space-like separated from both 'wings'
Free-choice	The measurement choices in the Bell measurement are independent of the rest of the experiment

Table 3.1: **Assumptions of Bell's Theorem for Temporal Order (see [71]).**

The argument presented in [71] is that, given the initial product state of the target systems, local operations performed in a definite order would not produce entanglement, even after conditioning on the control system. Therefore, if certain conditions are met, a violation of Bell inequalities implies that the operations were not performed in a definite order (for more details, see Table 3.1).

Another auxiliary assumption introduced in [71], which becomes a focal point of this work, is that any additional evolution of the target systems (including their free evolution) between the events of interest can be neglected. In this work, we examine the consequences of this additional assumption. We construct a scenario where neglecting the free evolution of the target is not feasible. We argue that this is a general feature and that finding exceptions where the

assumption holds requires theory-dependent analysis. For completeness, we start by presenting a scenario that can generate a violation of Bell inequalities and then discuss the possibility of verifying the existence of indefinite temporal order solely due to the violation of these inequalities.

3.1.2 Unruh-DeWitt coupling

In this section we define the interaction between a two-level system, the 'detector', and the scalar field inside the cavity via the pointlike Unruh-DeWitt Hamiltonian [202, 203]. We first discuss key properties of the field operators. We consider a scalar field of a mass m governed by the Klein-Gordon equation [1],

$$\left(\Box + m^2\right)\phi = 0, \tag{3.3}$$

in a cavity of length L fulfilling Dirichlet boundary conditions, $\phi(x=0) = \phi(x=L) = 0$. The field has the following mode solutions

$$u_n(x,t) = \frac{1}{\sqrt{\omega_n L}} \sin\left(k_n x\right) e^{-i\omega_n t} \equiv u_n(x) e^{-i\omega_n t}, \tag{3.4}$$

where $\omega_n = \sqrt{k_n^2 + m^2}$, $k_n = \frac{n\pi}{L}$, $n \in \mathbb{N}$. Using these modes, the field operator $\hat{\phi}$ can be decomposed as

$$\hat{\phi}(x) = \sum_n \left[\hat{a}_n^\dagger u_n(x) + \hat{a}_n u_n(x)\right], \tag{3.5}$$

where $\hat{a}_n$ and $\hat{a}_n^\dagger$ are annihilation and creation bosonic operators satisfying the canonical commutation relations, $\left[\hat{a}_n, \hat{a}_k^\dagger\right] = \delta_{nk}$ and $[\hat{a}_n, \hat{a}_k] = \left[\hat{a}_n^\dagger, \hat{a}_k^\dagger\right] = 0$. For the detector we consider a two-level system, the simplest model of an atom, with an energy gap Ω, and position parameter denoted x_d, (where the subscript d hereafter stands for the 'detector'). The full Hamiltonian consists of the free Hamiltonians of the scalar field and the detector, and an interaction Hamiltonian. One of the simplest choices of the interaction between a scalar field and a two-level system is the pointlike Unruh-DeWitt (UDW) Hamiltonian which in the Schrödinger picture has the following form

$$\hat{H}_{\mathrm{UDW}} = \lambda\, \chi_d(t)\, \hat{\mu}_{\mathrm{S}}\, \hat{\phi}(x_d), \tag{3.6}$$

where λ is a dimensionless coupling constant; the real function $\chi_d(t)$ is equal to 0 when the detector does not interact and 1 for any other time and is commonly referred to as the switching function; $\hat{\mu}_{\mathrm{S}}$ is the monopole operator $\hat{\mu}_{\mathrm{S}} = \hat{\sigma}^+ + \hat{\sigma}^- = |g\rangle\langle e| + |e\rangle\langle g|$, where $|g\rangle$ is the ground state of the two-level system and $|e\rangle$ is its excited state. The Hilbert space spanned by $|g\rangle$ and $|e\rangle$ will be called the internal Hilbert space of the detector. Finally, $\hat{\phi}(x_d)$ is the field operator

[1] For generality, we write everything for arbitrary m, although in the numerical calculations below we set $m = 0$.

evaluated at the position of the detector. As mentioned above, the full Hamiltonian includes also the time-independent free Hamiltonian of the field and of the two-level system, which reads $\hat{H}_0 = \sum_n \omega_n \hat{a}_n^\dagger \hat{a}_n \otimes \mathbb{1} + \mathbb{1} \otimes \Omega \hat{\sigma}^+ \hat{\sigma}^-$. Thus, the evolution of the state of the full system in the Dirac picture (also called the interaction picture) is here given by the unitary of the form

$$\hat{U} = \mathcal{T} \exp\left\{-i \int_{-\infty}^{\infty} \mathrm{d}t \hat{H}_{\mathrm{UDW}}^{(D)}(t)\right\}, \tag{3.7}$$

where (D) stands for the Dirac picture and $\mathcal{T}$ is the time-ordering operator. It can be shown that [204]

$$\hat{H}_{\mathrm{UDW}}^{(D)}(t) = \chi(t)\ \lambda\ \hat{\mu}^{(D)}\ \hat{\phi}^{(D)}, \tag{3.8}$$

where

$$\hat{\mu}^{(D)} = \left(e^{i\Omega t}\hat{\sigma}^+ + e^{-i\Omega t}\hat{\sigma}^-\right), \tag{3.9}$$

$$\hat{\phi}^{(D)}(x_d) = \sum_n \left(\hat{a}_n^\dagger u_n(x_d) e^{i\omega_n t} + H.c.\right). \tag{3.10}$$

The evolution operator (3.7) can be expanded into the Dyson series. For sufficiently small value of the coupling constant λ we can limit this series to the first order term. We further show in Appendix 3.4.1 that the next contributing term is λ^3. Thus, in the above approximation

$$\hat{U} = \mathbb{1} - i\lambda \int_{-\infty}^{\infty} \mathrm{d}t\ \chi_d(t) \left(e^{i\Omega t}\hat{\sigma}^+ + e^{-i\Omega t}\hat{\sigma}^-\right) \times \sum_n \left(\hat{a}_n^\dagger u_n(x_d) e^{i\omega_n t} + \hat{a}_n u_n(x_d) e^{-i\omega_n t}\right). \tag{3.11}$$

3.2 Protocol without gravity

In this section, we describe a setup where accelerating particles interact with quantum fields via their own internal clock degrees of freedom (DoFs). This approach uses only special relativity and does not require additional assumptions, as the effect on spacetime by the matter involved is minimal. A superposition of the clock states of motion induces the corresponding non-classical time dilation, as first investigated in [205]. By allowing particles to move in superposition along accelerating paths, we show that the interactions between particles and fields replicate the "entanglement of temporal order" observed in the gravitational case [71].

Remarkably, our study reveals that a violation of Bell inequalities persists even when the entangled events are space-like, challenging the interpretation that the protocol uniquely identifies

non-classical temporal order of necessarily time-like events. We find that this is due to the failure of one of the auxiliary assumptions made in [71]—specifically, that the superposed amplitudes differ only in event order, while all local evolutions are trivial, including the free evolution of the systems measured to reveal the violation of Bell inequalities. We argue that this assumption's failure is ubiquitous and would occur in a generic dynamical context, including a gravitational implementation of the protocol. We also propose an interpretation of the Bell inequality violation in scenarios where the non-classicality of temporal order cannot possibly explain the results (e.g., for space-like separated events mentioned above).

Our findings reveal a loophole in the previous theory i.e. [71], indicating that in realistic scenarios involving specific implementations of the protocol for violating Bell inequalities for temporal order, it is impossible to satisfy all the mathematical assumptions of the original theory (we will discuss it later in 3.2.6). While it is possible in principle, each system requires its own assumptions, making the procedure less universal than initially thought (detailed discussion of this issue will be the topic of 3.2.7). This raises a fundamental question: can we develop an operational scenario that clearly distinguishes the non-classicality of the causal structure of spacetime from the dynamical effects inherent in its physical implementations or other laboratory implementations of quantum causal structures [206–212]? We discuss potential extensions to the original protocol that might be necessary to achieve this goal.

Furthermore, a flat spacetime version of the protocol may allow for a laboratory implementation and provide further insights into the requirements of the original, gravitational argument. Finally, it seems likely that the quantum indeterminacy of spacetime structures is at the heart of the still unknown quantum theory of gravity [213, 214], and comparing special relativistic and gravitational schemes could also offer insights into potential violations of the equivalence principle due to quantum effects.

This part of the dissertation is structured as follows: First we focus on reproducing the gravitational protocol using special relativistic time dilation. We present an operational setting that incorporates the dynamics of all relevant degrees of freedom (DoFs), particularly those involved in realizing the four unitaries $\hat{U}^A$ and $\hat{U}^B$. In 3.2.6, we discuss our main finding: entanglement can be generated and Bell inequalities for temporal order can be violated even if the temporal order is classically defined. We attribute this to the failure of the additional assumption mentioned earlier, that target systems have trivial evolution apart from the unitaries marking the four spacetime events of interest. In 3.2.7, we provide a simplified example demonstrating the importance of free evolution. In 3.3, we discuss the implications of our results, including the fundamental question of how to isolate quantum features of a causal structure from other non-classical effects.

3.2.1 General setup

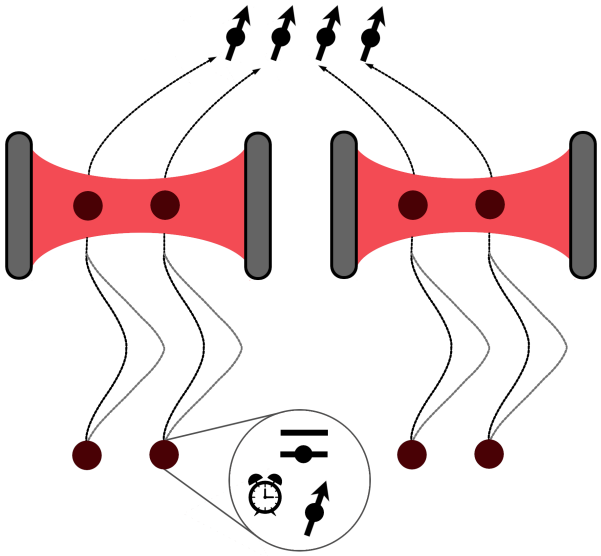

Figure 3.2: **General scheme of our protocol for a violation of Bell inequalities for temporal order.** In each 'wing' of the experiment we have a quantum field in a cavity, and two composite 'molecules'. After following entangled pairs of trajectories the molecules interact with the fields at a fixed proper time of their internal clocks. Due to time dilation, entangled state of motion gets transferred to the order of the interaction events (as well as to other degrees of freedom of the molecules and the cavities).

Instead of using a massive object to control the spacetime geometry—and thus temporal order via gravitational time dilation—here we want to control the trajectories of particles so as to induce special-relativistic time dilation. For clarity of this scheme, we decided to provide a simple comparison between our approach and the original one presented in [71] in the form of tab. 3.2. The protocol involves several degrees of freedom, which can be best thought of as multiple particles 'glued' together (up to the moment when we need to break them apart, as detailed later). We will refer to a bunch of joined particles as a 'molecule', although the details of what binds the particles together are irrelevant to the discussion.

Our protocol involves four molecules going through two optical cavities (two molecules per cavity). In further consideration, we will refer to everything that happens to these two cavities as two 'wings' of the protocol because they will play the same role as the 'wings' described in the previous section. Moreover, each molecule is composed of three particles: a 'clock', a 'detector', and a 'control'. Figure 3.2 presents a general scheme of our protocol.

The clock is simply a particle with some time-evolving internal state; if the molecule evolves

along a classical trajectory, the internal state evolves at a rate proportional to the trajectory's proper time. The role of the clock is to trigger an interaction between the detector and the cavity at the desired proper time. Thanks to the universality of time dilation, the protocol does not depend on the particular mechanism by which the clocks evolve—all we need is that the clock reaches two different orthogonal states depending on the two proper times involved in the protocol (see, e.g., Refs. [132, 215]). We decided to employ this particular realization of our idea to underscore the relativistic aspect of our study. One could propose an alternative mechanism to achieve a delay between two interactions, but such a mechanism would require external entities to manipulate the atoms and position them at specific times. Although this alternative mechanism could yield similar results, it would lack the relativistic nature. However, we would like to emphasize that the specifics of our model are not the focal point of our study. Our main goal is to demonstrate that the violation of Bell inequalities is not always an unambiguous consequence of the indefinite temporal order of interactions.

The detector is a particle with two internal energy levels that (at the proper time specified by the clock), interacts with a quantum field confined in a cavity. We use the Unruh-DeWitt detector model for the interaction; see 3.2.3 below and 3.1.2 for the details of the coupling. Finally, the control is a spin-$\frac{1}{2}$ particle, with its two orthogonal spin states, $|\uparrow\rangle$ and $|\downarrow\rangle$, defining the molecules' trajectories (refer to [216] for an example of coherent spin-dependent trajectories that could be utilized here). Although each detector interacts with the cavity at the same proper time according to its local clock, special-relativistic time dilation ensures that these interactions occur at different coordinate times based on the molecule's trajectory, which is determined by the spin.

In this protocol, the detectors in each molecule are initially prepared in their ground state $|g\rangle$, and the clocks are synchronized at a reference starting time τ_0. The spins of different molecules are prepared in an appropriate entangled state (defined below). Each molecule then follows a spin-dependent trajectory into a cavity. The clock triggers an interaction between the detector in the molecule and the field, creating entanglement between them. The proper time for the interaction is chosen so that the molecule remains in the cavity for either trajectory. At this stage, the molecule is 'broken apart': the detector and the clock remain next to the respective cavity, while all controls are brought together at a central location. A joint measurement on the controls prepares an entangled state of the remaining systems, enabling a violation of a Bell inequality.

In our setup, the 'target' system on each side, such as S_1, includes the field in the cavity and the two detectors passing through it. Crucially, the field-detector interaction does not affect the clock or control. This is essential to ensure that each operation U^A, U^B acts solely on the target system. Without this assumption, one could entangle each target system with an additional

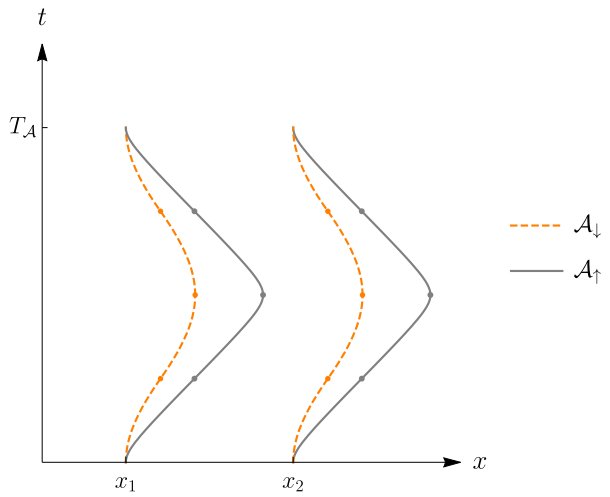

Figure 3.3: **Trajectories of the molecules in one cavity leading to the required time dilation.** x_1, x_2 represent the initial positions of the molecules. Each molecule's trajectory is determined by the spin of its 'control' particle. For spin $|\uparrow\rangle$, the trajectory follows the proper acceleration $\mathcal{A}_\uparrow$, and similarly for spin $|\downarrow\rangle$. Dots along the trajectories divide each curve into four geometrically identical hyperbolic segments. The trajectories of the molecules in the second cavity are analogous.

degree of freedom (DoF), such as an extra particle, bring these extra particles together, and, by measuring them, induce entanglement in the two target systems. This would be a form of entanglement swapping [217] that does not require any control of time ordering or control systems.

Furthermore, since the control DoF passes through the cavity along with the rest of the molecule, it is crucial to trust the involved devices to ensure that local operations leave the control unaffected. This necessity means that such a test for indefinite temporal order cannot be formulated in a device-independent manner (as in the gravitational protocol of [71], see also the discussion therein).

	Gravity	Cavity
Control system	massive body	spin-$\frac{1}{2}$ particles (one per molecule, two in each wing)
Target system	a single 2-level system (e.g., a spin-$\frac{1}{2}$ particle)	Optical cavity mode and two detectors
Local operations	unitaries on each system	Interaction between cavity and detectors

Table 3.2: **Comparison between the degrees of freedom involved in the gravitational scheme and ours**. Here we only consider the main scheme from [71] (variations of the scheme involve multiple control systems or different target DoFs.)

3.2.2 Trajectories

In this section, we will describe the trajectories of the molecules mentioned previously. Building on the concept presented in 3.1.1, we have decided to use the same trajectories in both wings of the experiment. This allows us to focus on one wing and its two molecules, simplifying the analysis of the trajectory's specific form in the overall protocol.

Each molecule has two possible trajectories depending on the spin state. The specific trajectories we propose for one wing of the experiment are shown in Fig. 3.3, with identical choices for the other wing. Each molecule always starts and ends its trajectory at the same events, which are identical for both possibilities. However, the proper time elapsed along the two trajectories is different. Both trajectories are constructed by joining four identical hyperbolic segments, characterized by proper accelerations $\mathcal{A}_\uparrow$ and $\mathcal{A}_\downarrow$ for spin up, $|\uparrow\rangle$, and spin down, $|\downarrow\rangle$, respectively.

These segments are rotated or flipped according to Fig. 3.3, so that the acceleration for each trajectory switches signs three times. Let's assume that the acceleration for the spin $|\uparrow\rangle$ is greater than the acceleration for the spin $|\downarrow\rangle$. Knowing the value of proper time along a generic hyperbolic trajectory (see, e.g., [77]), we can determine the difference between the proper times measured at the common endpoint of one such pair of trajectories

$$\Delta\tau = \underbrace{\frac{4}{\mathcal{A}_\downarrow}\text{asinh}(\frac{\mathcal{A}_\downarrow T_\mathcal{A}}{4})}_{\tau_\downarrow} - \underbrace{\frac{4}{\mathcal{A}_\uparrow}\text{asinh}(\frac{\mathcal{A}_\uparrow T_\mathcal{A}}{4})}_{\tau_\uparrow}, \tag{3.12}$$

where $\tau_{\uparrow/\downarrow}$ is the proper time measured along the trajectory of a $\uparrow$ / $\downarrow$ spin, and $T_\mathcal{A}$ is the total travel time in a common inertial frame of reference, such as the frame used to initially synchronize the clocks. Note that it is possible to achieve a large value of $\Delta\tau$ with a small value of proper acceleration. For a large value of $T_\mathcal{A}$, we have

$$\Delta\tau = 2\left(\frac{\log\left(\frac{\mathcal{A}_\downarrow^2}{4}\right)}{\mathcal{A}_\downarrow} - \frac{\log\left(\frac{\mathcal{A}_\uparrow^2}{4}\right)}{\mathcal{A}_\uparrow}\right) + 4\left(\frac{1}{\mathcal{A}_\downarrow} - \frac{1}{\mathcal{A}_\uparrow}\right)\log(T_\mathcal{A}) + \mathcal{O}\left(\frac{1}{T_\mathcal{A}^2}\right). \tag{3.13}$$

This indicates that we can achieve the required $\Delta\tau$ (to make the events defined by such time-dilated pair of clocks timelike) by accelerating for a sufficiently long time, even with arbitrarily small accelerations.

Finally, by taking the initial state of the spin of the two molecules to be entangled, one of the two clocks in each cavity will "age" more than the other in a correspondingly correlated manner. Thus, the order of operations, controlled by the clocks, will also be "entangled," as a direct result of the initial spin entanglement and time dilation. In this scenario, the joint spin state of the two

molecules acts as the control, analogous to the position of a massive object in the gravitational case [71]. Table 3.2 summarizes the differences between the gravitational and our cavity-based implementation of the protocol in terms of control systems, target(s), and local operations.

3.2.3 One Cavity - Two Molecules

Before discussing the full protocol, let's consider the interaction between one cavity and a pair of molecules, focusing on one wing of the protocol. Each molecule contains a clock, a control spin, and a two-level detector that interacts with the cavity via the Unruh-DeWitt (UDW) Hamiltonian, which in the Schrödinger picture has the following form (see also 3.1.2)

$$\hat{H}_{\mathrm{UDW}} = \lambda\, \chi_d(t)\, \hat{\mu}_{\mathrm{S}}\, \hat{\phi}(x_d), \tag{3.14}$$

where λ is a dimensionless coupling constant; the real function $\chi_d(t)$ is zero when the detector is inactive and one otherwise, commonly referred to as the switching function; $\hat{\mu}_{\mathrm{S}}$ is the monopole operator $\hat{\mu}_{\mathrm{S}} = \hat{\sigma}^{+} + \hat{\sigma}^{-} = |g\rangle\langle e| + |e\rangle\langle g|$, where $|g\rangle$ is the ground state and $|e\rangle$ is the excited state of the two-level system. The Hilbert space spanned by $|g\rangle$ and $|e\rangle$ is called the internal Hilbert space of the detector. Finally, $\hat{\phi}(x_d)$ is the field operator evaluated at the position of the detector.

At the beginning of the protocol, the cavity field is in the vacuum state, denoted $|0\rangle$, and the two detectors are in their respective ground states. We synchronize the clocks, preparing them in the same state $|\tau_0\rangle$, and prepare the two control spins in the entangled state $\frac{1}{\sqrt{2}}(|\uparrow\downarrow\rangle + |\downarrow\uparrow\rangle)$. After applying the spin-dependent accelerations described in 3.2.2, the joint state of the cavity and molecules is

$$\frac{1}{\sqrt{2}}(|\tau_\uparrow\tau_\downarrow\rangle\,|\uparrow\downarrow\rangle + |\tau_\downarrow\tau_\uparrow\rangle\,|\downarrow\uparrow\rangle)\,|gg\rangle\,|0\rangle\,, \tag{3.15}$$

where $|\tau_{\uparrow/\downarrow}\rangle$ is the state of the clock after evolving for time $\tau_{\uparrow/\downarrow}$. For convenience, we have grouped the degrees of freedom by type (clock, spin, detector), rather than by molecule. For example, instead of

$$\underbrace{|\tau_\uparrow\rangle\,|\uparrow\rangle\,|g\rangle}_{1^{st}\ molecule} \otimes \underbrace{|\tau_\downarrow\rangle\,|\downarrow\rangle\,|g\rangle}_{2^{nd}\ molecule}, \tag{3.16}$$

we write $|\tau_\uparrow\tau_\downarrow\rangle\,|\uparrow\downarrow\rangle\,|gg\rangle$, where within each 'ket' symbol, we first write the state relative to molecule 1 and then to molecule 2.

From (3.15), it is clear that after the spin-dependent accelerations, the clocks become entangled

with the remaining systems. This can be problematic because the final protocol aims to observe entanglement in the target systems (detectors and cavities) after projecting the control onto an appropriate state. Any correlation with the target, including the clocks, would degrade entanglement. We can circumvent this by re-synchronizing the clocks after they have passed through the cavity. This can be achieved, for example, by flipping the molecules' spins and applying accelerations identical to those in the first phase, ensuring all trajectories accrue equal proper times (similar to the decorrelation of clocks in the gravitational scenario discussed in [71]). This procedure allows us to ignore the clocks in the final state. The role of the clock is crucial to ensure events occur "at a given time" in the molecule's reference frame so that any conclusion about the order of events can be attributed to an intrinsic definition of events, similar to the gravitational case[2]. It is only after ensuring that the clock decorrelates from the rest of the system that we can remove it from the description. After tracing out the clock degrees of freedom, we simplify the notation and map $\left|\tau_{\uparrow/\downarrow}\right\rangle|\uparrow/\downarrow\rangle \to |\uparrow/\downarrow\rangle$, allowing us to denote the state (3.15) as

$$\left|\Psi_0^1\right\rangle = \frac{1}{\sqrt{2}}(|\uparrow\downarrow\rangle + |\downarrow\uparrow\rangle)\,|gg\rangle\,|0\rangle\,, \tag{3.17}$$

where the subscript 0 indicates that this is the initial state of the system (before the detectors and cavity interact) and the superscript 1 indicates the state of the field and two molecules in wing 1 (see Fig. 3.2).

According to the scheme presented above, the state $|\uparrow\downarrow\rangle$ corresponds to the case when the detector at position x_2 interacts first with the cavity (the spin of the molecule interacting earlier is $\downarrow$). Similarly, for the state $|\downarrow\uparrow\rangle$, the detector at x_1 interacts before the detector at x_2. In further calculations, we assume that the duration T of each detector's interaction with the cavity is shorter than the time dilation between the two trajectories, i.e., $T \leq \Delta\tau$, to ensure that the two detectors do not interact simultaneously from the perspective of the cavity's reference frame.

The interaction between each detector and the cavity is described by (3.7) from Appendix 3.1.2. Since the order of interactions is determined by the molecule's spin, we can write the final state as

$$\left|\Psi^1\right\rangle = \frac{1}{\sqrt{2}}\left(|\uparrow\downarrow\rangle\,\hat{U}_1\hat{U}_2\,|g\rangle\,|g\rangle\,|0\rangle + |\downarrow\uparrow\rangle\,\hat{U}_2\hat{U}_1\,|g\rangle\,|g\rangle\,|0\rangle\right). \tag{3.18}$$

Here, operators $\hat{U}_1$ and $\hat{U}_2$ act on the internal states of the first (left) and the second (right)

[2] One could also define the time of events relative to a common laboratory clock and correlate the time of each event with a control degree of freedom. This would effectively simulate time dilation by directly desynchronizing clocks. However, here we are interested in a relativistic definition of events and event order.

detector, respectively. For ease of notation, we define the state $|\psi_R\rangle := \hat{U}_1\hat{U}_2 |g\rangle |g\rangle |0\rangle$, where the subscript R denotes that the right (2^{nd}) detector interacts before the left (1^{st}) one, and similarly define $|\psi_L\rangle := \hat{U}_2\hat{U}_1 |g\rangle |g\rangle |0\rangle$. Thus, we have

$$\left|\Psi^1\right\rangle = \frac{1}{\sqrt{2}} |\uparrow\downarrow\rangle |\psi_R\rangle + \frac{1}{\sqrt{2}} |\downarrow\uparrow\rangle |\psi_L\rangle \,. \tag{3.19}$$

Using the evolution operator given by (3.7) from Appendix 3.1.2, we find the explicit form of $|\psi_R\rangle$ and $|\psi_L\rangle$ up to leading order in the interaction parameter λ using (3.11) from Appendix 3.1.2. The results of this calculation are

$$|\psi_R\rangle = \hat{U}_1\hat{U}_2 |g\rangle |g\rangle |0\rangle = |gg\rangle |0\rangle + |ge\rangle \left|\phi^R_{ge}\right\rangle + |eg\rangle \left|\phi^R_{eg}\right\rangle + \mathcal{O}(\lambda^2), \tag{3.20}$$

$$|\psi_L\rangle = \hat{U}_2\hat{U}_1 |g\rangle |g\rangle |0\rangle = |gg\rangle |0\rangle + |ge\rangle \left|\phi^L_{ge}\right\rangle + |eg\rangle \left|\phi^L_{eg}\right\rangle + \mathcal{O}(\lambda^2), \tag{3.21}$$

where $\left|\phi^{L/R}_{ge}\right\rangle$ and $\left|\phi^{L/R}_{eg}\right\rangle$ are first order in λ, describing field states containing a single excitation (see Appendix 3.4.1 for their explicit expression).

3.2.4 Two Cavities - Four Molecules

We now proceed to the complete protocol aimed at explicitly demonstrating indefinite temporal order. We consider two 'wings' of the experiment, where each wing involves two operations (see Fig. 3.2). The objective is to correlate the order of each pair of operations with a control system and, after measuring the control, produce an entangled state between the two wings, which would not be possible if the operations were realized in a definite order.

The target systems comprise the fields in both cavities and the detectors (two per cavity), while the four spin-$\frac{1}{2}$ particles serve as the control. The full protocol involves four molecules (two in each wing), each containing a clock, a detector, and a spin-$\frac{1}{2}$ particle. Initially, the state of these molecules is

$$|\tau_0\tau_0\tau_0\tau_0\rangle \frac{1}{\sqrt{2}}(|\uparrow\downarrow\uparrow\downarrow\rangle + |\downarrow\uparrow\downarrow\uparrow\rangle) |gggg\rangle \,, \tag{3.22}$$

where $|\tau_0\rangle$ is the initial state of one clock, synchronizing all four clocks, and each detector is in its ground state, while the spins are entangled.

This state is constructed so that the four molecules can be divided into two identical pairs, with analogous trajectories in each wing. These pairs are then accelerated as described in 3.2.2.

After acceleration, the state of all four molecules is

$$\frac{1}{\sqrt{2}}(|\tau_\uparrow\tau_\downarrow\tau_\uparrow\tau_\downarrow\rangle\,|\uparrow\downarrow\uparrow\downarrow\rangle + |\tau_\downarrow\tau_\uparrow\tau_\downarrow\tau_\uparrow\rangle\,|\downarrow\uparrow\downarrow\uparrow\rangle)\,|gggg\rangle\,. \tag{3.23}$$

Due to time dilation, after acceleration, one clock from each pair of molecules will be older than the other from the same pair. We cannot determine which one because the initial state of spins is a superposition of two different possibilities. Next, each pair of molecules enters a cavity. The first pair is placed in cavity 1 at positions x_1 and x_2 relative to the boundary of this cavity at $x = 0$. The second pair is placed in cavity 2 at analogous positions relative to that cavity. The field in each cavity is initially in the vacuum state. As discussed in the previous section, we can decorrelate the clock degrees of freedom by re-synchronizing the clocks after the molecules interact with the cavities. The role of the clocks is crucial to ensure events occur "at a given time" in the molecule's reference frame. After re-synchronization, the initial state of the total system including the two cavities is

$$\left|\Psi_0^{\text{tot}}\right\rangle = \frac{1}{\sqrt{2}}(|\uparrow\downarrow\uparrow\downarrow\rangle + |\downarrow\uparrow\downarrow\uparrow\rangle)\,\underbrace{|gg\rangle\,|0\rangle}_{\in S_1} \otimes \underbrace{|gg\rangle\,|0\rangle}_{\in S_2}, \tag{3.24}$$

where we use $\otimes$ to separate states from the two cavities and indicate which degrees of freedom comprise the targets S_1 and S_2 introduced in 3.1.1.

After the interactions between the detectors and the cavity fields, the state of the system is

$$\left|\Psi^{\text{tot}}\right\rangle = \frac{1}{\sqrt{2}}\left(|\uparrow\downarrow\uparrow\downarrow\rangle\,|\psi_R\rangle \otimes |\psi_R\rangle + |\downarrow\uparrow\downarrow\uparrow\rangle\,|\psi_L\rangle \otimes |\psi_L\rangle\right), \tag{3.25}$$

where the detectors and cavity states, $\left|\psi_{L/R}\right\rangle$, are as defined in (3.20) and (3.21).

Next, the molecules are 'broken apart'. All spins are sent to a common location where, at an event labeled D, they are jointly measured in the basis $\frac{1}{\sqrt{2}}(|\uparrow\downarrow\uparrow\downarrow\rangle \pm |\downarrow\uparrow\downarrow\uparrow\rangle)$. This measurement prepares the remaining systems—cavities and detectors (which stay next to their cavities)—in the state

$$\left|\Psi^{\pm}\right\rangle = \frac{1}{\sqrt{2}}\left(|\psi_R\rangle \otimes |\psi_R\rangle \pm |\psi_L\rangle \otimes |\psi_L\rangle\right), \tag{3.26}$$

where the sign $\pm$ depends on the measurement outcome. This state is entangled as long as $|\psi_L\rangle \neq |\psi_R\rangle$.

To determine whether the final state is entangled, we can consider a measurement on each detector pair in a basis that includes the vector $1/\sqrt{2}(|ge\rangle + |eg\rangle)$. The resulting conditional

states of the fields (from (3.20) and (3.21)) are

$$\frac{1}{\sqrt{2}}(\langle ge| + \langle eg|)\,|\psi_R\rangle = \frac{1}{\sqrt{2}}\left(\left|\phi^R_{ge}\right\rangle + \left|\phi^R_{eg}\right\rangle\right) + \mathcal{O}(\lambda^3), \tag{3.27}$$

$$\frac{1}{\sqrt{2}}(\langle ge| + \langle eg|)\,|\psi_L\rangle = \frac{1}{\sqrt{2}}\left(\left|\phi^L_{ge}\right\rangle + \left|\phi^L_{eg}\right\rangle\right) + \mathcal{O}(\lambda^3), \tag{3.28}$$

where the order of this result, $\mathcal{O}(\lambda^3)$, is explained in Appendix 3.4.3.

To summarize this method: one can measure each pair of detectors in the basis $1/\sqrt{2}\,(|ge\rangle + |eg\rangle)$ to obtain the field state given in (3.27) and (3.28), and then follow the previously described procedure by measuring the control. Upon measuring the control in the entangled basis, $\frac{1}{\sqrt{2}}(|\uparrow\downarrow\uparrow\downarrow\rangle \pm |\downarrow\uparrow\downarrow\uparrow\rangle)$, the joint state of the two cavities consists only of the field states because all other degrees of freedom were measured. This state of the fields, up to the leading order in λ, is

$$\left|\tilde{\Psi}^{\pm}\right\rangle \propto \underbrace{\left(\left|\phi^R_{ge}\right\rangle + \left|\phi^R_{eg}\right\rangle\right)}_{|\Phi_R\rangle} \otimes \underbrace{\left(\left|\phi^R_{ge}\right\rangle + \left|\phi^R_{eg}\right\rangle\right)}_{|\Phi_R\rangle} \pm \underbrace{\left(\left|\phi^L_{ge}\right\rangle + \left|\phi^L_{eg}\right\rangle\right)}_{|\Phi_L\rangle} \otimes \underbrace{\left(\left|\phi^L_{ge}\right\rangle + \left|\phi^L_{eg}\right\rangle\right)}_{|\Phi_L\rangle}. \tag{3.29}$$

The conditional state of the fields, $\left|\tilde{\Psi}^{\pm}\right\rangle$, is entangled as long as $|\Phi_R\rangle \neq |\Phi_L\rangle$, which is easier to verify than the condition $|\psi_R\rangle \neq |\psi_L\rangle$. We also note that the measurement on the detectors can result in different outcomes, not all of which lead to entangled field states. However, if the original state across S_1 and S_2 was a product state, all local detector measurements would yield product states of the fields. Thus, obtaining an entangled state for any outcome is sufficient to prove that the original state was entangled.

In conclusion, we have shown that using two cavities, four molecules, and the fundamental effects of special relativity, we can achieve the state given in (3.29). If this state is entangled, the next steps of the protocol can use this entanglement to violate Bell inequalities, thereby proving that the detector-field interaction events were not classically ordered.

3.2.5 Entanglement of the Final State

We now proceed to demonstrate that the state in (3.29) can indeed be entangled by showing that there exist parameters for which $|\Phi_R\rangle \neq |\Phi_L\rangle$. The scalar product between these states is given by

$$\langle\Phi_R|\Phi_L\rangle = \frac{\sum_k \frac{e^{-i\Delta\tau(\omega_k+\Omega)}}{(\omega_k+\Omega)^2}\left[1-\cos\left(T(\omega_k+\Omega)\right)\right]\left(u_k(x_1) + e^{i\Delta\tau(\omega_k+\Omega)}u_k(x_2)\right)^2}{2\sum_n \frac{\sin^2\frac{T(\omega_n+\Omega)}{2}}{(\omega_n+\Omega)^2}\left[u_n(x_2)^2 + 2u_n(x_2)u_n(x_1)\cos\left(\Delta\tau(\omega_n+\Omega)\right) + u_n(x_1)^2\right]}. \tag{3.30}$$

The explicit derivation is presented in Appendix 3.4.2. There, we further show how to choose parameters for which the states are not just different but orthogonal. To summarize this procedure, the parameters that have to be chosen are:

1. The length L of each cavity and the positions x_1, x_2 of the molecules relative to their respective cavity.
2. The energy gap Ω of the detectors.
3. The duration T of the interaction between each detector and the cavity field.
4. The time dilation $\Delta\tau$ between clocks within each pair of molecules (within each cavity), arising from the different accelerations $\mathcal{A}_{\uparrow/\downarrow}$.

Remarkably, it is also possible to find parameters such that $|\Phi_R\rangle \neq |\Phi_L\rangle$ even when the two field-detector interactions within each cavity are space-like separated, as shown in Fig. 3.4. This implies that it is possible to obtain an entangled state even when, in some reference frame, the relevant operations are performed in the same temporal order. From the perspective of such a reference frame, the operations would occur over four different coordinate regions, maintaining the same order in each amplitude. Therefore, the entanglement generated in this scheme cannot be solely attributed to non-classical temporal order. We discuss the implications and argue for the generality of this result in the following sections.

3.2.6 Ambiguity in the signature of indefinite temporal order

We have specifically modeled a special-relativistic variant of a protocol in which gravitational time dilation and quantum superposition result in an indefinite temporal order of events, as discussed in [71]. This protocol was designed in the context of a 'Bell inequality for temporal order.' The objective was to develop a protocol wherein operations conducted in a *definite* sequence would not produce an entangled state, given that a suitable set of assumptions is met. The final phase of the protocol necessitates measurements on the state to violate a Bell inequality and confirm the entanglement. The goal was to establish a test for temporal order that is *theory independent*, based on the observation that violating a Bell inequality would demonstrate indefinite temporal order without presuming that the final state is governed by quantum mechanics. In this section, we revisit the assumptions made in [71] and illustrate that the claim of theory-independence is problematic.

Initially, we note that the issue identified does not occur if we accept the validity of quantum mechanics, i.e., if we aim to provide experimental evidence for non-classical temporal order assuming the involved states and transformations are accurately described by quantum theory.

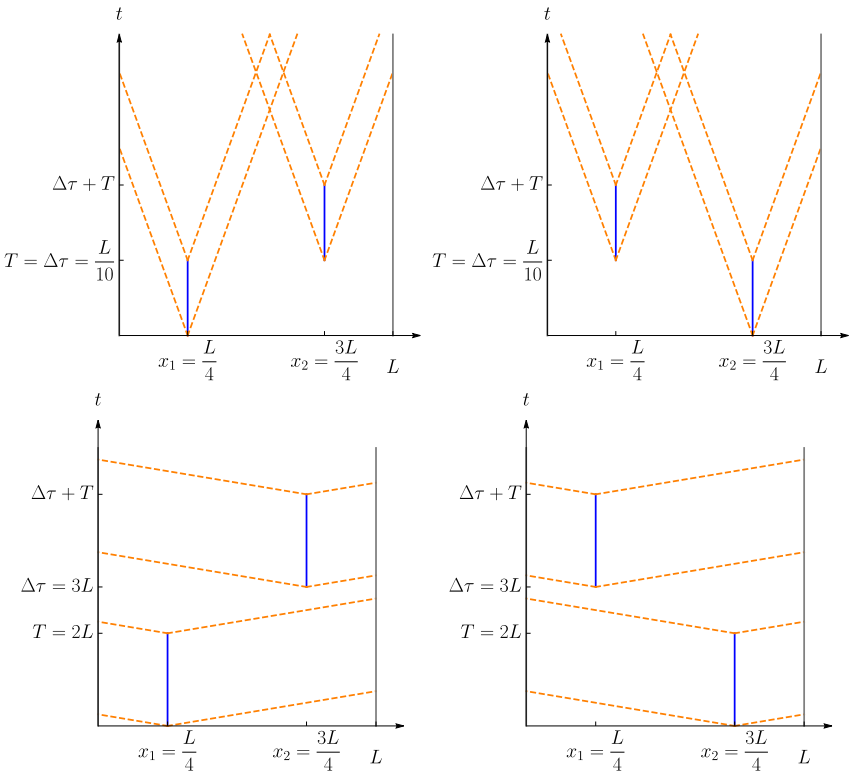

Figure 3.4: **Spacetime diagrams of interacting detectors.** Spacetime diagram showing the regions where the detector-field interactions lead to an entangled state, (3.29). The diagrams are for one cavity – the interaction regions are identically defined for the second cavity. The first row shows space-like separated regions which nevertheless yield entanglement. The second row shows time-like separation which yields maximal entanglement. The columns correspond to the two amplitudes of the process that are superimposed using the control (spin) state. See Appendix 3.4.2 for the supporting calculations.

In this scenario, even the one-cavity part of our protocol, as described in 3.2.3, or its gravitational equivalent, suffices. This is because, at an abstract level, these protocols implement a "quantum switch" [201] – a setup where two local operations, represented by unitary operators $\hat{U}^A$ and $\hat{U}^B$, act on a target system in an order dictated by a control system prepared in a superposition, thus yielding a final state of the form

$$|\psi_{\text{fin}}\rangle = \frac{1}{\sqrt{2}}\left(|0\rangle\,\hat{U}^A\hat{V}_0\hat{U}^B + |1\rangle\,\hat{U}^B\hat{V}_1\hat{U}^A\right)|\psi\rangle\,. \tag{3.31}$$

Here, $|0\rangle$ and $|1\rangle$ are two basis states of the control, and $|\psi\rangle$ is the initial state of the target system. $\hat{V}_0$ and $\hat{V}_1$ are two arbitrary unitary operators representing the target's evolution between the two

operations. Although most descriptions of the switch omit the intermediate evolution, we will demonstrate its importance in our context[3]. Given a realization of the switch, by performing suitable final measurements for a set of appropriately selected operations $\hat{U}^A$ and $\hat{U}^B$, it is possible to prove that the operations are not executed in a definite sequence. This procedure is referred to as measuring a *causal witness* [218, 219], and it could, in principle, be incorporated into a single-cavity variant of our protocol to demonstrate that, assuming the quantum description of the experiment is accurate, the cavity-detector interactions do not occur in a definite order.

Returning to the Bell inequality approach, it essentially becomes an 'entangled' version of the switch, resulting in the final state given by

$$|\psi_{\text{fin}}\rangle = \frac{1}{\sqrt{2}}\left(|0\rangle\,\hat{U}^{A_1}\hat{V}_0\hat{U}^{B_1}\,|\psi\rangle\otimes\hat{U}^{A_2}\hat{V}_0\hat{U}^{B_2}\,|\psi\rangle \;+\; |1\rangle\,\hat{U}^{B_1}\hat{V}_1\hat{U}^{A_1}\,|\psi\rangle\otimes\hat{U}^{B_2}\hat{V}_1\hat{U}^{A_2}\,|\psi\rangle\right). \tag{3.32}$$

To use such a state to refute classical temporal order among $\hat{U}^A$ and $\hat{U}^B$, the state must arise under conditions satisfying all assumptions used to derive the Bell inequality for temporal order, except for the classical order assumption itself. The assumptions used in Ref [71] to derive the inequality are: the initial state of the target systems S_1 and S_2 is separable; transformations on the targets are local (i.e., operations on target S_j act as the identity on other degrees of freedom); the events/spacetime regions where transformations and measurements occur are appropriately separated: both interaction events in one wing are spacelike separated from both interaction events in the other wing, and event D is spacelike from the events where Bell measurements are performed (which, as usual in Bell inequalities, are assumed to be spacelike from each other); the choice of bases for Bell measurements is independent of all other aspects of the experiment (often called the 'free choice' assumption); and finally, the assumption that events where transformations and measurements are performed are classically ordered.

The unexpected result identified in 3.2.5 is that entanglement is produced while *all* the above assumptions, including the classical order assumption, are met. Clearly, some other assumption was made to derive the inequality and is violated in our implementation. Indeed, as previously mentioned, the additional implicit assumption made in [71] is that the target systems do not undergo non-trivial evolution aside from the transformations $\hat{U}^A$ and $\hat{U}^B$. Below, we explain why this assumption is violated in the present implementation, and in 3.2.6, we argue that this will remain true in a generic dynamical implementation. As a result, our considerations apply to any generic scheme attempting to verify the indefinite temporal order of events implemented in a fully quantum mechanical manner.

[3] For the sake of completeness, one can also include a control-dependent initial state, but this is unnecessary for our analysis.

To see where the assumption of no free evolution comes into play and why it is the cause, it is sufficient to examine one wing of our setup. Comparing a single-cavity scenario, (3.18), and a generic quantum switch, (3.31), one finds that the evolution operators $\hat{U}_1$ and $\hat{U}_2$ in (3.18) do not directly represent the local operations $\hat{U}^A$ and $\hat{U}^B$. The reason is that $\hat{U}_1$ and $\hat{U}_2$ are written in the Dirac (interaction) picture, which necessarily includes time evolution with respect to the free Hamiltonian (starting from an initial time established in a common reference frame). By unraveling this time evolution, one finds precisely a state of the form (3.31), where $\hat{V}_0$ and $\hat{V}_1$ represent the free evolution of the targets (i.e., cavity and detectors) between the interactions. Note that the time intervals between events, and thus intervals of free evolution, are equal in the reference frame of the cavity, meaning that in that frame $\hat{V}_0 = \hat{V}_1$. On the other hand, $\hat{U}^A$ and $\hat{U}^B$ describe *only* the field-cavity interactions in the Schrödinger picture[4].

This is relevant because if the free Hamiltonian does not commute with the interaction, the free evolution does not commute with $\hat{U}^A$ and $\hat{U}^B$, which explains the presence of entanglement in the state in (3.32) in a frame where $\hat{V}_0 = \hat{V}_1$ and the events are spacelike separated. Note that in that case, there is a reference frame where $A_j \prec B_j$ for both states of the control; however, as mentioned above, in that frame necessarily $\hat{V}_0 \neq \hat{V}_1$ since the time intervals of free evolution along the worldlines of molecules 1 and 2 are necessarily different. In such a frame, the final state in the two-wing scenario becomes

$$|\psi_{\text{fin}}\rangle = \frac{1}{\sqrt{2}}\Big(|0\rangle\,\hat{U}^{B_1}\hat{V}_0\hat{U}^{A_1}\,|\psi\rangle\otimes\hat{U}^{B_2}\hat{V}_0\hat{U}^{A_2}\,|\psi\rangle \;+\; |1\rangle\,\hat{U}^{B_1}\hat{V}_1\hat{U}^{A_1}\,|\psi\rangle\otimes\hat{U}^{B_2}\hat{V}_1\hat{U}^{A_2}\,|\psi\rangle\Big)\,, \tag{3.33}$$

and the presence of entanglement is thus interpreted as due to overall different dynamics depending on the control, $\hat{U}^{B_i}\hat{V}_0\hat{U}^{A_i} \neq \hat{U}^{B_i}\hat{V}_1\hat{U}^{A_i}$ i.e., in that frame while the order of operations is common, when they take place relative to periods of free dynamics, and thus the overall evolution, depends on the control. Crucially, in this case, temporal order among events cannot even be defined as it depends on the reference frame.

Further discussion of the role played by free evolution in this protocol is presented in the next section.

In fact, if free evolution and the applied operations do not commute, even simpler scenarios can illustrate the issue. Consider that one of the operations is trivial, say $\hat{U}^B = \hat{\mathbb{I}}$, so in fact only *one* operation is applied. The non-commutativity between $\hat{U}_A$ and $\hat{V} = \hat{V}_0 = \hat{V}_1$ (we are in the reference frame of the cavity) would again result in different final states depending on when $\hat{U}^A$

[4]Strictly speaking, we should add free-evolution operators also before and after the two local unitaries—not only in between. However, free evolution acts trivially on the vacuum state (our initial state), while the final evolution can be absorbed into the definition of the measurement basis.

is applied relative to $\hat{V}$. This would again lead to an entangled final state in a two-wing scenario, even though in this case, there is no time order of events to speak of.

Finally, we note that in all quantum switch scenarios, including the entangled switch, there is an assumption that each local operation is performed 'only once'. This condition is, however, naturally satisfied in relativistic implementations such as ours, as each operation is performed at a specific time on a local clock.

We have focused so far on a particular realization of the entangled switch protocol—with two-level 'detectors' and cavity-confined quantum field modes as targets, and the position degrees of freedom of the detectors as the control. However, our main result and its explanation apply to any physical realization of the protocol. Indeed, we have shown that entanglement can be generated for spacelike separated operations and identified that this is due to the free evolution of the targets. For any physical implementation of the protocol, if the applied operations do not commute with the free evolution, the final state will generally be entangled regardless of the commutation relations between the operations themselves, and thus also regardless of their temporal order. Entanglement can arise even if only one operation is applied, as discussed in the previous section.

3.2.7 Entanglement Generation for Spacelike Events and Its Implications

The results from the previous section demonstrate that Bell inequalities for temporal order can be violated even when the interaction events are spacelike separated. This statement seems paradoxical because for spacelike separated events, their temporal order cannot be defined—it depends on the reference frame. Here, we examine the compatibility of this fact with the locality of evolution.

Consider the cavity and two molecules placed near its boundaries. We know that entanglement at spacelike separation appears for a short interaction time and small time dilation (see Fig. 3.4). By definition, in such scenarios, information about the interaction with the field cannot be transferred from the first to the second detector before the latter interacts with the field. To illustrate the problem with this situation, we can divide the whole cavity into three parts (see Fig. 3.5). Let us denote these as F_L, F, and F_R. The field F_L refers to the part of the cavity near the left detector, and similarly, F_R describes the right part of the cavity. The field F refers to the middle segment of the entire cavity. The lengths of each part are chosen to ensure that information about the interaction with the left/right molecule can be localized only within the left/right part of the cavity. This division allows us to capture the two alternative orders of events as follows.

For one order, the left molecule interacts first, $L \prec R$; for the other, the right molecule interacts

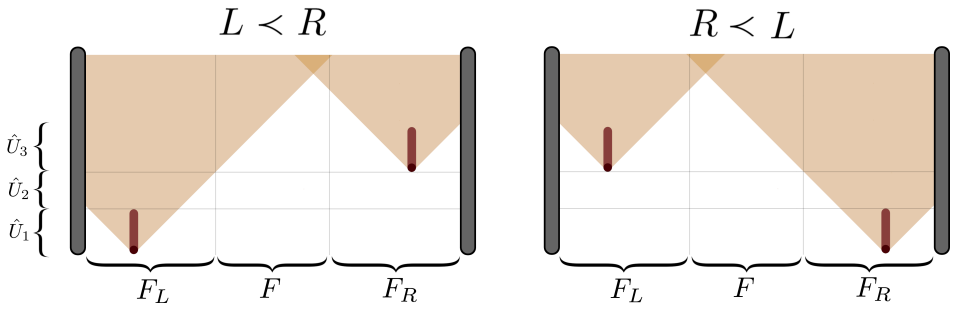

Figure 3.5: **Spacetime diagram of a cavity interacting with two detectors.** Operators $\hat{U}_1$ and $\hat{U}_3$ describe the evolution of the system according to the interaction, and $\hat{U}_2$ is an operator of the free evolution that occurs between interactions. F_L and F_R are parts of the cavity that can interact with the detector in some finite time. F is a middle segment of the cavity that evolves only due to the free evolution operator between interactions.

first, $R \prec L$. The entire evolution $\hat{U}$ of the system containing the two molecules and three parts of the cavity can then be represented as $\hat{U} = \hat{U}_3\ \hat{U}_2\ \hat{U}_1$, where:

- $\hat{U}_1$ – interaction of the left (right) molecule with F_L (F_R) and free evolution of the remaining parts.
- $\hat{U}_2$ – free evolution of the entire cavity.
- $\hat{U}_3$ – interaction of the right (left) molecule with F_R (F_L) and free evolution of the remaining parts.

The two scenarios appear to differ solely by the order of events at which the detectors and the field interact. If these events are spacelike, one would not expect any difference between the two scenarios based on the original argument. However, the free evolution always includes components that are timelike relative to one of the interaction events, and generally, the three evolution operators do not commute.

Thus, despite the spacelike separation of the interaction events, the free part of the evolution still influences the system, resulting in a different state of the targets for the two wings of the protocol. This implies that for such a case, we cannot argue that the violation of Bell inequalities signifies an indefinite order of events because we violate an additional assumption: there is an extra part of the evolution of the target systems, and it is this evolution that causes a different final state despite the spacelike separation of the events at which the interactions defining the order occur.

However, we contend that this assumption is unavoidable in a generic realization of the studied protocol, including its gravitational version. Indeed, it is possible to identify implementations where the assumption of no free evolution of the targets holds (e.g., with polarization or angular momentum degrees of freedom of photons) or where the operations are performed within a degenerate subspace of the Hamiltonian of the targets (and thus commute with free evolution), making only the non-commutativity between the two local operations relevant. Such strategies would lead to an entangled final state only if the local operations are timelike and applied in a non-classical order. However, identifying such implementations requires a theoretical description of the states and dynamics of the involved systems. In other words, theory-dependent assumptions are needed to interpret a violation of the final Bell inequalities as a signature of indefinite temporal order, while a theory-independent method to certify non-classical time order was one of the key motivations of [71].

Furthermore, the above observation is not dependent on the special-relativistic setting studied in this work and equally applies to gravitational protocols. Indeed, nothing in our argument depends on how the time dilation of the clocks is achieved. For example, the position of a massive body can determine—through gravitational time dilation—the time at which a single operation occurs (relative to some mass-independent coordinates). This can lead to the same situation described earlier: the creation of entanglement (in a two-wing scenario) even with a single operation per wing. Again, theory-dependent assumptions would be required to ensure that entanglement can only arise as a result of an indefinite order of events.

3.3 Conclusions of the chapter

In this section, we constructed a non-gravitational scenario where accelerating particles, interacting with quantum fields according to their own internal clock degrees of freedom, can lead to a violation of the temporal Bell inequalities similar to the gravitational case. In 3.2.1, we introduced the formalism required to replicate the gravitational protocol using special relativistic time dilation. We defined the kinematics of all particles involved in the protocol and the appropriate coupling between them and the quantum field. We discussed the complete protocol that explicitly demonstrated a violation of Bell inequalities, which are claimed to test the indefinite temporal order of events.

We described the procedure that would lead to the violation of Bell inequalities for the proposed system, occurring even when the events responsible for the entanglement are spacelike, which we interpreted as an ambiguity in the signature of indefinite temporal order. We found that this surprising conclusion results from the failure of the additional assumption that target systems have no other evolution except the one governed by unitaries applied in a specific time order.

We presented a detailed discussion of this problem in the last two sections of our work.

We argued that to satisfy all assumptions of the Bell theorem for time order—including the auxiliary one (of no free evolution of the targets)—it is essential to invoke theory-dependent arguments. Moreover, in a generic implementation—including a gravitational version of the protocol—this assumption is not met. The present work is the first in the existing literature to investigate this assumption and its consequences. Our chosen model thus clarifies the overlooked aspect of Bell inequalities for temporal order. Consequently, our conclusions hold significance for any theoretical or experimental pursuit of indefinite temporal order.

Being able to describe and experimentally test entangled temporal order (i.e., even working fully within quantum mechanics) is of interest in its own right. Our result, however, raises the question of whether it is possible to formulate a stronger, theory-independent test of temporal order. The insight from this study is that it is problematic to separate the effect of the free dynamics of the system from that of the local operations. A possible avenue to circumvent this is to consider more general operations than the fixed unitaries discussed thus far: they can involve a measurement of the system, producing a classical variable as the outcome. Furthermore, a setting variable for each party can model a choice among different operations. In this manner, one can consider directly the causal relations between parties—understood operationally as correlations between settings and outcomes—without relying on a theory-dependent description of the transformations. We leave further investigation of this possibility to future work.

3.4 Appendices

3.4.1 Details of calculations of the final state

Using the form of evolution operator (3.7) we can find that

$$|\psi_R\rangle = \hat{U}_1\hat{U}_2 |g\rangle |g\rangle |0\rangle = |g\rangle |g\rangle |0\rangle - i\lambda \int \mathrm{d}t_2 \chi_{2R}(t_2) \sum_k \frac{1}{\sqrt{\omega_k L}} e^{i(\omega_k+\Omega)t_2} \sin\left(\frac{k\pi}{L}x_2\right) |g\rangle |e\rangle \hat{a}_k^\dagger |0\rangle$$
$$-i\lambda \int \mathrm{d}t_1 \chi_{1R}(t_1) \sum_k \frac{1}{\sqrt{\omega_k L}} e^{i(\omega_k+\Omega)t_1} \sin\left(\frac{k\pi}{L}x_1\right) |e\rangle |g\rangle \hat{a}_k^\dagger |0\rangle + \mathcal{O}(\lambda^2), \tag{3.34}$$

where: χ_{1R}–switching function for the first detector in the case that right detector interacts before the left one, χ_{2R}–switching function for the second detector in the case that right detector interacts earlier. We assume that the interaction starts and ends rapidly, so that $\chi_{2R}(t) = 1$ for $t \in (0, T)$ and $\chi_{2R}(t) = 0$ for any other time. Similarly, $\chi_{1R}(t) = 1$ for $t \in (\Delta\tau, \Delta\tau + T)$ and

$\chi_{1R}(t) = 0$ for any other time. We can proceed with the same calculation for $|\psi_L\rangle$

$$|\psi_L\rangle = \hat{U}_2\hat{U}_1 |g\rangle |g\rangle |0\rangle = |g\rangle |g\rangle |0\rangle - i\lambda \int \mathrm{d}t_2 \chi_{2L}(t_2) \sum_k \frac{1}{\sqrt{\omega_k L}} e^{i(\omega_k+\Omega)t_2} \sin\left(\frac{k\pi}{L}x_2\right) |g\rangle |e\rangle \hat{a}_k^\dagger |0\rangle$$
$$-i\lambda \int \mathrm{d}t_1 \chi_{1L}(t_1) \sum_k \frac{1}{\sqrt{\omega_k L}} e^{i(\omega_k+\Omega)t_1} \sin\left(\frac{k\pi}{L}x_1\right) |e\rangle |g\rangle \hat{a}_k^\dagger |0\rangle + \mathcal{O}(\lambda^2), \tag{3.35}$$

where: χ_{1L}–switching function for the first detector in the case that right detector interacts before the left one, χ_{2L}–switching function for the second detector in the case that right detector interacts earlier. In this case we have that $\chi_{1L}(t) = 1$ for $t \in (0, T)$ and $\chi_{1L}(t) = 0$ for any other time. Similarly, $\chi_{2L}(t) = 1$ for $t \in (\Delta\tau, \Delta\tau + T)$ and $\chi_{2L}(t) = 0$ for any other time. It worth noticing that $\chi_{1L} = \chi_{2R}$ and $\chi_{2L} = \chi_{1R}$. After using this property describing relation between switching functions, we have

$$|\psi_R\rangle = \hat{U}_1\hat{U}_2 |g\rangle |g\rangle |0\rangle = |g\rangle |g\rangle |0\rangle - i\lambda \int \mathrm{d}t_2 \chi_{2R}(t_2) \sum_k \frac{1}{\sqrt{\omega_k L}} e^{i(\omega_k+\Omega)t_2} \sin\left(\frac{k\pi}{L}x_2\right) |g\rangle |e\rangle \hat{a}_k^\dagger |0\rangle$$
$$-i\lambda \int \mathrm{d}t_1 \chi_{1R}(t_1) \sum_k \frac{1}{\sqrt{\omega_k L}} e^{i(\omega_k+\Omega)t_1} \sin\left(\frac{k\pi}{L}x_1\right) |e\rangle |g\rangle \hat{a}_k^\dagger |0\rangle + \mathcal{O}(\lambda^2), \tag{3.36}$$

$$|\psi_L\rangle = \hat{U}_2\hat{U}_1 |g\rangle |g\rangle |0\rangle = |g\rangle |g\rangle |0\rangle - i\lambda \int \mathrm{d}t_2 \chi_{2R}(t_2) \sum_k \frac{1}{\sqrt{\omega_k L}} e^{i(\omega_k+\Omega)t_2} \sin\left(\frac{k\pi}{L}x_1\right) |e\rangle |g\rangle \hat{a}_k^\dagger |0\rangle$$
$$-i\lambda \int \mathrm{d}t_1 \chi_{1R}(t_1) \sum_k \frac{1}{\sqrt{\omega_k L}} e^{i(\omega_k+\Omega)t_1} \sin\left(\frac{k\pi}{L}x_2\right) |g\rangle |e\rangle \hat{a}_k^\dagger |0\rangle + \mathcal{O}(\lambda^2). \tag{3.37}$$

For simplicity of further calculation, let us introduce the following notation

$$|\psi_R\rangle = \hat{U}_1\hat{U}_2 |g\rangle |g\rangle |0\rangle = |gg\rangle |0\rangle + |ge\rangle \left|\phi_{ge}^R\right\rangle + |eg\rangle \left|\phi_{eg}^R\right\rangle + \mathcal{O}(\lambda^2), \tag{3.38}$$

$$|\psi_L\rangle = \hat{U}_2\hat{U}_1 |g\rangle |g\rangle |0\rangle = |gg\rangle |0\rangle + |ge\rangle \left|\phi_{ge}^L\right\rangle + |eg\rangle \left|\phi_{eg}^L\right\rangle + \mathcal{O}(\lambda^2), \tag{3.39}$$

where: $\left|\phi_{ge}^L\right\rangle$–a state of a field when the left detector interacts first but the right detector is excited, $\left|\phi_{eg}^L\right\rangle$–a state of a field when the left detector interacts first and the left detector is excited, $\left|\phi_{ge}^R\right\rangle$–a state of a field when the right detector interacts first and the right detector is excited, $\left|\phi_{eg}^R\right\rangle$–a state of a field when the right detector interacts first but the left detector is excited as a consequence of the interaction between atoms and the field.

3.4.2 Method of finding appropriate parameters

In this section we will find an appropriate set of parameters that orthogonalize $|\Phi_R\rangle$ and $|\Phi_L\rangle$ vectors

$$\begin{aligned}
|\Phi_R\rangle &= -i\lambda \sum_k \frac{1}{\sqrt{\omega_k L}} \int \mathrm{d}t \left(\chi_{2R}(t) \sin\left(\frac{k\pi}{L} x_2\right) + \chi_{1R}(t) \sin\left(\frac{k\pi}{L} x_1\right) \right) e^{i(\omega_k+\Omega)t} \hat{a}_k^\dagger |0\rangle \\
&= -i\lambda \sum_k \int \mathrm{d}t \left(\chi_{2R}(t) u_k(x_2) + \chi_{1R}(t) u_k(x_1) \right) e^{i(\omega_k+\Omega)t} \hat{a}_k^\dagger |0\rangle \\
&= -\lambda \sum_k \frac{e^{iT(\omega_k+\Omega)} - 1}{\omega_k + \Omega} \left(e^{i\Delta\tau(\omega_k+\Omega)} u_k(x_1) + u_k(x_2) \right) \hat{a}_k^\dagger |0\rangle \qquad (3.40) \\
|\Phi_L\rangle &= -i\lambda \sum_k \frac{1}{\sqrt{\omega_k L}} \int \mathrm{d}t \left(\chi_{2R}(t) \sin\left(\frac{k\pi}{L} x_1\right) + \chi_{1R}(t) \sin\left(\frac{k\pi}{L} x_2\right) \right) e^{i(\omega_k+\Omega)t} \hat{a}_k^\dagger |0\rangle \\
&= -\lambda \sum_k \frac{e^{iT(\omega_k+\Omega)} - 1}{\omega_k + \Omega} \left(e^{i\Delta\tau(\omega_k+\Omega)} u_k(x_2) + u_k(x_1) \right) \hat{a}_k^\dagger |0\rangle \qquad (3.41)
\end{aligned}$$

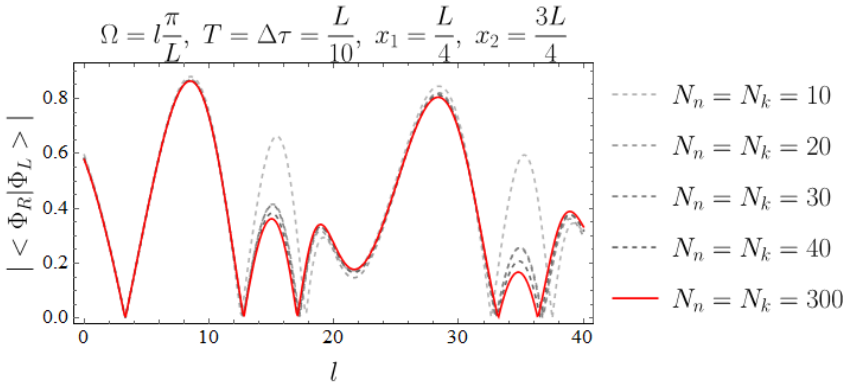

Figure 3.6: **The analysis of an orthogonality between $|\Phi_L\rangle$ and $|\Phi_R\rangle$.**The absolute value of the scalar product as a function of the energy gap of the detector Ω.

Where the form of the state $|\Phi_L\rangle$ we get by changing $x_1 \longleftrightarrow x_2$. Now it is easy to see that the scalar product can be written as:

$$\begin{aligned}
\langle\Phi_R|\Phi_L\rangle &\cong \lambda^2 \sum_k \frac{\left| e^{iT(\omega_k+\Omega)} - 1 \right|^2}{(\omega_k+\Omega)^2} \left(e^{-i\Delta\tau(\omega_k+\Omega)} u_k(x_1) + u_k(x_2) \right) \left(e^{i\Delta\tau(\omega_k+\Omega)} u_k(x_2) + u_k(x_1) \right) \\
&\cong 2\lambda^2 \sum_k \frac{e^{-i\Delta\tau(\omega_k+\Omega)}}{(\omega_k+\Omega)^2} \left[1 - \cos\left(T(\omega_k+\Omega) \right) \right] \left(u_k(x_1) + e^{i\Delta\tau(\omega_k+\Omega)} u_k(x_2) \right)^2 \qquad (3.42)
\end{aligned}$$

We have to remember that states $|\Phi_L\rangle$ and $|\Phi_R\rangle$ were not properly normalized so now we can find the norm

$$\||\Phi_R\rangle\| = \sqrt{\langle\Phi_R|\Phi_R\rangle} = \sqrt{\lambda^2 \sum_k \frac{\left|e^{iT(\omega_k+\Omega)}-1\right|^2}{(\omega_k+\Omega)^2}\left|e^{i\Delta\tau(\omega_k+\Omega)}u_k(x_1)+u_k(x_2)\right|^2}$$

$$= 2\lambda\sqrt{\sum_k \frac{\sin^2\frac{T(\omega_k+\Omega)}{2}}{(\omega_k+\Omega)^2}\left[u_k(x_1)^2+2u_k(x_1)u_k(x_2)\cos\left(\Delta\tau(\omega_k+\Omega)\right)+u_k(x_2)^2\right]} \tag{3.43}$$

$$\||\Phi_L\rangle\| = \sqrt{\langle\Phi_L|\Phi_L\rangle} = 2\lambda\sqrt{\sum_k \frac{\sin^2\frac{T(\omega_k+\Omega)}{2}}{(\omega_k+\Omega)^2}\left[u_k(x_2)^2+2u_k(x_2)u_k(x_1)\cos\left(\Delta\tau(\omega_k+\Omega)\right)+u_k(x_1)^2\right]} \tag{3.44}$$

We can notice that $\||\Phi_R\rangle\| = \||\Phi_L\rangle\|$ and finally the scalar product has the following form

$$\langle\Phi_R|\Phi_L\rangle = \frac{\langle\Phi_R|\Phi_L\rangle}{\||\Phi_R\rangle\|\||\Phi_L\rangle\|} = \frac{\sum_k \frac{e^{-i\Delta\tau(\omega_k+\Omega)}}{(\omega_k+\Omega)^2}\left[1-\cos\left(T(\omega_k+\Omega)\right)\right]\left(u_k(x_1)+e^{i\Delta\tau(\omega_k+\Omega)}u_k(x_2)\right)^2}{2\sum_n \frac{\sin^2\frac{T(\omega_n+\Omega)}{2}}{(\omega_n+\Omega)^2}\left[u_n(x_2)^2+2u_n(x_2)u_n(x_1)\cos\left(\Delta\tau(\omega_n+\Omega)\right)+u_n(x_1)^2\right]} \tag{3.45}$$

This function can be estimated as a finite sum. Let us denote the upper limits of these two sums as N_n for the sum over n and N_k for the sum over k.

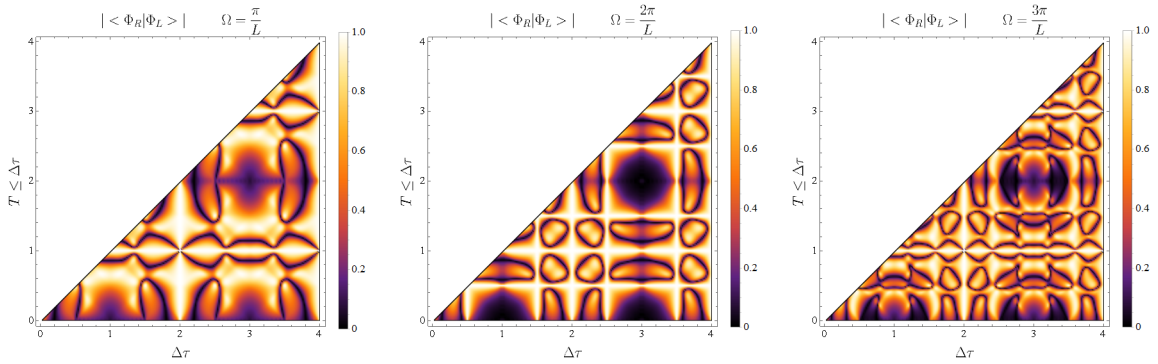

Figure 3.7: **The analysis of an orthogonality between $|\Phi_L\rangle$ and $|\Phi_R\rangle$ for different parameters describing interaction.**
An absolute value of the scalar product for two detectors standing at $x_1 = L/4$ and $x_2 = 3L/4$. The energy gap Ω is chosen as one of the cavity frequencies. Scalar product approximated as a finite sum of 30 modes i.e. $N_k = N_n = 30$.

Fig. 3.6 shows the absolute value of the scalar product as a function of the energy gap Ω plotted

for different numbers of modes N_n and N_k. We can see that we can produce entanglement for very short times $\Delta\tau = T = L/10$. Thus, it proves that there is an entanglement between two cavities also for spacelike separated events of interaction.

Fig. 3.6 look quite random. Let us analyze the scalar product for the case of two detectors standing in the positions $x_1 = L/4$ and $x_2 = 3L/4$. Fig. 3.7 show the absolute value of the scalar product for different parameters $\Delta\tau$ and $T \leq \Delta\tau$ for different values of the energy gap Ω. We can notice that there are many parameters minimizing the scalar product between two states.

Based on Fig. 3.7 we can conjecture that point $(\Delta\tau, T) = (3L, 2L)$ is a good candidate for the orthogonalization of the states $|\Phi_R\rangle$ and $|\Phi_L\rangle$. To verify this hypothesis let us consider the following calculation: Let $L = 1$, $x_1 = 1/4$, $x_2 = 3/4$, $\Omega = \pi$, $\Delta\tau = 3$, $T = 2 + \epsilon$, where $\epsilon \in \mathbb{R}_+$ is a small parameter. Then

$$\langle\Phi_R|\Phi_L\rangle = -\frac{\sum_k \frac{e^{-3ik\pi}}{k(k+1)^2}\left[\cos\left((1+k)(2+\epsilon)\pi\right) - 1\right]\left(\sin\frac{k\pi}{4} - e^{3ik\pi}\sin\frac{3k\pi}{4}\right)^2}{2\sum_n \frac{\sin^2\frac{(n+1)\pi\epsilon}{2}}{2n(n+1)^2}\left[(1+2(-1)^n)\cos\frac{n\pi}{2} + \cos\frac{3n\pi}{2} - 4\right]}. \tag{3.46}$$

Each of these sums can be done analytically for arbitrary ϵ. Then we expand the numerator and denominator around $\epsilon = 0$, to get

$$|\langle\Phi_R|\Phi_L\rangle| = \left|\frac{\frac{1}{2\pi}\left(2\log 20\log(1-i) - \log(1+i)\right)\epsilon^2 + \mathcal{O}(\epsilon^3)}{\frac{1}{6\pi}\left(9 + \log 8 - 6\log\pi - 6\log\epsilon\right)\epsilon^2 + \mathcal{O}(\epsilon^3)}\right| \approx \frac{\log 8}{9 + \log 8 - 6\log\pi\epsilon}. \tag{3.47}$$

And we see that

$$\lim_{\epsilon\to 0^+} |\langle\Phi_R|\Phi_L\rangle| = 0 \tag{3.48}$$

3.4.3 Second order of the Dyson series

In this section, We will show that second-order Dyson expansion does not affect on $|\Phi_R\rangle$ and $|\Phi_L\rangle$.

One can ask the question why (3.42) depends on λ^2. Previously we limited our calculation only to the first-order expansion of the Dyson series. We have to verify that second-order expansion does not produce lambda square terms too. Otherwise, there is a possibility that results from (3.42) will cancel out with these additional terms. Let us write the general evolution operator

in the following form

$$\hat{U} = \mathbb{1} - i\lambda \int_{-\infty}^{\infty} \mathrm{d}t\ \chi_d(t) \left(e^{i\Omega t}\hat{\sigma}^+ + e^{-i\Omega t}\hat{\sigma}^-\right) \sum_n \left(\hat{a}_n^\dagger u_n(x_d) e^{i\omega_n t} + \hat{a}_n u_n(x_d) e^{-i\omega_n t}\right) \tag{3.49}$$
$$-\lambda^2 \int_{-\infty}^{\infty} \mathrm{d}t_2 \int_{-\infty}^{t_2} \mathrm{d}t_1\ \chi_d(t_2)\chi_d(t_1) \left(e^{i\Omega t_2}\hat{\sigma}^+ + e^{-i\Omega t_2}\hat{\sigma}^-\right) \left(e^{i\Omega t_1}\hat{\sigma}^+ + e^{-i\Omega t_1}\hat{\sigma}^-\right)$$
$$\times \sum_n \left(\hat{a}_n^\dagger u_n(x_d) e^{i\omega_n t_2} + \hat{a}_n u_n(x_d) e^{-i\omega_n t_2}\right) \sum_m \left(\hat{a}_m^\dagger u_m(x_d) e^{i\omega_m t_1} + \hat{a}_m u_m(x_d) e^{-i\omega_m t_1}\right),$$

where x_d is a position of a detector and $\hat{\sigma}^\pm$ acts on the internal state of this detector. In our case we have two detectors and two Hilbert spaces of internal degrees of freedom. We can simplify the notation to write operators of the evolution as

$$\hat{U}_1 = \mathbb{1} - i\lambda \sum_n \left(\hat{U}_{1n}^+ \hat{\sigma}_1^+ + \hat{U}_{1n}^- \hat{\sigma}_1^-\right) - \lambda^2 \sum_{n,m} \left(\hat{U}_{1nm}^{++} \hat{\sigma}_1^+ \hat{\sigma}_1^+ + \hat{U}_{1nm}^{+-} \hat{\sigma}_1^+ \hat{\sigma}_1^- + \hat{U}_{1nm}^{-+} \hat{\sigma}_1^- \hat{\sigma}_1^+ + \hat{U}_{1nm}^{--} \hat{\sigma}_1^- \hat{\sigma}_1^-\right), \tag{3.50}$$

$$\hat{U}_2 = \mathbb{1} - i\lambda \sum_n \left(\hat{U}_{2n}^+ \hat{\sigma}_2^+ + \hat{U}_{2n}^- \hat{\sigma}_2^-\right) - \lambda^2 \sum_{n,m} \left(\hat{U}_{2nm}^{++} \hat{\sigma}_2^+ \hat{\sigma}_2^+ + \hat{U}_{2nm}^{+-} \hat{\sigma}_2^+ \hat{\sigma}_2^- + \hat{U}_{2nm}^{-+} \hat{\sigma}_2^- \hat{\sigma}_2^+ + \hat{U}_{2nm}^{--} \hat{\sigma}_2^- \hat{\sigma}_2^-\right), \tag{3.51}$$

where $U_{1n}^\pm$, $U_{2n}^\pm$ are operators from the first-order order expansion and $U_{1nm}^{\pm\pm}$ and $U_{2nm}^{\pm\pm}$ are operators from the second-order expansion of the Dyson series. $\hat{\sigma}_1^\pm$ and $\hat{\sigma}_2^\pm$ are operators $\hat{\sigma}^\pm$ acting on the internal space of the first or the second detector respectivly. To find contributions proportional to the λ^2 to the value of (3.42), we have to find new terms in the $|\psi_R\rangle$ and $|\psi_L\rangle$ proportional to $|ge\rangle$ or $|eg\rangle$. Knowing that $|\psi_R\rangle = \hat{U}_1\hat{U}_2 |gg\rangle |0\rangle$, $|\psi_L\rangle = \hat{U}_2\hat{U}_1 |gg\rangle |0\rangle$, $\hat{\sigma}^- |g\rangle = 0$ and $\hat{\sigma}^+ |e\rangle = 0$ we can write

$$|\psi_R\rangle = \left[\mathbb{1} - i\lambda \sum_n \hat{U}_{1n}^+ \hat{\sigma}_1^+ - \lambda^2 \sum_{n,m} \hat{U}_{1nm}^{-+} \hat{\sigma}_1^- \hat{\sigma}_1^+\right] \left[\mathbb{1} - i\lambda \sum_n \hat{U}_{2n}^+ \hat{\sigma}_2^+ - \lambda^2 \sum_{n,m} \hat{U}_{2nm}^{-+} \hat{\sigma}_2^- \hat{\sigma}_2^+\right] |gg\rangle |0\rangle, \tag{3.52}$$

$$|\psi_L\rangle = \left[\mathbb{1} - i\lambda \sum_n \hat{U}_{2n}^+ \hat{\sigma}_2^+ - \lambda^2 \sum_{n,m} \hat{U}_{2nm}^{-+} \hat{\sigma}_2^- \hat{\sigma}_2^+\right] \left[\mathbb{1} - i\lambda \sum_n \hat{U}_{1n}^+ \hat{\sigma}_1^+ - \lambda^2 \sum_{n,m} \hat{U}_{1nm}^{-+} \hat{\sigma}_1^- \hat{\sigma}_1^+\right] |gg\rangle |0\rangle. \tag{3.53}$$

We can observe that second-order contributions from the same detector do not change the internal state, i.e. $\hat{\sigma}^-\hat{\sigma}^+ |g\rangle = |g\rangle$, while the product of first order terms from both detectors gives $\hat{\sigma}_1^+\hat{\sigma}_2^+ |gg\rangle = \hat{\sigma}_2^+\hat{\sigma}_1^+ |gg\rangle = |ee\rangle$. Thus, the second order terms do not have support on the subspace spanned by the states $|ge\rangle, |eg\rangle$. Note that the states $|ge\rangle$ or $|eg\rangle$ appear in this

expansion at order λ^3 or higher. This means that second-order terms from the Dyson series do not affect the states $|\Phi_R\rangle$ and $|\Phi_L\rangle$ in our approximation.

4 Conclusions

This dissertation has explored the relativistic aspects of time in quantum mechanics, divided into two main areas: the study of quantum time dilation and the examination of indefinite temporal order, including the implications of temporal Bell inequalities.

A major focus of this research was to understand how time dilation operates within the quantum domain. Known from relativity, time dilation implies that time pases slower for objects at high velocities or in strong gravitational fields. Our research showed that this well-known phenomenon can be generalized to the case of an atom moving in a superposition of velocities or in a superposition of positions in the case of gravitational time dilation. We also discovered that kinematical quantum time dilation is universal, much like its classical counterpart. In this context, universality means that it is independent of the type of mechanism used as a clock.

In section 2.2, we demonstrated a spectroscopic signature of quantum time dilation, observed in the spontaneous emission rate or the lifetime of an excited atom moving in a superposition of relativistic momentum wave packets. Our analysis indicated that the total transition rate is significantly affected by the momentum coherence in the atom's center-of-mass state. Notably, the quantum contribution to the observed time dilation could be positive or negative, depending on the relative phase between the superposed momentum states. These quantum effects are accessible with current experimental setups, such as optical clocks [79, 105–108].

Additionally, we observed a correspondence between quantum time dilation in atomic lifetimes and that observed by an ideal clock in a different physical system [54, 157]. This finding underscores the universality of quantum time dilation, indicating that it affects all clocks similarly, regardless of their underlying mechanisms.

Our spectroscopic approach highlighted the role of coherence across relativistic momentum wave packets. By probing proper time superpositions in this regime, our study provided a unique view of the interplay between quantum theory and relativity.

We also investigated the presence of a quantum Doppler effect, which arises when an atom's center-of-mass is in a superposition of momentum wave packets. This effect manifests in the shape of the emission spectrum, particularly smoothing the contrast between the typical Doppler-shifted peaks.

In section 2.3, we examined a realistic scenario where quantum time dilation in a gravitational field is anticipated. By analyzing the spontaneous emission process of a two-level atom at rest in an external gravitational field, modeled as an accelerated frame of reference according to the equivalence principle, we showed that the atom's spontaneous emission rate depends on its wave function in position space. Specifically, this rate is influenced by spatial coherence in the atom's center-of-mass state. Our findings, consistent with [126] for a realistic clock model, confirm that quantum time dilation occurs in practical scenarios. This further substantiates that quantum time dilation is not merely theoretical but can be observed in real-world conditions. By applying the equivalence principle to describe the gravitational effect on the clock, we concluded similarly to a post-Newtonian analysis, suggesting our results validate the equivalence principle for quantum systems.

Our analysis proposed a method to detect quantum time dilation by placing a decaying particle in a superposition of heights and observing the decay rate's dependence on the particle's initial state. Similarly, a spectroscopic method involves positioning a clock (either ionic or atomic) in a superposition of heights and measuring either the spontaneous decay or the fractional frequency shift. According to our findings, the coherence effect becomes significant when the spread of two position wave packets is comparable to the distance between them. The quantum correction to classical time dilation can match the classical gravitational time dilation factor for appropriately chosen state parameters. Thus, if gravitational time dilation can be measured at such distances, the quantum time dilation effect should also be detectable.

Typically, experimental measurements of gravitational time dilation involve comparing two clocks at different heights, as demonstrated in tabletop experiments [173], flight-based clocks [174], or clocks separated by large distances [175]. Future advancements include satellite-based experiments aimed at improving accuracy by orders of magnitude [176, 177]. Recent developments with optical lattice clocks have shown the potential to resolve gravitational redshift within a single sample on a sub-millimeter scale [178, 179]. Specifically, a frequency change consistent with the linear gravitational field was measured along a system of 100,000 strontium atoms [178], with the atoms uncorrelated to suppress corrections due to quantum coherence across the sample.

We demonstrated that for an optimally prepared state in a simple spectroscopic system, the gravitational quantum time dilation effect is comparable to the gravitational redshift caused by a millimeter-sized height difference near Earth's surface. In the best-case scenario, with two overlapping wave packets of opposite relative phase, the change in the total emission rate scales as $\frac{g\Delta}{4c^2}\Gamma_0$, where Δ is the spatial spread of the wave packets. For micrometer-scale superpositions [180–183], this results in a 10^{-23} change in the total emission rate or the fractional frequency shift. Although current measurements of atomic lifetimes and emission rates lack the precision to detect such a small correction—typically determined up to tenths of a percent [184–186]—the correction

to the fractional frequency shift is just below the sensitivity of state-of-the-art measurements, which detect gravitational time dilation on millimeter scales [178, 179, 187, 188]. Increasing the spatial superposition scale from micrometers to millimeters would result in a correction of the order of 10^{-20}, within the reach of current technology. With recent advances in optical clocks, the next step is to develop a method to prepare the optimal superposition state and observe quantum time dilation unambiguously using present-day technology.

Finally, in section 2.4, we demonstrated that while kinematic quantum time dilation is universal, gravitational quantum time dilation is not. Our proof of universality provided a necessary condition for quantum reference frames to be well-defined [189]. We also argued that defining quantum time dilation depends on an arbitrary choice of the classical reference state, and for other equally valid choices, the effect disappears. However, we derived an alternative quantum time dilation effect that appears with higher-order coupling terms between translational and internal degrees of freedom. Here, the quantum noncommutativity of the involved position and momentum operators ensures that the effect has no classical counterpart. Our findings clarify the current understanding of quantum time dilation, offering insights into its universality and fundamental nature.

The second major part of this dissertation, chapter 3, explored the concept of indefinite temporal order. In classical physics, events occur in a definite sequence: one event happens before or after another. In the quantum realm, however, events can occur in a superposition of different orders, meaning the sequence of events is not fixed and can be indefinite.

We devised a non-gravitational scenario where accelerating particles, interacting with quantum fields according to their own internal clock degrees of freedom, could lead to a violation of temporal Bell inequalities similar to the gravitational case. In 3.2.1, we introduced the formalism needed to replicate the gravitational protocol using special relativistic time dilation. We defined the kinematics of all particles involved and the appropriate coupling between them and the quantum field. We outlined the complete protocol that clearly demonstrated a violation of Bell inequalities, which are intended to test the indefinite temporal order of events.

We described the procedure that would lead to the violation of Bell inequalities for the proposed system, occurring even when the events responsible for the entanglement are spacelike, which we interpreted as ambiguity in the signature of indefinite temporal order. We found this surprising conclusion resulted from the failure of the assumption that target systems have no other evolution besides the one governed by unitaries applied in a specific time order.

We argued that to satisfy all assumptions of Bell's theorem for time order—including the auxiliary assumption of no free evolution of the targets—it is crucial to use theory-dependent arguments. Moreover, in a generic implementation—including a gravitational version of the protocol—this assumption is not satisfied. This work is the first to investigate this assumption and

its implications in the existing literature. Our model clarifies an overlooked aspect of Bell inequalities for temporal order, making our conclusions significant for theoretical and experimental pursuits of indefinite temporal order.

Describing and experimentally testing entangled temporal order within quantum mechanics is intriguing. However, our results raise the question of whether it is possible to create a stronger, theory-independent test of temporal order. The insight from this study shows that separating the free dynamics of the system from local operations is problematic. A possible solution is to consider more general operations than the fixed unitaries discussed so far: these could involve measuring the system, producing a classical variable as the outcome. Additionally, a setting variable for each party could model different operational choices. This approach allows for the study of causal relations between parties—understood as correlations between settings and outcomes—without relying on a theory-dependent description of transformations. Further investigation of this possibility is left for future work.

In summary, our findings revealed that the assumptions needed to prove Bell inequalities for temporal order are not always met in practical scenarios. This prompted us to rethink these assumptions and recognize the complexity of separating a system's free dynamics from local operations. These insights are vital for both theoretical and experimental studies on the nature of time.

To address these challenges, we propose using more general operations that include measurements producing classical outcomes. This method allows direct study of causal relationships between different events without relying on specific theoretical models.

Finally, this dissertation opens new research opportunities, expanding our understanding of time and causality in the quantum realm. Future studies could aim to develop more robust, theory-independent tests of temporal order and practical methods to observe quantum time dilation in experimental settings.

In conclusion, this dissertation challenges our understanding of quantum time dilation and indefinite temporal order, questioning traditional views of time and causality. It provides new insights into the universe's fundamental nature. As research progresses in this field, exploring quantum mechanics and the nature of time will continue to be an engaging and significant endeavor.

Bibliography

[1]P. T. Grochowski, A. R. H. Smith, A. Dragan, and K. Dębski, "Quantum time dilation in atomic spectra", Phys. Rev. Res. **3**, 023053 (2021).

[2]J. Paczos, K. Dębski, P. T. Grochowski, A. R. H. Smith, and A. Dragan, "Quantum time dilation in a gravitational field", Quantum **8**, 1338 (2024).

[3]K. Dębski, P. T. Grochowski, R. Demkowicz-Dobrzański, and A. Dragan, "Universality of quantum time dilation", Class. Quantum Grav. (accepted manuscript) (2024).

[4]K. Dębski, M. Zych, F. Costa, and A. Dragan, "Indefinite temporal order without gravity", Phys. Rev. A **108**, 062204 (2023).

[5]K. Dębski and A. Dragan, "Multimode theory of gaussian states in uniformly accelerated frames", Phys. Rev. D **98**, 025003 (2018).

[6]J. A. Szypulski, P. T. Grochowski, K. Dębski, and A. Dragan, "Effect of relativistic acceleration on tripartite entanglement of gaussian states", Int. J. Mod. Phys. D **32**, 2350032 (2023).

[7]K. Dębski, P. T. Grochowski, and A. Dragan, "Probing the casimir-polder potential with unruh-dewitt detector excitations", Phys. Lett. B **815**, 136160 (2021).

[8]B. Markowicz, K. Dębski, M. Kolanowski, W. Kamiński, and A. Dragan, "Casimir effect in conformally flat spacetimes", Class. Quantum Grav. **37**, 235009 (2020).

[9]A. Dragan, K. Dębski, S. Charzyński, K. Turzyński, and A. Ekert, "Relativity of superluminal observers in 1+3 spacetime", Class. Quantum Grav. **40**, 025013 (2022).

[10]J. Paczos, K. Dębski, S. Cedrowski, S. Charzyński, K. Turzyński, A. Ekert, and A. Dragan, "Covariant quantum field theory of tachyons", Phys. Rev. D (accepted manuscript) (2024).

[11]A. of Hippo, *The confessions of st. augustine*, trans. by J. G. Pilkington, Original work published ca. 400 AD (Forgotten Books, 2008) Chap. Book XI, Chapter 14.

[12]J. Levine, "The history of time and frequency from antiquity to the present day", Eur. Phys. J. H **41**, 1–67 (2016).

[13]H. E. Winlock, "The origin of the ancient egyptian calendar", Proc. Am. Philos. Soc. **83**, 447–464 (1940).

[14]V. R. Bricker, "The origin of the maya solar calendar", Curr. Anthropol. **23**, 101–103 (1982).

[15]H. J. Birx, ed., *Encyclopedia of time: science, philosophy, theology, and culture* (Sage Publications, Los Angeles, 2009).

[16]A. N. Balslev and N. Mohanty, *Religion and time* (Brill, Leiden, The Netherlands, 1992).

[17]A. Bareau, "The notion of time in early buddhism", East and West **7**, 353–364 (1957).

[18]J. Hintikka, "Time, truth, and knowledge in ancient greek philosophy", Am. Philos. Q. **4**, 1–14 (1967).

[19]A. Grunbaum, "Modern science and refutation of the paradoxes of zeno", The Scientific Monthly **81**, 234–239 (1955).

[20]A. Bardon, *A brief history of the philosophy of time* (Oxford University Press, New York, 2013).

[21]G. Hatfield, *Kant on the perception of space (and time)*, edited by P. Guyer (Cambridge University Press, 2006), pp. 61–93.

[22]N. K. Smith, "A commentary to kant's "critique of pure reason"", in *A commentary to kant's 'critique of pure reason'* (Palgrave Macmillan UK, London, 2003), pp. 1–78.

[23]S. Holte, "Nietzsche's eternal return and the question of hope", Stud. Theol. - Nord. J. Theol. **74**, 139–158 (2020).

[24]R. Pfeffer, "Eternal recurrence in nietzsche's philosophy", The Review of Metaphysics **19**, 276–300 (1965).

[25]P. J. Kain, "Nietzsche, eternal recurrence, and the horror of existence", Journal of Nietzsche Studies, 49–63 (2007).

[26]G. W. Leibniz, M. Frankiewicz, and J. Kopania, *Teodycea: o dobroci boga, wolności człowieka i pochodzeniu zła* (Wydawn. Naukowe PWN, 2001).

[27]I. Dilman, *Free will: an historical and philosophical introduction* (Routledge, 2013).

[28]R. Staley, *Einstein's generation: the origins of the relativity revolution* (University of Chicago Press, 2008).

[29]A. Einstein, "The Theory of Relativity", in *Out of my Later Years* (Wings Books, New York, 1996), pp. 39–46.

[30]R. Shankar, *Principles of quantum mechanics* (Springer Science & Business Media, 2012).

[31]W. Pauli, *General Principles of Quantum Mechanics* (Springer-Verlag, Berlin Heidelberg New York, 1980).

[32]P. W. Bridgman, *The logic of modern physics* (Macmillan, Oxford, England, 1927).

[33]A. Peres, "Measurement of time by quantum clocks", Am. J. Phys. **48**, 552–557 (1980).

[34]C. W. Helstrom, *Quantum detection and estimation theory*, Vol. 123, Mathematics in Science and Engineering (Academic Press, New York, 1976).

[35]A. S. Holevo, *Probabilistic and statistical aspects of quantum theory*, Vol. 1, Statistics and Probability (North-Holland, Amsterdam, 1982).

[36]S. L. Braunstein and C. M. Caves, "Statistical distance and the geometry of quantum states", Phys. Rev. Lett. **72**, 3439–3443 (1994).

[37]S. L. Braunstein, C. M. Caves, and G. J. Milburn, "Generalized Uncertainty Relations: Theory, Examples, and Lorentz Invariance", Ann. Phys. **247**, 135–173 (1996).

[38]P. Busch, M. Grabowski, and P. J. Lahti, *Operational Quantum Physics*, Vol. 31, Lecture Notes in Physics Monographs (Springer, Verlag Berlin Heidelberg).

[39]P. Busch, P. J. Lahti, J. P. Pellonpää, and K. Ylinen, *Quantum Measurement*, Theoretical and Mathematical Physics (Springer International Publishing, 2016).

[40]P. Busch, M. Grabowski, and P. J. Lahti, "Time observables in quantum theory", Phys. Lett. A **191**, 357–361 (1994).

[41]R. Brunetti, K. Fredenhagen, and M. Hoge, "Time in quantum physics: from an external parameter to an intrinsic observable", Found. Phys. **40**, 1368–1378 (2010).

[42]A. R. H. Smith and M. Ahmadi, "Quantizing time: Interacting clocks and systems", Quantum **3**, 160 (2019).

[43]L. Loveridge, T. Miyadera, and P. Busch, "Symmetry, Reference Frames, and Relational Quantities in Quantum Mechanics", Found. Phys. **48**, 135–198 (2018).

[44]P. A. Höhn, A. R. H. Smith, and M. P. E. Lock, "Trinity of relational quantum dynamics", Phys. Rev. D **104**, 066001 (2021).

[45]P. A. Höhn, A. R. H. Smith, and M. P. E. Lock, "Equivalence of approaches to relational quantum dynamics in relativistic settings", Front. Phys. **9** (2021).

[46]M. Zych, F. Costa, I. Pikovski, T. C. Ralph, and Č. Brukner, "General relativistic effects in quantum interference of photons", Class. Quantum Grav. **29**, 224010 (2012).

[47]I. Pikovski, M. Zych, F. Costa, and Č. Brukner, "Universal decoherence due to gravitational time dilation", Nat. Phys. **11**, 668–672 (2015).

[48]Y. Margalit, Z. Zhou, S. Machluf, D. Rohrlich, Y. Japha, et al., "A self-interfering clock as a "which path" witness", Science **349**, 1205–1208 (2015).

[49]B. H. Pang, Y. Chen, and F. Y. Khalili, "Universal Decoherence under Gravity: A Perspective through the Equivalence Principle", Phys. Rev. Lett. **117**, 090401 (2016).

[50]M. Zych, I. Pikovski, F. Costa, and Č. Brukner, "General relativistic effects in quantum interference of "clocks"", J. Phys.: Conf. Ser. **723**, 012044 (2016).

[51]P. A. Bushev, J. H. Cole, D. Sholokhov, N. Kukharchyk, and M. Zych, "Single electron relativistic clock interferometer", New J. Phys. **18**, 093050 (2016).

[52]S. Loriani, A. Friedrich, C. Ufrecht, F. D. Pumpo, S. Kleinert, et al., "Interference of clocks: A quantum twin paradox", Sci. Adv. **5**, eaax8966 (2019).

[53]A. Roura, "Gravitational Redshift in Quantum-Clock Interferometry", Phys. Rev. X **10**, 021014 (2020).

[54]A. R. H. Smith and M. Ahmadi, "Quantum clocks observe classical and quantum time dilation", Nat. Commun. **11**, 5360 (2020).

[55]E. Castro-Ruiz, F. Giacomini, A. Belenchia, and Č. Brukner, "Quantum clocks and the temporal localisability of events in the presence of gravitating quantum systems", Nat. Commun. **11**, 2672 (2020).

[56]J. Foo, S. Onoe, and M. Zych, "Unruh-dewitt detectors in quantum superpositions of trajectories", Phys. Rev. D **102**, 085013 (2020).

[57]G. Chiribella, G. M. D'Ariano, P. Perinotti, and B. Valiron, "Quantum computations without definite causal structure", Phys. Rev. A **88**, 022318 (2013).

[58]R. Pierini, K. Turzyński, and A. Dragan, "Can a charged decaying particle serve as an ideal clock in the presence of a magnetic field?", Phys. Rev. D **97**, 045006 (2018).

[59]K. Lorek, J. Louko, and A. Dragan, "Ideal clocks—a convenient fiction", Class. Quantum Grav. **32**, 175003 (2015).

[60]A. Peres and D. R. Terno, "Quantum information and relativity theory", Rev. Mod. Phys. **76**, 93–123 (2004).

[61]L. C. Barbado, E. Castro-Ruiz, L. Apadula, and Č. Brukner, "Unruh effect for detectors in superposition of accelerations", Phys. Rev. D **102**, 045002 (2020).

[62]P. A. Höhn, A. R. H. Smith, and M. P. E. Lock, "Trinity of relational quantum dynamics", Phys. Rev. D **104**, 066001 (2021).

[63]F. Giacomini, E. Castro-Ruiz, and Č. Brukner, "Quantum mechanics and the covariance of physical laws in quantum reference frames", Nat. Commun. **10**, 494 (2019).

[64]L. J. Henderson, A. Belenchia, E. Castro-Ruiz, C. Budroni, M. Zych, et al., "Quantum temporal superposition: the case of quantum field theory", Phys. Rev. Lett. **125**, 131602 (2020).

[65]L. Viola and R. Onofrio, "Testing the equivalence principle through freely falling quantum objects", Phys. Rev. D **55**, 455–462 (1997).

[66]C. Anastopoulos and B. L. Hu, "Equivalence principle for quantum systems: dephasing and phase shift of free-falling particles", Class. Quantum Grav. **35**, 035011 (2018).

[67]S. Bose, A. Mazumdar, G. W. Morley, H. Ulbricht, M. Toroš, M. Paternostro, A. A. Geraci, P. F. Barker, M. S. Kim, and G. Milburn, "Spin entanglement witness for quantum gravity", Phys. Rev. Lett. **119**, 240401 (2017).

[68]C. Marletto and V. Vedral, "Gravitationally Induced Entanglement between Two Massive Particles is Sufficient Evidence of Quantum Effects in Gravity", Phys. Rev. Lett. **119**, 240402 (2017).

[69]H. Weyl, *The theory of groups and quantum mechanics*, Originally published in German as *Gruppentheorie und Quantenmechanik* in 1928 (Dover Publications, New York, 1950).

[70]A. R. H. Smith and M. Ahmadi, "Quantizing time: Interacting clocks and systems", Quantum **3**, 160 (2019).

[71]M. Zych, F. Costa, I. Pikovski, and Č. Brukner, "Bell's theorem for temporal order", Nat. Commun. **10**, 3772 (2019).

[72]V. Vedral and F. Morikoshi, "Schrödinger's Cat Meets Einstein's Twins: A Superposition of Different Clock Times", English, Int. J. Theor. Phys. **47**, 2126–2129 (2008).

[73]J. Lindkvist, C. Sabín, I. Fuentes, A. Dragan, I.-M. Svensson, et al., "Twin paradox with macroscopic clocks in superconducting circuits", Phys. Rev. A **90**, 052113 (2014).

[74]M. Zych, F. Costa, I. Pikovski, and Č. Brukner, "Quantum interferometric visibility as a witness of general relativistic proper time", Nat. Commun. **2**, 505 (2011).

[75]P. A. Bushev, J. H. Cole, D. Sholokhov, N. Kukharchyk, and M. Zych, "Single electron relativistic clock interferometer", New J. Phys. **18**, 093050 (2016).

[76]A. J. Paige, A. D. K. Plato, and M. S. Kim, "Classical and Nonclassical Time Dilation for Quantum Clocks", Phys. Rev. Lett. **124**, 160602 (2020).

[77]A. Dragan, *Unusually special relativity* (World Scientific, London, Dec. 2021).

[78]B. Maybee, D. Hodgson, A. Beige, and R. Purdy, "A Physically-Motivated Quantisation of the Electromagnetic Field on Curved Spacetimes", Entropy **21**, 844 (2019).

[79]C. W. Chou, D. B. Hume, T. Rosenband, and D. J. Wineland, "Optical Clocks and Relativity", Science **329**, 1630–1633 (2010).

[80]Z. Białynicka-Birula, P. Meystre, E. Schumacher, and M. Wilkens, "Velocity-dependent spontaneous emission", Opt. Commun. **85**, 315–318 (1991).

[81]K. Rzążewski and W. Żakowicz, "Spontaneous emission from an extended wavepacket", J. Phys. B At. Mol. Opt. Phys. **25**, L319 (1992).

[82]O. Steuernagel and H. Paul, "Decoherence from spontaneous emission", Phys. Rev. A **52**, 905–908 (1995).

[83]M. V. Fedorov, M. A. Efremov, A. E. Kazakov, K. W. Chan, C. K. Law, et al., "Spontaneous emission of a photon: Wave-packet structures and atom-photon entanglement", Phys. Rev. A **72**, 032110 (2005).

[84]N. Stritzelberger and A. Kempf, "Coherent delocalization in the light-matter interaction", Phys. Rev. D **101**, 036007 (2020).

[85]M. Zych, *Quantum Systems under Gravitational Time Dilation*, Springer Theses (Springer International Publishing, 2017).

[86]M. Wilkens, "Spurious velocity dependence of free-space spontaneous emission", Phys. Rev. A **47**, 671–673 (1993).

[87]M. Wilkens, "Significance of Röntgen current in quantum optics: Spontaneous emission of moving atoms", Phys. Rev. A **49**, 570–573 (1994).

[88]S. M. Barnett and M. Sonnleitner, "The vacuum friction paradox and related puzzles", Contemp. Phys. **59**, 145–154 (2018).

[89]M. Sonnleitner, N. Trautmann, and S. M. Barnett, "Will a decaying atom feel a friction force?", Phys. Rev. Lett. **118**, 053601 (2017).

[90]M. Sonnleitner and S. M. Barnett, "Mass-energy and anomalous friction in quantum optics", Phys. Rev. A **98**, 042106 (2018).

[91]W. C. Röntgen, "Ueber die durch bewegung eines im homogenen electrischen felde befindlichen dielectricums hervorgerufene electrodynamische kraft", Ann. Phys. Chem. **35**, 264 (1888).

[92]M. Babiker, "Theory of momentum changes in atomic translation due to irradiation with resonant light", J. Phys. B At. Mol. Phys. **17**, 4877 (1984).

[93]L. G. Boussiakou, C. R. Bennett, and M. Babiker, "Quantum theory of spontaneous emission by real moving atoms", Phys. Rev. Lett. **89**, 123001 (2002).

[94]J. D. Cresser and S. M. Barnett, "The rate of spontaneous decay of a moving atom", J. Phys. B: At. Mol. Opt. Phys. **36**, 1755–1759 (2003).

[95]R. Matloob, "Decay rate of an excited atom in a moving medium", Phys. Rev. Lett. **94**, 050404 (2005).

[96]M. Sonnleitner and S. M. Barnett, "Mass-energy and anomalous friction in quantum optics", Phys. Rev. A **98**, 042106 (2018).

[97]P. K. Schwartz and D. Giulini, "Post-Newtonian Hamiltonian description of an atom in a weak gravitational field", Phys. Rev. A **100**, 052116 (2019).

[98]F. Shafieiyan, E. Amooghorban, and A. Mahdifar, "Spontaneous emission of a moving atom in the presence of magnetodielectric material: A relativistic approach", Opt. Commun. **426**, 63–69 (2018).

[99]R. Lopp and E. Martín-Martínez, "Quantum delocalization, gauge, and quantum optics: light-matter interaction in relativistic quantum information", Phys. Rev. A **103**, 013703 (2021).

[100]V. Weisskopf and E. Wigner, "Berechnung der natürlichen linienbreite auf grund der diracschen lichttheorie", Z. Phys. **63**, 54–73 (1930).

[101]B. Welz, *Atomic absorption spectrometry* (Wiley-VCH, Weinheim New York, 1999).

[102]S. M. Brewer, J. S. Chen, A. M. Hankin, E. R. Clements, C. W. Chou, et al., "$^{27}Al^{+}$ Quantum-Logic Clock with a Systematic Uncertainty below 10^{-18}", Phys. Rev. Lett. **123**, 033201 (2019).

[103]K. G. Johnson, J. D. Wong-Campos, B. Neyenhuis, J. Mizrahi, and C. Monroe, "Ultrafast creation of large Schrödinger cat states of an atom", Nat. Commun. **8**, 1–7 (2017).

[104]A. D. Cronin, J. Schmiedmayer, and D. E. Pritchard, "Optics and interferometry with atoms and molecules", Rev. Mod. Phys. **81**, 1051–1129 (2009).

[105]P. Cladé, S. Guellati-Khélifa, F. Nez, and F. Biraben, "Large momentum beam splitter using bloch oscillations", Phys. Rev. Lett. **102**, 240402 (2009).

[106]S.-w. Chiow, T. Kovachy, H.-C. Chien, and M. A. Kasevich, "102$\hbar k$ Large area atom interferometers", Phys. Rev. Lett. **107**, 130403 (2011).

[107]G. D. McDonald, C. C. N. Kuhn, S. Bennetts, J. E. Debs, K. S. Hardman, et al., "80$\hbar k$ Momentum separation with bloch oscillations in an optically guided atom interferometer", Phys. Rev. A **88**, 053620 (2013).

[108]J. Rudolph, T. Wilkason, M. Nantel, H. Swan, C. M. Holland, et al., "Large momentum transfer clock atom interferometry on the 689 nm intercombination line of strontium", Phys. Rev. Lett. **124**, 083604 (2020).

[109]M. Kasevich and S. Chu, "Atomic interferometry using stimulated raman transitions", Phys. Rev. Lett. **67**, 181–184 (1991).

[110]Z.-K. Hu, B.-L. Sun, X.-C. Duan, M.-K. Zhou, L.-L. Chen, et al., "Demonstration of an ultrahigh-sensitivity atom-interferometry absolute gravimeter", Phys. Rev. A **88**, 043610 (2013).

[111]I. Dutta, D. Savoie, B. Fang, B. Venon, C. L. Garrido Alzar, et al., "Continuous cold-atom inertial sensor with 1 nrad/sec rotation stability", Phys. Rev. Lett. **116**, 183003 (2016).

[112]S. Abend, M. Gebbe, M. Gersemann, H. Ahlers, H. Müntinga, et al., "Atom-chip fountain gravimeter", Phys. Rev. Lett. **117**, 203003 (2016).

[113]R. Geiger, A. Landragin, S. Merlet, and F. P. D. Santos, "High-accuracy inertial measurements with cold-atom sensors", AVS Quantum Sci. **2**, 024702 (2020).

[114]N. Hinkley, A. Sherman, N. B. Phillips, M. Schioppo, N. D. Lemke, et al., "An atomic clock with 10^{-18} instability", Science **341**, 1215–1218 (2013).

[115]A. D. Ludlow, M. M. Boyd, J. Ye, E. Peik, and P. O. Schmidt, "Optical atomic clocks", Rev. Mod. Phys. **87**, 637 (2015).

[116]Ł. Dobrek, M. Gajda, M. Lewenstein, K. Sengstock, G. Birkl, et al., "Optical generation of vortices in trapped bose-einstein condensates", Phys. Rev. A **60**, R3381–r3384 (1999).

[117]J. Denschlag, J. E. Simsarian, D. L. Feder, C. W. Clark, L. A. Collins, et al., "Generating solitons by phase engineering of a bose-einstein condensate", Science **287**, 97–101 (2000).

[118]H. Y. Lo, D. Kienzler, L. De Clercq, M. Marinelli, V. Negnevitsky, et al., "Spin-motion entanglement and state diagnosis with squeezed oscillator wavepackets", Nature **521**, 336–339 (2015).

[119]T. Kovachy, P. Asenbaum, C. Overstreet, C. A. Donnelly, S. M. Dickerson, et al., "Quantum superposition at the half-metre scale", Nature **528**, 530–533 (2015).

[120]J. M. McGuirk, M. J. Snadden, and M. A. Kasevich, "Large area light-pulse atom interferometry", Phys. Rev. Lett. **85**, 4498–4501 (2000).

[121]P. W. Graham, J. M. Hogan, M. A. Kasevich, and S. Rajendran, "New method for gravitational wave detection with atomic sensors", Phys. Rev. Lett. **110**, 171102 (2013).

[122]B. Plotkin-Swing, D. Gochnauer, K. E. McAlpine, E. S. Cooper, A. O. Jamison, et al., "Three-path atom interferometry with large momentum separation", Phys. Rev. Lett. **121**, 133201 (2018).

[123]C. J. Kennedy, E. Oelker, J. M. Robinson, T. Bothwell, D. Kedar, et al., "Precision metrology meets cosmology: improved constraints on ultralight dark matter from atom-cavity frequency comparisons", Phys. Rev. Lett. **125**, 201302 (2020).

[124]M. Saba, T. A. Pasquini, C. Sanner, Y. Shin, W. Ketterle, et al., "Light scattering to determine the relative phase of two bose-einstein condensates", Science **307**, 1945–1948 (2005).

[125]N. R. Thomas, A. C. Wilson, and C. J. Foot, "Double-well magnetic trap for bose-einstein condensates", Phys. Rev. A **65**, 063406 (2002).

[126]S. Khandelwal, M. P. E. Lock, and M. P. Woods, "Universal quantum modifications to general relativistic time dilation in delocalised clocks", Quantum **4**, 309 (2020).

[127]F. Giacomini, "Spacetime Quantum Reference Frames and superpositions of proper times", Quantum **5**, 508 (2021).

[128]N. Stritzelberger and A. Kempf, "Coherent delocalization in the light-matter interaction", Phys. Rev. D **101**, 036007 (2020).

[129]R. Lopp and E. Martín-Martínez, "Quantum delocalization, gauge, and quantum optics: Light-matter interaction in relativistic quantum information", Phys. Rev. A **103**, 013703 (2021).

[130]R. Colella, A. W. Overhauser, and S. A. Werner, "Observation of Gravitationally Induced Quantum Interference", Phys. Rev. Lett. **34**, 1472–1474 (1975).

[131]M. Kasevich and S. Chu, "Measurement of the gravitational acceleration of an atom with a light-pulse atom interferometer", Appl. Phys. B **54**, 321–332 (1992).

[132]M. Zych, F. Costa, I. Pikovski, and Č. Brukner, "Quantum interferometric visibility as a witness of general relativistic proper time", Nat. Commun. **2**, 505 (2011).

[133]I. Pikovski, M. Zych, F. Costa, and Č. Brukner, "Universal decoherence due to gravitational time dilation", Nat. Phys. **11**, 668 (2015).

[134]B. H. Pang, Y. Chen, and F. Y. Khalili, "Universal Decoherence under Gravity: A Perspective through the Equivalence Principle", Phys. Rev. Lett. **117**, 090401 (2016).

[135]D.-F. Gao, J. Wang, and M.-S. Zhan, "Atomic Interferometric Gravitational-Wave Space Observatory (AIGSO)", Commun. Theor. Phys. **69**, 37 (2018).

[136]D. Schlippert, J. Hartwig, H. Albers, L. L. Richardson, C. Schubert, et al., "Quantum Test of the Universality of Free Fall", Phys. Rev. Lett. **112**, 203002 (2014).

[137]M. Zych and Č. Brukner, "Quantum formulation of the Einstein equivalence principle", Nature Phys **14**, 1027–1031 (2018).

[138]K.-P. Marzlin, "Dipole coupling of atoms and light in gravitational fields", Phys. Rev. A **51**, 625–631 (1995).

[139]P. K. Schwartz and D. Giulini, "Post-newtonian hamiltonian description of an atom in a weak gravitational field", Phys. Rev. A **100**, 052116 (2019).

[140]V. J. Martínez-Lahuerta, S. Eilers, T. E. Mehlstäubler, P. O. Schmidt, and K. Hammerer, "Ab initio quantum theory of mass defect and time dilation in trapped-ion optical clocks", Phys. Rev. A **106**, 032803 (2022).

[141]M. Zych, Ł. Rudnicki, and I. Pikovski, "Gravitational mass of composite systems", Phys. Rev. D **99**, 104029 (2019).

[142]C. Lämmerzahl, "A Hamilton operator for quantum optics in gravitational fields", Phys. Lett. A **203**, 12–17 (1995).

[143]C. Gerry and P. Knight, *Introductory Quantum Optics* (Cambridge University Press, Cambridge, 2004).

[144]P. Lambropoulos and D. Petrosyan, *Fundamentals of Quantum Optics and Quantum Information* (Springer Berlin Heidelberg, Berlin, Heidelberg, 2007).

[145]G. Grynberg, A. Aspect, and C. Fabre, *Introduction to Quantum Optics: From the Semiclassical Approach to Quantized Light* (Cambridge University Press, Cambridge, 2010).

[146]K. Lorek, J. Louko, and A. Dragan, "Ideal clocks—a convenient fiction", Class. Quantum Grav. **32**, 175003 (2015).

[147]A. M. Eisele, "On the behaviour of an accelerated clock", Helv. Phys. Acta **60** (1987).

[148]R. Pierini, K. Turzyński, and A. Dragan, "Can a charged decaying particle serve as an ideal clock in the presence of a magnetic field?", Phys. Rev. D **97**, 045006 (2018).

[149]N. D. Birrell, N. D. Birrell, and P. Davies, *Quantum fields in curved space* (Cambridge university press, 1984).

[150]C. Rovelli, "Relational quantum mechanics", Int. J. Theor. Phys. **35**, 1637–1678 (1996).

[151]V. Vedral and F. Morikoshi, "Schrödinger's cat meets einstein's twins: a superposition of different clock times", Int. J. Theor. Phys. **47**, 2126–2129 (2007).

[152]S. Reinhardt, G. Saathoff, H. Buhr, L. A. Carlson, et al., "Test of relativistic time dilation with fast optical atomic clocks at different velocities", Nat. Phys. **3**, 861–864 (2007).

[153]P. A. Bushev, J. H. Cole, D. Sholokhov, N. Kukharchyk, and M. Zych, "Single electron relativistic clock interferometer", New J. Phys. **18**, 093050 (2016).

[154]E. C. Ruiz, F. Giacomini, and Č. Brukner, "Entanglement of quantum clocks through gravity", Pnas **114**, 2303–2309 (2017).

[155]S. Loriani, A. Friedrich, C. Ufrecht, F. D. Pumpo, S. Kleinert, et al., "Interference of clocks: A quantum twin paradox", Sci. adv. **5**, 8966 (2019).

[156]A. J. Paige, A. D. K. Plato, and M. S. Kim, "Classical and Nonclassical Time Dilation for Quantum Clocks", Phys. Rev. Lett. **124**, 160602 (2020).

[157]A. R. Smith, "Quantum time dilation: a new test of relativistic quantum theory", arXiv:2004.10810 (2020).

[158]A. Roura, C. Schubert, D. Schlippert, and E. M. Rasel, "Measuring gravitational time dilation with delocalized quantum superpositions", Phys. Rev. D **104**, 084001 (2021).

[159]T. Chiba and S. Kinoshita, "Quantum clocks, gravitational time dilation, and quantum interference", Phys. Rev. D **106**, 124035 (2022).

[160]H.-P. Breuer and F. Petruccione, *The Theory of Open Quantum Systems* (Oxford University Press, Jan. 2007).

[161]W. Pauli, *General Principles of Quantum Mechanics* (Springer Science & Business Media, Dec. 2012).

[162]P. Busch, M. Grabowski, and P. J. Lahti, "Time observables in quantum theory", Phys. Lett. A **191**, 357–361 (1994).

[163]A. Peres, "Measurement of time by quantum clocks", Am. J. Phys. **48**, 552–557 (1980).

[164]C. W. Helstrom, "Quantum detection and estimation theory", J. Stat. Phys. **1**, 231–252 (1969).

[165]A. Holevo, *Probabilistic and Statistical Aspects of Quantum Theory* (Edizioni della Normale, Pisa, 2011).

[166]S. L. Braunstein and C. M. Caves, "Statistical distance and the geometry of quantum states", Phys. Rev. Lett. **72**, 3439–3443 (1994).

[167]S. L. Braunstein, C. M. Caves, and G. J. Milburn, "Generalized Uncertainty Relations: Theory, Examples, and Lorentz Invariance", Ann. Phys. **247**, 135–173 (1996).

[168]P. Busch, M. Grabowski, and P. J. Lahti, *Operational Quantum Physics* (Springer Science & Business Media, Nov. 1997).

[169]P. Busch, P. Lahti, J.-P. Pellonpää, and K. Ylinen, *Quantum Measurement* (Springer, Aug. 2016).

[170]H. Hadi, K. Atazadeh, and F. Darabi, "Quantum time dilation in the near-horizon region of a black hole", Phys. Lett. B, 137471 (2022).

[171]C. Cepollaro and F. Giacomini, "Quantum generalisation of einstein's equivalence principle can be verified with entangled clocks as quantum reference frames", arXiv:2112.03303 (2021).

[172]C. Cepollaro, F. Giacomini, and M. G. Paris, "Gravitational time dilation as a resource in quantum sensing", Quantum **7**, 946 (2023).

[173]C. W. Chou, D. B. Hume, T. Rosenband, and D. J. Wineland, "Optical Clocks and Relativity", Science **329**, 1630–1633 (2010).

[174]J. C. Hafele and R. E. Keating, "Around-the-World Atomic Clocks: Predicted Relativistic Time Gains", Science **177**, 166–168 (1972).

[175]M. Takamoto, I. Ushijima, N. Ohmae, T. Yahagi, K. Kokado, et al., "Test of general relativity by a pair of transportable optical lattice clocks", Nat. Photonics **14**, 411–415 (2020).

[176]P. Laurent, D. Massonnet, L. Cacciapuoti, and C. Salomon, "The ACES/PHARAO space mission", C. R. Phys. **16**, 540–552 (2015).

[177]G. M. Tino, A. Bassi, G. Bianco, K. Bongs, P. Bouyer, et al., "SAGE: A proposal for a space atomic gravity explorer", Eur. Phys. J. D **73**, 228 (2019).

[178]T. Bothwell, C. J. Kennedy, A. Aeppli, D. Kedar, J. M. Robinson, et al., "Resolving the gravitational redshift across a millimetre-scale atomic sample", Nature **602**, 420–424 (2022).

[179]X. Zheng, J. Dolde, V. Lochab, B. N. Merriman, H. Li, et al., "Differential clock comparisons with a multiplexed optical lattice clock", Nature **602**, 425–430 (2022).

[180]R. Charrière, M. Cadoret, N. Zahzam, Y. Bidel, and A. Bresson, "Local gravity measurement with the combination of atom interferometry and bloch oscillations", Phys. Rev. A **85**, 013639 (2012).

[181]X. Zhang, R. P. del Aguila, T. Mazzoni, N. Poli, and G. M. Tino, "Trapped-atom interferometer with ultracold sr atoms", Phys. Rev. A **94**, 043608 (2016).

[182]V. Xu, M. Jaffe, C. D. Panda, S. L. Kristensen, L. W. Clark, et al., "Probing gravity by holding atoms for 20 seconds", Science **366**, 745–749 (2019).

[183]C. D. Panda, M. Tao, J. Egelhoff, M. Ceja, V. Xu, and H. Müller, "Minute-scale gravimetry using a coherent atomic spatial superposition", arXiv:2210.07289 (2022).

[184]R. J. Rafac, C. E. Tanner, A. E. Livingston, K. W. Kukla, H. G. Berry, et al., "Precision lifetime measurements of the $6p^2P_{1/2,3/2}$ states in atomic cesium", Phys. Rev. A **50**, R1976(r) (1994).

[185]D. L. Moehring et al., "Precision lifetime measurements of a single trapped ion with ultrafast laser pulses", Phys. Rev. A **73**, 023413 (2006).

[186]M. Seidlitz et al., "Precision lifetime measurements of the first 2^+ and 4^+ states in ^{56}cr at the $N = 32$ subshell closure", Phys. Rev. C **84**, 034318 (2011).

[187]R. B. Hutson, A. Goban, G. E. Marti, L. Sonderhouse, C. Sanner, et al., "Engineering quantum states of matter for atomic clocks in shallow optical lattices", Phys. Rev. Lett. **123**, 123401 (2019).

[188]X. Zheng, J. Dolde, M. C. Cambria, H. M. Lim, and S. Kolkowitz, "A lab-based test of the gravitational redshift with a miniature clock network", Nat. Commun. **14**, 4886 (2023).

[189]R. M. Angelo, N. Brunner, S. Popescu, A. J. Short, and P. Skrzypczyk, "Physics within a quantum reference frame", J. Phys. A: Math. Theor. **44**, 145304 (2011).

[190]F. W. Nietzsche, *Philosophy and truth: selections from nietzsche?s notebooks of the early 1870?s*, edited by D. Breazeale (Humanities Press, Atlantic Highlands, N.J., 1979).

[191]J. Butterfield and C. Isham, "Spacetime and the philosophical challenge of quantum gravity", in *Physics meets philosophy at the planck scale*, edited by C. Callender and N. Huggett (Cambridge University Press, 2001), p. 33.

[192]L. Hardy, "Towards quantum gravity: a framework for probabilistic theories with non-fixed causal structure", J. Phys. A: Math. Gen. **40**, 3081–3099 (2007).

[193]D. Oriti, ed., *Approaches to quantum gravity: toward a new understanding of space, time and matter* (Cambridge University Press, 2009).

[194]C. Kiefer, *Quantum gravity: third edition*, International Series of Monographs on Physics (OUP Oxford, 2012).

[195]J. S. Bell, "On the einstein podolsky rosen paradox", Phys. Phys. Fiz. **1**, 195–200 (1964).

[196]J. F. Clauser, M. A. Horne, A. Shimony, and R. A. Holt, "Proposed experiment to test local hidden-variable theories", Phys. Rev. Lett. **23**, 880–884 (1969).

[197]S. J. Freedman and J. F. Clauser, "Experimental test of local hidden-variable theories", Phys. Rev. Lett. **28**, 938–941 (1972).

[198]B. Hensen et al., "Loophole-free bell inequality violation using electron spins separated by 1.3 kilometres.", Nature **526**, 682–686 (2015).

[199]M. Giustina, M. A. M. Versteegh, S. Wengerowsky, J. Handsteiner, A. Hochrainer, et al., "Significant-loophole-free test of bell's theorem with entangled photons", Phys. Rev. Lett. **115**, 250401 (2015).

[200]L. K. Shalm, E. Meyer-Scott, B. G. Christensen, P. Bierhorst, M. A. Wayne, et al., "Strong loophole-free test of local realism", Phys. Rev. Lett. **115**, 250402 (2015).

[201]G. Chiribella, G. M. D'Ariano, P. Perinotti, and B. Valiron, "Quantum computations without definite causal structure", Phys. Rev. A **88**, 022318 (2013).

[202]W. G. Unruh, "Notes on black-hole evaporation", Phys. Rev. D **14**, 870 (1976).

[203]W. G. Unruh and R. M. Wald, "What happens when an accelerating observer detects a rindler particle", Phys. Rev. D **29**, 1047–1056 (1984).

[204]L. C. B. Crispino, A. Higuchi, and G. E. A. Matsas, "The unruh effect and its applications", Rev. Mod. Phys. **80**, 787–838 (2008).

[205]A. Dimić, M. Milivojević, D. Gočanin, N. S. Móller, and Č. Brukner, "Simulating indefinite causal order with rindler observers", Front. Phys. **8**, 470 (2020).

[206]L. M. Procopio, A. Moqanaki, M. Araújo, F. Costa, I. A. Calafell, et al., "Experimental superposition of orders of quantum gates", Nat. Commun. **6**, 7913 (2015).

[207]G. Rubino, L. A. Rozema, A. Feix, M. Araújo, J. M. Zeuner, et al., "Experimental verification of an indefinite causal order", Sci. adv. **3**, e1602589 (2017).

[208]G. Rubino, L. A. Rozema, F. Massa, M. Araújo, M. Zych, et al., "Experimental entanglement of temporal orders", Opt. InfoBase Conf. Pap., `10.1364/qim.2019.s3b.3` (2017).

[209]K. Goswami, C. Giarmatzi, M. Kewming, F. Costa, C. Branciard, et al., "Indefinite causal order in a quantum switch", Phys. Rev. Lett. **121**, 090503 (2018).

[210]Y. Guo, X.-M. Hu, Z.-B. Hou, H. Cao, J.-M. Cui, et al., "Experimental transmission of quantum information using a superposition of causal orders", Phys. Rev. Lett. **124**, 030502 (2020).

[211]K. Wei, N. Tischler, S.-R. Zhao, Y.-H. Li, J. M. Arrazola, et al., "Experimental quantum switching for exponentially superior quantum communication complexity", Phys. Rev. Lett. **122**, 120504 (2019).

[212]M. M. Taddei, J. Cariñe, D. Martínez, T. García, N. Guerrero, et al., "Experimental computational advantage from superposition of multiple temporal orders of quantum gates", PRX Quantum **2**, 010320 (2020).

[213]S. Bose, A. Mazumdar, G. W. Morley, H. Ulbricht, M. Toroš, et al., "Spin entanglement witness for quantum gravity", Phys. Rev. Lett. **119**, 240401 (2017).

[214]C. Marletto and V. Vedral, "Gravitationally induced entanglement between two massive particles is sufficient evidence of quantum effects in gravity", Phys. Rev. Lett. **119**, 240402 (2017).

[215]I. Pikovski, M. Zych, F. Costa, and Č. Brukner, "Time dilation in quantum systems and decoherence", New J. Phys. **19**, 025011 (2017).

[216]Y. Margalit, O. Dobkowski, Z. Zhou, O. Amit, Y. Japha, et al., "Realization of a complete stern-gerlach interferometer: toward a test of quantum gravity", Sci. adv. **7**, 2879 (2021).

[217]B. Yurke and D. Stoler, "Bell's-inequality experiments using independent-particle sources", Phys. Rev. A **46**, 2229–2234 (1992).

[218]M. Araújo, C. Branciard, F. Costa, A. Feix, C. Giarmatzi, et al., "Witnessing causal nonseparability", New J. Phys. **17**, 102001 (2015).

[219]C. Branciard, "Witnesses of causal nonseparability: an introduction and a few case studies", Sci. Rep. **6**, 26018 (2016).